AD NUMBER
AD360623
CLASSIFICATION CHANGES
TO: unclassified
FROM: secret
LIMITATION CHANGES
TO: Approved for public release, distribution unlimited
FROM: Distribution authorized to DoD only; Administrative/Operational Use; JUN 1961. Other requests shall be referred to Defense Threat Reduction Agency, 8725 John J. Kingman Rd., MS 6201, Fort Belvoir, VA 22060-6201.
AUTHORITY
DNA/ISST ltr dtd 29 Jan 1996; DNA/ISST ltr dtd 29 Jan 1996

WT-1630

This document consists of 158 pages

No. 11 of 170 copies, Series A

Operation HARDTACK

April - October 1958

BEHAVIOR OF DEEP REINFORCED-CONCRETE SLABS IN HIGH-OVERPRESSURE REGIONS (U)

Issuance Date: June 30, 1961

HEADQUARTERS FIELD COMMAND
DEFENSE ATOMIC SUPPORT AGENCY
SANDIA BASE ALBUQUERQUE, NEW MEXICO

Inquiries relative to this report may be made to

Chief, Defense Atomic Support Agency
Washington 25, D. C.

When no longer required, this document may be destroyed in accordance with applicable security regulations.

DO NOT RETURN THIS DOCUMENT

USAEC Office of Technical Information Extension
Oak Ridge, Tennessee

WT-1030

OPERATION HARDTACK — PROJECT 3.6

BEHAVIOR OF DEEP REINFORCED-CONCRETE SLABS IN HIGH-OVERPRESSURE REGIONS (U)

E. H. Bultmann, Jr., Capt, USAF
Project Officer
J. D. Haltiwanger
R. N. Wright III
J. T. Hanley

University of Illinois
Urbana, Illinois

Air Force Special Weapons Center
Kirtland Air Force Base, New Mexico

Defense Atomic Support Agency
Washington, D. C. 20301

ABSTRACT

The primary objective was to determine the dynamic behavior of deep reinforced-concrete slabs in the overpressure region of 200 to 600 psi, and thereby to provide a basis for establishing design criteria for massive reinforced-concrete structures under blast loads.

Both one-way and two-way slabs placed flush with the ground surface were tested. The ratios of effective span to depth varied from 1.43 to 7.0. It was expected that, for slabs of these proportions, shearing strength would prove to be the controlling design parameter. Consequently, the test specimens were designed to study particularly shear strength of slabs both with and without shear reinforcement, though flexural strength was also considered. The slabs were tested during Shot Koa, and the weapon yield was given as about 1 Mt.

Instrumentation included self-recording overpressure-versus-time gages at each site and self-recording acceleration-versus-time gages on the slab-supporting structures. Measurements before and after test were made to determine the magnitude and character of the permanent deformations and, if possible, the modes of failure.

As a result of foundation failures, no usable data was obtained on the response of the deep two-way slabs. Thus, no effort was made to evaluate current resistance criteria for these members. However, sufficient usable data was obtained on the one-way slabs to justify detailed analyses of those members.

Recent research on the static behavior of deep beams is summarized. Data available from these static tests indicates that the shear-strength criteria originally applied to the Project 3.6 slabs are very conservative. In addition, the data indicates possible modes of failure of deep one-way slabs that were not considered in the pretest analyses. Using deflection data from laboratory static tests, new empirical expressions were developed for yield and ultimate deflections of deep one-way slabs and for the fundamental period of vibration of such members.

Consideration was given to the effects of axial loads, base disturbance, and rebound on the flexural behavior of the deep one-way slabs. It is shown that axial forces are very important and may account for increases in the yield resistances of the deeper slabs by as much as 300 percent. For estimates of base-disturbance effects, data from nearby stations was used, because the records of the accelerometers on the slabs themselves were destroyed by the action of sea water before recovery. Rebound computations correlated well with observed crack patterns.

Application of available criteria for the resistances or strengths of the slabs in brittle modes of failure, including shear-compression, shear-anchorage, bond, bearing, and pure bond shear indicate that much remains to be learned about the failure of deep one-way slabs in these modes. Of those mentioned, only the shear-compression and bearing-strength criteria do not appear to be excessively conservative.

Further research on the static and dynamic behavior of deep one-way slabs is recommended. In addition, research on static behavior of deep two-way slabs is required to establish the probable modes of failure and criteria for resistance in those modes. Revised interim design criteria are recommended for simply supported deep one-way slabs subjected to uniformly distributed dynamic load.

FOREWORD

This report presents the final results of one of the projects participating in the military-effect programs of Operation Hardtack. Overall information about this and the other military-effect programs can be obtained from ITR-1660, the "Summary Report of the Commander, Task Unit 3." This technical summary includes: (1) tables listing each detonation with its yield, type, environment, meteorological conditions, etc., (2) maps showing shot locations, (3) discussions of results by programs, (4) summaries of objectives, procedures, results, etc., for all projects, and (5) a listing of project reports for the military-effect programs.

PREFACE

The work reported herein was planned and carried out by personnel of the Structural Research Laboratory of the University of Illinois under Contract AF 29(601)-544 between the University of Illinois and the Air Force Special Weapons Center (AFSWC), Kirtland Air Force Base, New Mexico.

The project was under the general direction of Dr. N. M. Newmark, Head, Department of Civil Engineering, and under the immediate supervision of Dr. J. D. Haltiwanger, Professor of Civil Engineering. The planning and field test phases of this program were carried out by Dr. Haltiwanger; Mr. S. L. Paul, Instructor in Civil Engineering; Mr. R. N. Wright III, Instructor in Civil Engineering; and Mr. C. P. Mangelsdorf, formerly Instructor in Civil Engineering. The posttest analyses of the data accumulated from the field test and other supporting and allied studies significant to this work were carried out by Mr. Wright and Mr. J. T. Hanley, Research Associate in Civil Engineering.

The instrumentation program was installed and operated by personnel of the Ballistic Research Laboratories, Aberdeen Proving Ground, Maryland, under the supervision of Mr. J. J. Meszaros. The cooperation of this organization during the test program as well as during the data-reduction phases following the test was appreciated.

The Project Officer was Captain E. H. Bultmann, Jr., USAF, of AFSWC. The cooperation of Lt R. L. Player, USAF, also of AFSWC, throughout the period of the project is gratefully acknowledged. Recognition is also given to Professor G. K. Sinnamon of the University of Illinois for his interest, advice, and general guidance during the field test.

CONTENTS

FIGURES

Chapter 1

INTRODUCTION

1.1 OBJECTIVES

The original objective of this project was to determine the behavior of deep reinforced-concrete slabs in the overpressure region of 200 to 1,000 psi, and thereby to provide a basis for establishing design criteria for massive reinforced-concrete structures under blast loading. The upper limit of overpressure was subsequently reduced to 600 psi to avoid the possibility of losing the slabs in the crater formed by the surface test shot.

The term "deep" as used here is intended to include slabs having span-to-depth ratios as low as 1.28. It was expected that, for slabs of these proportions, shear would prove to be the most significant strength parameter.

Simply supported slabs reinforced in only one direction, as well as square slabs simply supported on all four edges and reinforced flexurally in two mutually perpendicular directions, were tested. Approximately half of the slabs were reinforced for shear by means of conventional vertical stirrups.

1.2 BACKGROUND

The design of reinforced-concrete beams and slabs has long been the subject of extensive experimental and theoretical studies. Literally thousands of laboratory tests have been made, and the results have been reported in the technical literature over the last several decades. A complete bibliography of such tests would constitute a sizable report in itself.

Despite the existence of a massive amount of information having to do with the strength of concrete beams and slabs, there are at least two areas of vital importance to the design of protective structures on which data is sorely lacking. The first of these areas has to do with the behavior of reinforced-concrete beams and slabs under dynamic loads —practically all previous tests have been restricted to static loads.

The second area concerns the need for experimental studies on the alteration of normal beam and slab proportions to resist high pressures. Prior to the need for structures to resist pressures from atomic or nuclear blasts, the load intensities of interest were, relatively speaking, low, and led to beams and slabs of what might be called normal proportions. Under the high pressures (hundreds of psi) that protective structures must resist, the beam and slab proportions must necessarily be severely altered. For such structures, slabs having span-to-depth ratios as low as 2.0 to 2.5 are not at all unrealistic. For slabs of such proportions, experimental studies are very few, and, for dynamic loads, virtually nonexistent.

Another area where the need for information is urgent is the design of doors and covers

for entranceways into underground protective structures. This is particularly true for structures to be designed and built as a part of our retaliatory installations, the doors for which may have to be power-operated. In such cases, the weight of the door is important and must be kept to a practical minimum consistent with requirements for blast and radiation protection.

For beams or one-way slabs, adequate ultimate strength design criteria are available for sections of normal proportions under statically applied loads (Reference 1). Application of these criteria to deep sections would require extrapolation that could lead to rather serious errors, because the basic criteria are largely empirical. This is particularly true in regard to shear strength which, it is believed, will prove to be the most significant strength parameter for the very deep sections.

For two-way slabs, ultimate strength design criteria, even for static loads on sections of normal proportions, particularly where shear phenomena are concerned, are not very well established. Consequently, for dynamically loaded deep slabs, proportions would have to be guessed at rather than designed on a sound basis. As a result, such slabs would have to be proportioned more conservatively and, therefore, less economically than they should be.

In 1958, while the field operations for this project were underway, the first extensive series of laboratory tests on deep beams (essentially one-way slabs) was begun at the University of Illinois under Contract AF 29(601)-468. The results of these tests are reported in References 2 and 3. In Chapter 4 of this report, these test results are considered in the evaluation of the behavior of the slabs for this project.

1.3 THEORY: BASIS FOR DESIGN OF ONE-WAY SLABS

When the slabs for this project were designed, it was believed that one-way slabs were susceptible to failure in pure shear, flexure, or diagonal tension. The results of the laboratory testing described in References 2 and 3, and the results of the field test itself have shown that the critical modes of failure are pure shear, flexure, shear-compression, bearing, shear-anchorage and bond. These tests appear to indicate that deep members, uniformly loaded, are not susceptible to failure in diagonal tension. The modes of failure and the test results are discussed in Chapter 4.

The parameters that affect the static strength of a simply supported reinforced-concrete slab in the three modes of failure mentioned above (pure shear, flexure, or diagonal tension) are as follows: concrete strength, steel strength, depth of slab, percentage of tensile reinforcement, percentage of compression reinforcement, and percentage of shear reinforcement. When loaded dynamically, the strength of the slabs is also influenced by the ductility factor, natural period of vibration, and load duration. Because the yield of the weapon was in the megaton range, the expected effective load duration was long, relative to the natural period of vibration (on the order of 0.005 second) of the slabs. Therefore it was assumed that the load duration was infinite, thereby simplifying the design computations considerably. It is realized, of course, that this is not quite true; however, the resulting errors are small, compared to the other uncertainties existing in the design of these slabs.

On the basis of the preceding remarks, criteria were developed in terms of the aforementioned parameters for the loads required to produce failure in each of the three specified modes. The development of these criteria is presented in the following paragraphs.

1.3.1 Pure Shear. A pure shear failure would be exemplified by failure along a vertical section in the region of maximum shear, that is, at the supports. If the effective

depth of the slab is assumed to be nine-tenths of the total depth, and the shearing resistance of the longitudinal reinforcement is neglected, the average shearing stress across a vertical section at the face of the support is

$$v = \frac{V}{A} = \frac{(r_{sp})(l/2)}{(10/9)(d)} \tag{1.1}$$

Where: r_{sp} = the uniform pressure (static)

l = the clear span

d = the effective depth (All symbols are defined in Appendix C.)

If the shearing strength of plain concrete is taken as $0.2 f'_c$ where f'_c is the ultimate strength of concrete (Reference 4), and is equated to the shearing stress as given in Equation 1.1, then the uniform pressure required to produce a shearing stress equal to the shearing strength of concrete is obtained by equating Equation 1.1 to $0.2 f'_c$ and results in Equation 1.2:

$$r_{sp} = 0.44 f'_c (d/l) \tag{1.2}$$

Shear failures, by their very nature, tend to be brittle. If this factor is taken into consideration, then the relationship between the dynamically applied pressure of infinite duration required to produce a specified degree of damage and the static resistance is given by the following:

$$p_m/q_y = 1 - \frac{1}{2\mu} \tag{1.3}$$

Where: μ = the ductility factor

p_m = the dynamically applied constant pressure

q_y = the static yield resistance

The ductility factor, that is, the ratio between maximum or, in this case, collapse deflection, and yield deflection for shear failures in reinforced concrete is rather uncertain. However, it was assumed that the ductility factor probably was at least two. Assuming then, that μ is equal to two, Equation 1.2 is reduced by 25 percent and becomes

$$r'_{sp} = 0.33 f'_c (d/l) \tag{1.4}$$

Where: r'_{sp} = the uniform pressure (dynamic).

Equation 1.4 has been plotted in Figure 1.1(a) for a 28-day cylinder strength of 4,000 psi and a span of 72 inches. Equation 1.2 has also been plotted in Figure 1.1(a).

1.3.2 Flexure. The static moment (M) at the center of a simply supported slab of unit width, uniformly loaded at an intensity of r_f is as given by Equation 1.5.

$$M = \frac{1}{8} r_f l^2 \tag{1.5}$$

Thus, there must be equal to the internal resisting moment of the slab which, if under-reinforced, will fail by yielding of the steel. If the moment arm on the cross-section at the center of the slab between the resultant force in the concrete and the resultant force in the steel at yield is taken as 0.9d, then the internal resisting moment for a unit width of slab is

$$M \quad \frac{\phi}{100} \; d \; f_y \; (0.9d) \tag{1.6}$$

Where: ϕ the percentage of flexural reinforcement

f_y - the yield stress in the steel

Equating Equations 1.5 and 1.6 yields an expression for the load required to produce yielding of the steel in terms of the yield stress in the steel, the span, the percentage of flexural steel and the depth.

$$r_f - 0.072 \; f_y \phi \; (d/l)^2 \tag{1.7}$$

Because flexural failures in under-reinforced slabs are usually ductile, the ductility factor is rather large (on the order of about 10) and, as shown in Equation 1.3, the correction for ductility would be so small as to be negligible, in comparison to other uncertainties. Accepting this, the relation given in Equation 1.7 has been plotted in Figure 1.1(b) for an estimated value of f_y of 50,000 psi, for a span of 72 inches and for a range of values of ϕ normally considered in under-reinforced beams.

1.3.3 Diagonal Tension. The design of slabs for diagonal tension was based on an empirical relation developed in Reference 1 and given here as Equation 1.8.

$$r_{sw} = 86.5 \; (d/l)^2 \left(\frac{\phi}{2\phi + \phi'}\right) \left(1 + \frac{2\phi_w \, f_{yw}}{10^5}\right) \sqrt{f'_c \; \phi} \tag{1.8}$$

Where: r_{sw} = the static resistance or failure pressure

ϕ' = the percentage of compression steel

ϕ_w - the percentage of web steel assumed constant over the length of the beam

f_{yw} the yield stress in the web steel

The other terms are as previously defined. If the span is taken as 72 inches, the steel yield stress as 50,000 psi, f'_c as 4,000 psi, ϕ' as zero, and the percentage of flexural steel ϕ is assumed for the time being to be 1, then the above expression reduces to:

$$r_{sw} \quad 0.86 \; \phi^2 \; (1 + \phi_w) \tag{1.9}$$

which, for various values of ϕ_w, has been plotted in Figure 1.1(c). The assumption that ϕ' (the percentage of compression steel reinforcement) is zero is true in this case. For given values of pressures, slab depths, and ϕ, and for a percentage of main tension steel not equal to 1, the value of ϕ_w required to withstand the specified pressure can be found from the correction as indicated in Equation 1.10:

$$\rho_w = \frac{\rho_{w_1}}{\sqrt{\rho}} - 1 \qquad (1.10)$$

Where: ρ_{w_1} = the value given in Figure 1.1(c) for the prescribed depth and pressure as the percentage of web steel consistent with a percentage of tension steel of 1 percent

Figure 1.1(c) includes a line labeled $\rho_w = -0.5$, which is an actual impossibility, but negative values of ρ_{w_1} can be used in the above correction to determine positive values of ρ_w for percentages of flexural steel less than 1. If the final value of ρ_w is negative then, for the given depth and percentage of flexural steel, the beam should not fail in diagonal tension, even with no web steel at the pressure assigned.

Although diagonal tension can bring about brittle failures, particularly in beams without web reinforcement, no correction for ductility factor was applied to Equation 1.8 and 1.9. Rather, the value for r_{gw} found from those expressions was taken as an upper limit of a range of probable failure pressures for which 0.75 r_{sw} (assumed ductility factor of two in Equation 1.3) is the lower limit.

1.4 THEORY: BASIS FOR DESIGN OF TWO-WAY SLABS

The design of the two-way slab test specimens was considerably more complex than was the design of the one-way slab specimens. The principle reason for this increased complexity was the lack of information available on the strength of two-way slabs insofar as it may be controlled by diagonal tension. The information available in this area, even under static loads, is extremely limited and, for dynamic loads, totally nonexistent. Consequently, the design techniques employed in the proportioning of the two-way slabs can be considered, at best, little more than educated guesses. It was recognized that such slabs might fail in either one of the three common modes of failure, that is, flexure, pure shear, or diagonal tension. As in the case of the one-way slabs, most of the two-way slabs were proportioned so that the probable mode of failure would be diagonal tension. The criteria used for the design of these slabs in each of the several modes of failure are developed in the following paragraphs.

1.4.1 Flexure. The design of the slabs for ultimate flexural resistance is based on the yield line theory (Reference 5), which assumes that a square panel simply supported on all four edges and subjected to a uniform load will fail in flexure along two diagonal lines connecting opposite corners of the slab. In other words, the failure cracks would occur on the bottom of the slab dividing the panel into four congruent right triangles whose hypotenuses are the sides of the square panel. Due to symmetry, there will be no shear across a section along either of the diagonal lines so that each triangle may be separated as a free body with a uniform (yield) moment acting along the two cutting planes, a uniform load whose resultant is at the centroid of the triangle, and a distributed support reaction whose resultant acts at the center of the hypotenuse. For equilibrium, the moment per unit of length along the cutting plane can be found as,

$$M = \frac{1}{24} r_f l^2 \qquad (1.11)$$

in which l is the panel side dimension, or span, in either direction. Equating the above expression to Equation 1.6, the internal moment, results in the expression,

$$r_f = 0.216 f_y \rho (d/l) \qquad (1.12)$$

in which ρ now represents the percentage of flexural steel in each direction because it is the same in two perpendicular directions. This indicates that for flexure a two-way slab is three times as strong as a one-way slab having the same percentage of tensile steel. If f_y is 50,000 psi and l is 72 inches, as before, then the values given for ρ or r_f in Figure 1.1(b) can be corrected by a factor of 3.0 to find similar values for two-way slabs. That is, for a given pressure and depth the slab needs only one-third as much steel in each direction as a beam, or for a given depth and percentage of steel, the slab can resist three times as much load as the beam.

1.4.2 Pure Shear and Diagonal Tension. With respect to shear and diagonal tension in the two-way slabs, the simplifying assumption was made that any strip of slab parallel to two of the four sides of the panel could be designed as a beam spanning 72 inches and subjected to a load of just half the pressure acting on the slab. Although this approximation is unconservative for some particular strips, notably those through the center, the absence of precedent for shear reinforcement in slabs and the approximate nature of the design relations used, even for beams, do not justify a more precise determination of the shear conditions within the slab at this time. Consequently, Figures 1.1(a) and 1.1(c) may be used after multiplying the design pressure by one-half.

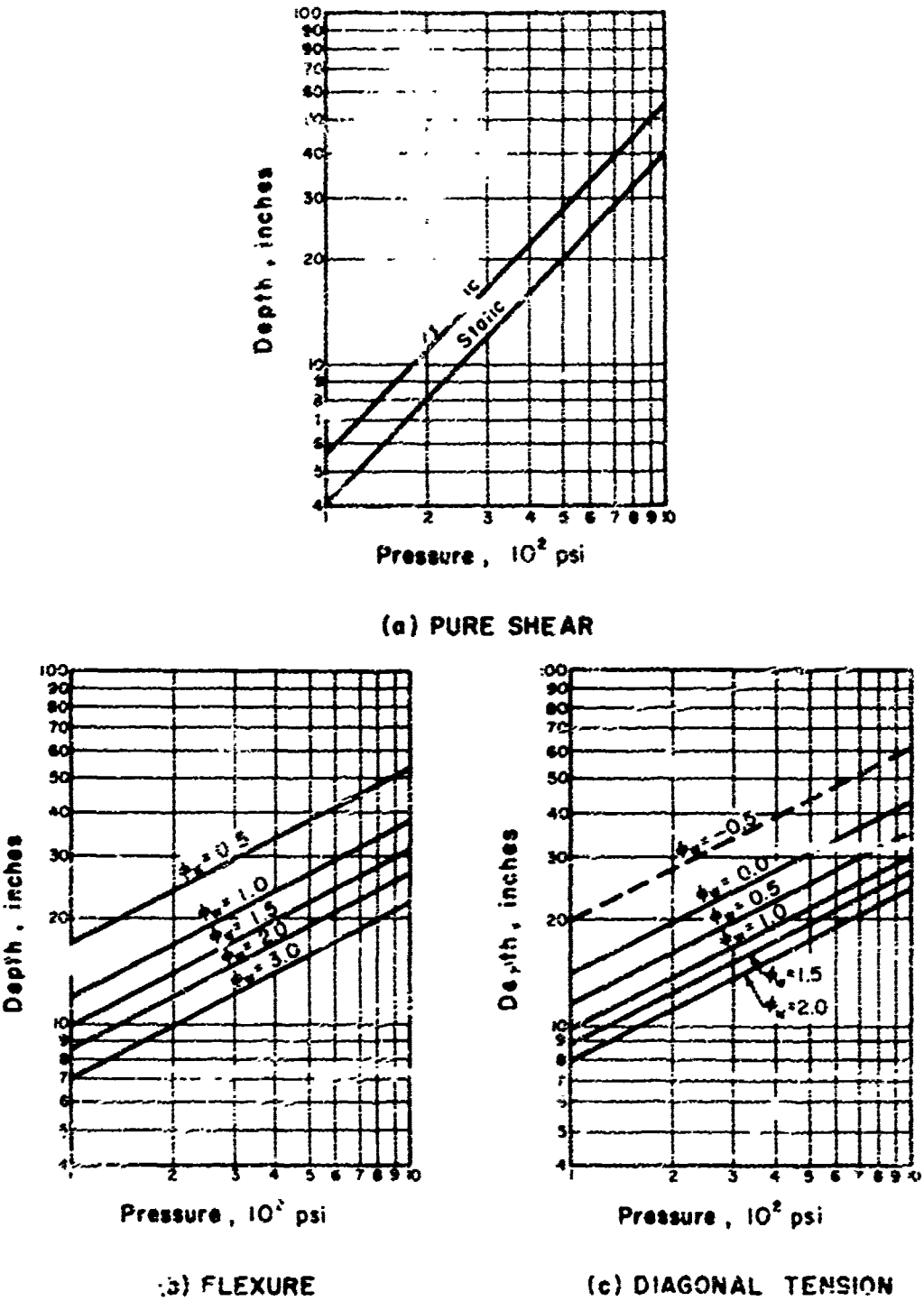

Figure 1.1 Design relations for the predicted modes of failure.

Chapter 2

PROCEDURE

The span lengths and overpressure levels used in these tests were chosen to create conditions for which current design specifications and data are inadequate for reliable use. The uncertainty is greatest in the area of diagonal tension; therefore, the span-to-depth ratios were chosen so as to make this phenomenon critical in most of the slabs. Approximately half the slabs were reinforced for diagonal tension.

The slabs of both types were designed with spans of 6.0 feet with their tops flush with the ground surface so that only the overpressure would act on them.

Because the instrumentation in this project was extremely limited, the information gained from the tests depended primarily upon the differences between those slabs which failed and those which did not. To provide such information, one specimen of each series had to be so weak that it was almost certain to fail, even at the lowest probable pressure, while one other specimen had to be so strong that it would not fail even at the highest probable pressure. Between these extremes, the strengths of the specimens were varied as uniformly as possible by varying depth, flexural reinforcement and shear reinforcement.

Because of the gross lack of data concerning dynamic diagonal-tension strength, an extensive instrumentation program seemed inappropriate. Consequently, the results of these tests are not expected to yield complete design specifications. Rather, it is expected that they will serve only to further limit and define the significance of the numerous parameters affecting the strength of such slabs. It is hoped that the results of these tests will define sufficiently well the significance of the several parameters so that, by means of further studies, definitive design criteria can be determined. Until such time as further studies can be performed, the results of these tests will undoubtedly give to the designer of blast-resistant slabs confidence in excess of that which he now possesses.

2.1 ONE-WAY SLABS

The one-way slabs were designed for peak overpressure levels of 600 and 175 psi, which were originally predicted on the basis of a nuclear device yield of 1.5 Mt to occur at ranges of 1,830 feet and 3,100 feet, respectively, from ground zero. At each of these locations, 15 such slabs were tested. The weakest of these were proportioned so that they should fail at pressures as low as 400 and 150 psi, respectively. The strongest were proportioned so that they should remain unharmed, even though the overpressure levels present at each of the test locations were to reach 800 and 250 psi, respectively. The remaining 13 slabs at each site were proportioned so that they should fail at pressures intermediate between these extremes. At the predicted 600-psi location, the slabs had effective depths which varied from 20 to 56 inches, and, at the predicted 175 psi location, from 11 to 31 inches.

As an illustration of the method used, consider the case of Slab 36-4 which had an assigned effective depth of 36 inches. From Figure 1.1(a), the resistance to shear proper is 650 psi. If 1.6 percent of tensile steel is assigned to this beam, the flexural resistance

is 1,350 psi from Equation 1.7), which is more than adequate. The web reinforcement then must be designed for a pressure consistent with 660 psi. The range of pressures from 600 to 800 psi is therefore considered. Use of the depth of 36 inches and 800 psi in Figure 1.1(c) results in a value of ρ_{w_t} of approximately 0.2. Introduction of this value into Equation 1.10 indicates that, in this instance, no web steel is required to resist a pressure of 800 psi. As indicated in Section 1.3, this represents an upper limit of the probable strength in diagonal tension with the lower limit being equal to 75 percent of 800 psi, or 600 psi.

At each of the two predicted overpressure levels, the slabs were tested in groups having a common depth, the diagonal tensile strength within any given depth group being varied by variation in the percentages of flexural and web steel. These variations were chosen by trial and error within any given group so that the range in diagonal tensile strengths within the group would be wide enough to bracket the probable variations in overpressure which could be expected on the basis of the range of predicted device yield, plus an additional range in strengths to account for the uncertainties in the theory whereby the predicted strengths were determined.

Though most of the slabs were proportioned so that failures should occur as a result of weakness in diagonal tension, it was expected that some of the failures might be of a flexural or pure shear nature, since the basis for ultimate strength computations, particularly under dynamic loads, is admittedly rather uncertain.

2.1.1 Choice of Test Specimens. As indicated previously, 15 test specimens were placed at each of the two nominal overpressure levels of 600 and 175 psi. The slabs were so proportioned that their strengths depended primarily upon their strength in diagonal tension as determined on the basis of the criteria developed in the preceding section. In some instances, the slab strengths in diagonal tension were approximately equal to their strengths in pure shear and/or flexure. The proportions of the one-way slab test specimens, together with their predicted failure overpressure levels in each of the three modes of failure, are summarized in Table 2.1. The revised diagonal tensile strength predictions given therein were made on the assumption that Equation 1.8 was applicable, even though the concrete strengths were considerably in excess of the range of [illegible] which this equation was empirically developed. The revised flexural strength predictions take into account the dynamic yield value of 63 kips per square inch (ksi) determined from the laboratory testing of the slab reinforcing steel. The results of the laboratory testing of the reinforcing steel are given in detail in Section 4.2.1.

2.1.2 Details of Test Specimens. All of the test specimens were designed on the basis of an assumed 28-day cylinder strength of 4,000 psi for the concrete and an assumed dynamic yield stress in the steel of 50,000 psi. The construction contractor was directed to provide concrete with a strength of from 3,500 to 4,500 psi as indicated by three test cylinders taken from each batch, one cylinder of which was to be tested at the Eniwetok Proving Ground (EPG) at the time of the slab tests. The construction contractor was further directed to take all principal reinforcing from the same lot of intermediate-grade billet steel conforming to ASTM Specification A-305. Twenty-four 3-foot lengths of each steel were sent to the Structural Research Laboratory, Department of Civil Engineering, University of Illinois.

The actual sizes and number of bars used and their locations are summarized in Table 2.2 and Figure 2.1. All flexural reinforcing was of No. 6 bars. The error between the area of steel called for in Table 2.1 and the area provided in Table 2.2 is in all cases less

than 5 percent which, considering the degree of approximation thus far employed, did not warrant any adjustment of Table 2.1.

Figures 2.2, 2.3, and 2.4 show the supporting structures for the test slabs. To insure uniform support, the slabs were rested, not on the concrete foundation directly which might be uneven but rather on washers and nuts (Figure 2.4) adjusted to the proper elevation and surrounded by a dry-packed grout covering the entire support area which would conform to any irregularities in either the slab or the support. When set, the grout provided a nearly uniform support. The same threaded rods that supported the slab were extended through holes in the slab and provided with nuts and washers to resist any uplift during the negative pressure phase.

For the experiment to function properly, it was essential that the pressures act only on the top surfaces of the slabs. To this end, the pressure seals shown in Figure 2.4 were designed to seal off the bottoms of the slabs without significantly increasing the resistance of the slabs.

2.2 TWO-WAY SLABS

Ten two-way slabs were designed for test under the higher predicted pressure level of 600 psi. As in the case of the one-way slabs, they were designed so that their strengths appeared to be dependent primarily upon the diagonal tensil strength of the slabs. However, since for two-way slabs there is no information available relative to the ultimate strength of such slabs in diagonal tension under dynamic loads, the predicted strengths may be considerably in error. Consequently, even though the slabs were designed for a nominal pressure of 600 psi, they were proportioned so that at least some usable data would be obtained even though the actual pressures present should depart from this nominal value by as much as ±400 psi. Actually, this wide range of strengths of the two-way slabs was chosen not so much because of uncertainty relative to the pressures that might be expected at the chosen location, although this was certainly a consideration, but rather because of lack of knowledge as to the diagonal tensile strength of two-way slabs.

2.2.1 Choice of Test Specimens. The same parameters which influence the strength of the one-way slabs apply equally well to two-way slabs. In this investigation the strength of the concrete and the strength of the steel were held constant, thereby reducing the important parameters to be considered to these three: d, effective slab depth, ϕ, the percentage of flexural steel; and ϕ_w, the percentage of web reinforcement. As in the case of the one-way slabs, here also several slabs were tested at each of several different depths. For each depth the strength in diagonal tension was varied over a reasonably wide range by varying the percentage of flexural steel and the percentage of web steel. Because the area of uncertainty insofar as the prediction of diagonal tensile strength of two-way slabs is concerned is greater than it was in the case of the one-way slabs, the range of predicted strengths had to be greater in order to give equal assurance of obtaining reasonably good data. Consequently, for each depth of slab, one was designed to fail at a very low pressure, another was designed to fail at a rather high pressure, and the remaining slabs were given reinforcement percentages so that their strengths varied more or less uniformly between these two extremes. The proportions of the two-way slab test specimens together with their predicted failure overpressure levels in each of the three modes of failure are summarized in Table 2.3.

As an example of design, consider Slab 20-4 which has an assigned depth of 20 inches. From Figure 1.1(a) a beam of 20 inches in depth could resist by pure shear a pressure of

370 psi, therefore, the slab can resist 740 psi. If the resistance in flexure is taken as 800 psi, Figure 1.1(b) indicates a percentage of 2.7 flexural steel required for a beam, hence, 0.9 percent will be used in the slab. If, finally, an assumed range for diagonal tension of from 600 to 800 psi is used, then entering Figure 1.1(c) with a depth of 26 inches and a pressure of 400 psi (half the upper limit of 800 psi) results in a required ϕ_w of 0.9 if ϕ were equal to 1. Therefore, the required percentage of web steel is given by Equation 1.10 as 1.0. At this depth, other probable strengths were obtained by varying ϕ and ϕ_w.

2.2.2 Details of Test Specimens. The actual sizes and numbers of bars to be used and their locations are summarized in Table 2.4 and Figure 2.5. Ideally, the shear reinforcement should have been placed so that the effective segments of the bars were vertical when viewed in any section. This would have made the effectiveness of each bar equal in all directions. Unfortunately, bar fabrication and placement restrictions made this impracticable. Therefore, the stirrups were placed as indicated with the realization that the departure from the ideal condition indicated above was small and probably inconsequential.

The slab support details are shown in Figure 2.6. Those remarks given in Section 2.1.2 relative to the strength of the concrete, strength of the steel, and handling of samples of both for the one-way slabs apply also to the two-way slabs.

2.3 FABRICATION OF TEST SPECIMENS

The agency responsible for the construction of the test specimens and supporting structures recommended precasting of the slabs and beams in the U.S. It was felt that closer control of concrete strength could be obtained at a stateside site rather than at the EPG. The specimens were precast at a site in California and shipped by surface transportation to the EPG. Test cylinders for each slab and beam were also provided in order to determine concrete strength on shot day.

The results of the 28-day concrete-strength tests by the contractor were received in the project after the beams and slabs had been delivered to the EPG. The [illegible] revealed that the 28-day strengths exceeded the 4,500-psi upper limit of specified concrete strength by 15 to 20 percent. Because there was not sufficient time remaining to recast all the specimens, it was decided not to recast any. It was felt that any advantage obtained by recasting a few beams or slabs would be offset by the additional variations in concrete properties that would be introduced. A secondary consideration was that a revision of the predicted yield for Shot Koa indicated the probability of higher overpressures at the two stations. It was recognized that if these higher overpressures occurred, the increase in concrete strengths might be advantageous.

The static and dynamic tests of the slab reinforcing steel conducted in the Structural Research Laboratory of the University of Illinois indicated the yield resistance of the reinforcing steel was also considerably higher than anticipated. The revised predicted resistances in pure shear, diagonal tension, and flexure considering the actual steel and concrete strengths are given in Tables 2.1 and 2.3.

2.4 DATA REQUIREMENTS AND INSTRUMENTATION

The minimum data considered necessary for the success of this project included the free-field overpressure at each site and the maximum deflection and mode of failure of each specimen that was damaged. The present lack of knowledge concerning the relative

significance of the several strength parameters made a more comprehensive instrumentation program impractical. The simple instrumentation system used was intended primarily to define the relative significance of the strength parameters—flexure, shear, and diagonal tension.

2.4.1 Free-Field Overpressure. Overpressure measurements were made at each of the two sites by the Ballistic Research Laboratories (BRL) with self-recording pressure-time gages, as described in the Reference 6. These gages were mounted on the supporting structures of the slabs and were designed to measure maximum pressures of 1,000 and 300 psi at the high- and low-pressure stations respectively.

2.4.2 Acceleration. Six self-recording accelerometers were used. Two were placed on the supporting structure of each of the three groups of slabs. These devices were designed to record accelerations up to 150 times that of gravity. It was expected that information obtained from these accelerometers would be of limited value insofar as the analysis and interpretation of the data obtained on this particular project are concerned; however, it was hoped that they would yield additional and much needed information relative to the magnitude of the peak accelerations that the structure experienced.

2.4.3 Permanent Deflections. The response of each slab to the applied loading was determined primarily by deflection measurements. Bolts were cast in the tops of the slabs in a pattern such that their elevations would define the deflected shapes of the slabs. On the one-way slabs, five bolts were equally spaced down the centerline, the end bolts being located over the inside edge of the supports. On the two-way slabs, the bolts were placed in the same manner on both centerlines and on both diagonals. It was possible to measure the elevations of the bolts accurately to within 0.02 inch.

TABLE 2.1 PROPERTIES OF ONE-WAY SLABS

Slab*			Design Predictions of Failure Overpressures			Ultimate Concrete Strength†	Revised Predictions of Failure Overpressures‡		
			Pure Shear	Flexure	Diagonal Tension		Pure Shear	Flexure	Diagonal Tension
	in.	%	psi	psi	psi	psi	psi	psi	psi
Mat'l [illegible], ground range 1,750 ft., predicted pressure 600 psi:									
[illegible]	[illegible]	1.5	373	[illegible]	150 to [illegible]	5,110	[illegible]	[illegible]	[illegible]
24-1	[illegible]	[illegible]	525	[illegible]	300 to [illegible]	4,670	[illegible]	[illegible]	[illegible]
24-2	1.0	0.5	525	[illegible]	[illegible] to [illegible]	4,500	[illegible]	[illegible]	[illegible]
24-3	1.0	1.0	525	[illegible]	[illegible] to [illegible]	4,171	[illegible]	[illegible]	[illegible]
30-1	1.0	[illegible]	660	[illegible]	450 to 650	6,845	1,130	1,130	650 to 950
30-2	1.0	0.5	660	[illegible]	750 to 1,000	7,020	1,160	1,150	1,110 to 1,150
30-3	[illegible]	[illegible]	660	[illegible]	[illegible] to [illegible]	6,722	1,120	[illegible]	[illegible] to [illegible]
30-4	1.0	[illegible]	660	1,320	[illegible] to [illegible]	6,150	1,130	1,130	[illegible] to 1,310
30-5	0.5	0.5	660	450	[illegible] to 750	6,325	1,015	[illegible]	[illegible] to [illegible]
44-1	1.0	[illegible]	880	1,350	750 to 1,000	6,210	1,260	1,650	950 to 1,295
44-2	0.75	1.0	880	[illegible]	1,000 to 1,770	6,205	1,210	[illegible]	1,500 to 2,360
44-3	0.5	[illegible]	[illegible]	950	525 to 700	6,744	1,310	910	700 to 910
44-4	0.25	0.5	[illegible]	340	450 to 600	6,330	1,230	450	600 to 800
36-1	0.5	1.0	1,100	1,100	1,050 to 2,000	6,614	1,420	1,370	2,050 to 3,410
36-2	0.5	[illegible]	1,100	1,100	900 to 1,667	6,586	1,410	1,370	1,150 to 1,510
Mat'l 36,02, ground range 3,150 ft., predicted pressure 175 psi:									
11-1	1.0	1.5	290	130	150 to 200	5,628	280	160	200 to 270
16-1	1.0	0.5	300	170	150 to 200	5,445	420	225	190 to 255
16-2	1.5	[illegible]	300	260	130 to 170	5,605	420	335	145 to 195
16-3	1.5	0.5	300	260	190 to 250	5,535	415	335	[illegible]
21-1	1.0	[illegible]	300	300	170 to 230	6,082	670	345	230 to 305
21-2	1.0	0.5	300	300	250 to 330	6,117	295	295	250 to 470
21-3	0.5	0.5	300	150	170 to 230	6,357	640	155	260 to 345
21-4	0.5	[illegible]	300	150	110 to 150	6,273	610	195	155 to 205
21-5	1.5	[illegible]	300	460	190 to 250	5,821	570	300	260 to 345
21-6	0.75	0.25	300	220	190 to 250	5,651	550	290	235 to 315
26-1	0.75	1.0	480	230	490 to 640	6,688	805	140	675 to 900
26-2	0.5	[illegible]	480	220	190 to 250	5,932	710	295	250 to 395
26-3	1.0	[illegible]	[illegible]	[illegible]	[illegible] to [illegible]	7,[illegible]	[illegible]	[illegible]	[illegible] to [illegible]
31-1	0.5	1.0	570	220	340 to 700	5,917	840	420	340 to 785
31-2	0.5	[illegible]	570	330	240 to 320	6,092	955	420	345 to 460

* Each slab is designated first by its effective depth and then by its code number at that depth.

† Based on concrete strength of 4,000 psi and dynamic yield of 50 ksi for reinforcing steel.

‡ From cylinders tested on shot date.

§ Based on shot date cylinder strengths and dynamic yield value of 65 ksi for reinforcing steel.

TABLE 2.2 DIMENSIONS OF ONE-WAY SLABS.

Slab	b*	Reinforcing Steel: Longitudinal d_1*	No. of Bars	d_2*	No. of Bars	Longitudinal d_3*	No. of Bars	Vertical: Type*	Bar Size	h'*	Spacing
	in	in		in		in			No	in	in
20-1	$22\frac{1}{2}$	21	8	19	8			B	5	21	$5\frac{1}{4}$
28-1	$30\frac{1}{2}$	29	8	27	7						
28-2	$30\frac{1}{2}$	29	8	27	7			A	5	29	$10\frac{1}{4}$
28-3	$30\frac{1}{2}$	29	8	27	7			B	5	29	$7\frac{1}{4}$
36-1	$39\frac{1}{2}$	37	10	35	10						
36-2	$39\frac{1}{2}$	37	10	35	10			A	5	37	$10\frac{1}{4}$
36-3	$39\frac{1}{2}$	37	8	35	7						
36-4	$39\frac{1}{2}$	38	10	36	10	31	9				
36-5	$39\frac{1}{2}$	36	10					A	5	36	$10\frac{1}{4}$
44-1	$47\frac{1}{2}$	46	8	44	8	42	8				
44-2	$47\frac{1}{2}$	45	9	43	9			A	5	45	$5\frac{3}{4}$
44-3	$47\frac{1}{2}$	45	6	43	6						
44-4	$47\frac{1}{2}$	44	6					A	3	44	$9\frac{1}{4}$
56-1	$58\frac{1}{2}$	57	8	55	7			B	5	57	$6\frac{1}{2}$
56-2	$58\frac{1}{2}$	57	8	55	7						
11-1	$12\frac{1}{2}$	11	9					A	5	11	$3\frac{1}{2}$
16-1	$18\frac{1}{2}$	16	9					A	4	16	$6\frac{3}{4}$
16-2	$18\frac{1}{2}$	17	7	15	6						
16-3	$18\frac{1}{2}$	17	7	15	6			A	4	17	$6\frac{3}{4}$
21-1	$23\frac{1}{2}$	22	6	20	5						
21-2	$23\frac{1}{2}$	22	6	20	5			A	4	22	$6\frac{3}{4}$
21-3	$23\frac{1}{2}$	21	6					A	4	21	$6\frac{3}{4}$
21-4	$23\frac{1}{2}$	21	6								
21-5	$23\frac{1}{2}$	22	9	20	8						
	$23\frac{1}{2}$	21	9					A	3	21	$7\frac{1}{4}$
26-1	$28\frac{1}{2}$	27	6	25	5			B	5	27	$7\frac{3}{4}$
26-2	$28\frac{1}{2}$	26	7								
26-3	$28\frac{1}{2}$	27	7	25	7						
31-1	$32\frac{1}{2}$	31	8					B	5	31	$9\frac{1}{4}$
31-2	$32\frac{1}{2}$	31	8								

* see Figure 2.1 for guide to dimensions.

TABLE 2.3 PROPERTIES OF TWO-WAY SLABS

Slab *	p	p'	Design Predictions of Failure Overpressures †			Ultimate Concrete Strength ‡	Revised Predictions of Failure Overpressures §		
			Pure Shear	Flexure	Diagonal Tensile		Pure Shear	Flexure	Diagonal Tensile
	pct	pct	psi	psi	psi	psi	psi	psi	psi
Station 360,91, ground range 1,830 ft., predicted pressure 600 psi:									
10-1	1.5	0	370	300	95 to 130	5,151	475	391	110 to 145
15-1	1.2	1.3	550	600	450 to 600	6,421	885	706	650 to 870
15-2	1.2	0	550	600	170 to 230	5,249	720	706	225 to 300
20-1	0.6	0	740	500	220 to 300	6,485	1,200	630	310 to 415
20-2	0.6	1.0	740	500	470 to 630	6,368	1,180	630	700 to 930
20-3	0.9	0	740	800	300 to 400	6,137	1,190	915	380 to 510
20-4	0.9	1.0	740	800	600 to 800	6,236	1,150	915	850 to 1,130
25-1	0.5	0	930	800	300 to 400	6,946	1,610	825	160 to 615
25-2	0.5	1.8	930	800	660 to 800	5,609	1,365	825	810 to 1,110
30-1	1.0	1.5	1,110	1,000	1,800 to 2,400	6,752	1,870	1,370	2,680 to 3,580

* Each slab is designated first by its effective depth and then by its code number at that depth.
† Based on concrete strength of 4,000 psi, and dynamic yield of 50 ksi for reinforcing steel.
‡ From cylinders tested on shot date.
§ Based on shot date cylinder strengths and dynamic yield value of 63 ksi for reinforcing steel.

TABLE 2.4 DIMENSIONS OF TWO-WAY SLABS

Slab	h *	Reinforcing Steel								
		Longitudinal *				Vertical				
		d_1 *	s *	d_2 *	s *	Bar Size	h' *	a *	l *	l *
	in						in	in	in	in
10-1	12	3								
15-1	17	$15\frac{1}{2}$	$2\frac{1}{2}$			5	$15\frac{1}{2}$	10	[illegible]	5
15-2	17	$15\frac{1}{2}$	$2\frac{1}{2}$							
20-1	22	$20\frac{1}{2}$	$3\frac{3}{4}$							
20-2	22	$20\frac{1}{2}$	$3\frac{3}{4}$			5	$20\frac{1}{2}$	$7\frac{1}{2}$	75	$7\frac{1}{2}$
20-3	22	$20\frac{1}{2}$	$2\frac{1}{2}$							
20-4	22	$20\frac{1}{2}$	$2\frac{1}{2}$			4	$20\frac{1}{2}$	5	75	$7\frac{1}{2}$
25-1	27	$25\frac{1}{2}$	$3\frac{1}{2}$							
25-2	27	$25\frac{1}{2}$	$3\frac{1}{2}$			5	$25\frac{1}{2}$	7	77	$10\frac{1}{2}$
30-1	$32\frac{1}{2}$	$31\frac{1}{4}$	3	$29\frac{1}{2}$	3	5	$29\frac{1}{2}$	4	78	6

* See Figure 2.5 for guide to dimensions. † Both way

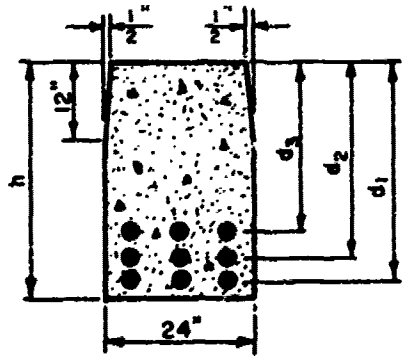

TYPICAL CROSS SECTION

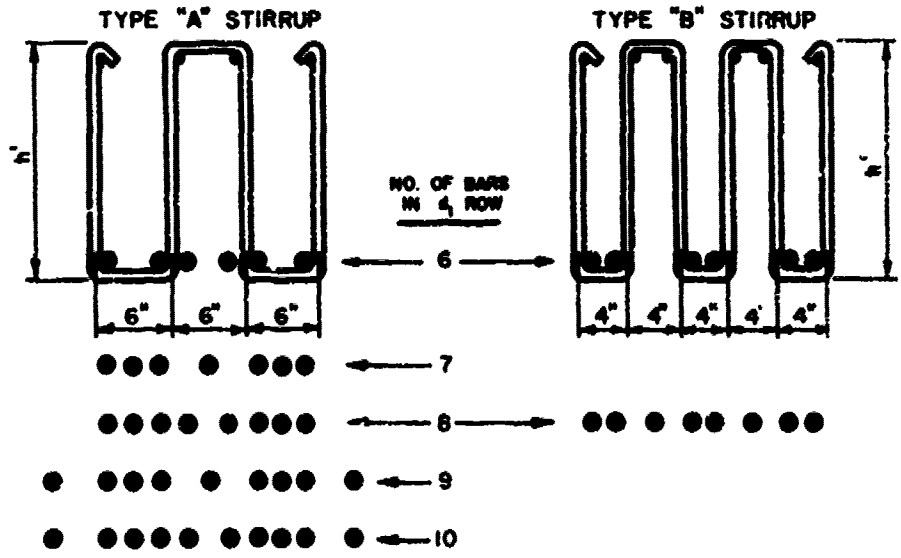

TYPE "A" AND "B" STIRRUPS SHOWING PLACEMENT PATTERNS FOR LONGITUDINAL STEEL

Figure 2.1 One-way slab details.

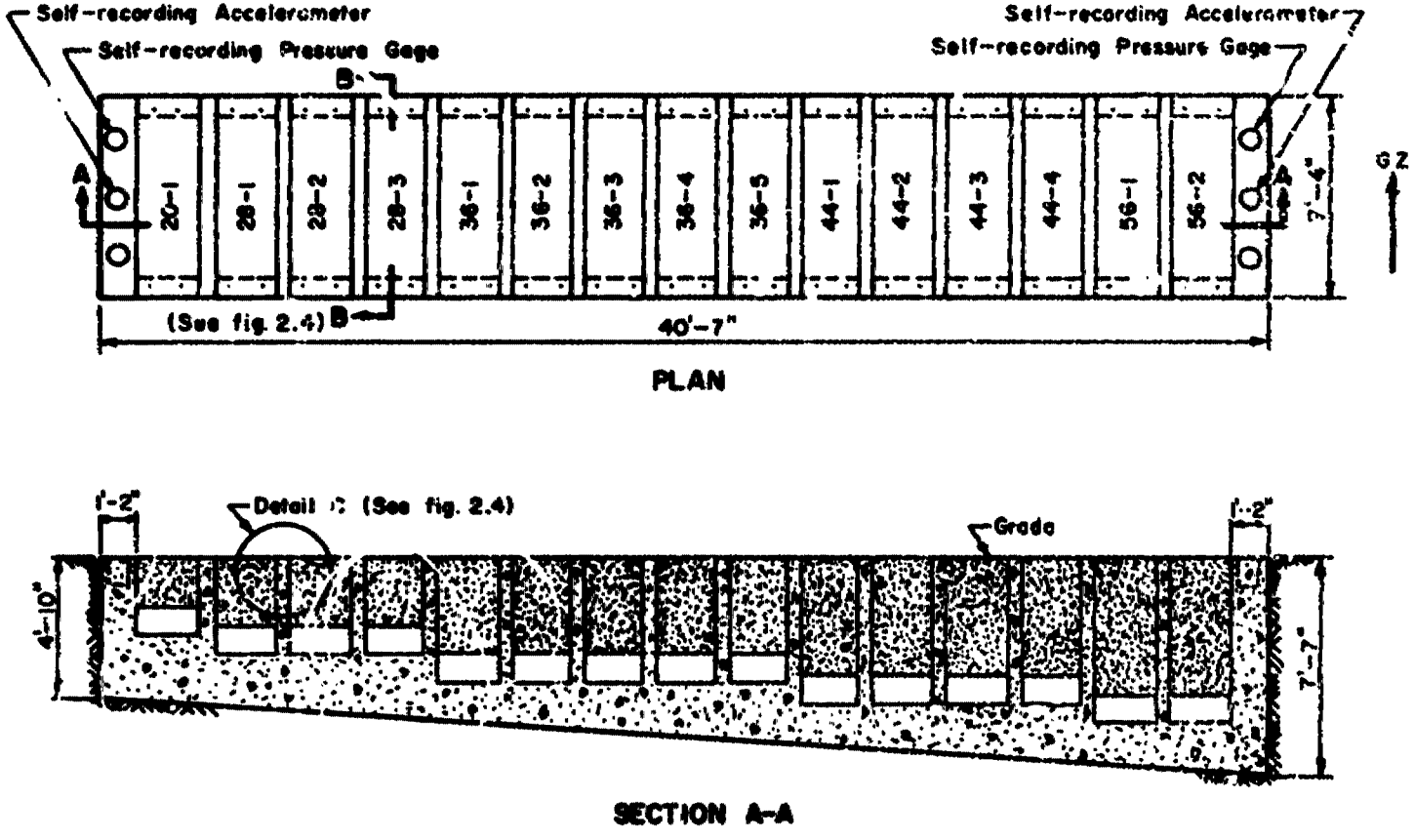

Figure 2.2 One-way slab supports at Station 560.01.

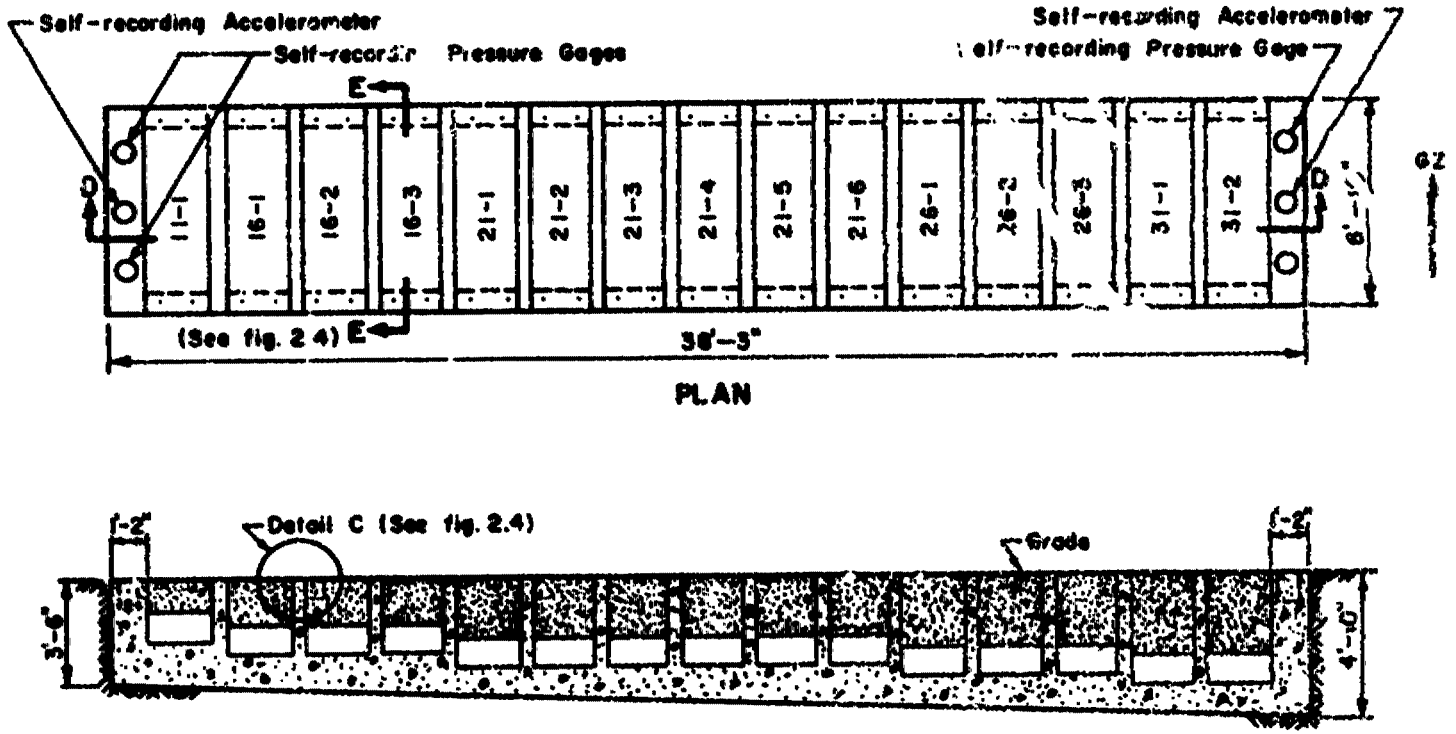

Figure 2.1 One-way slab supports at Station 360.02.

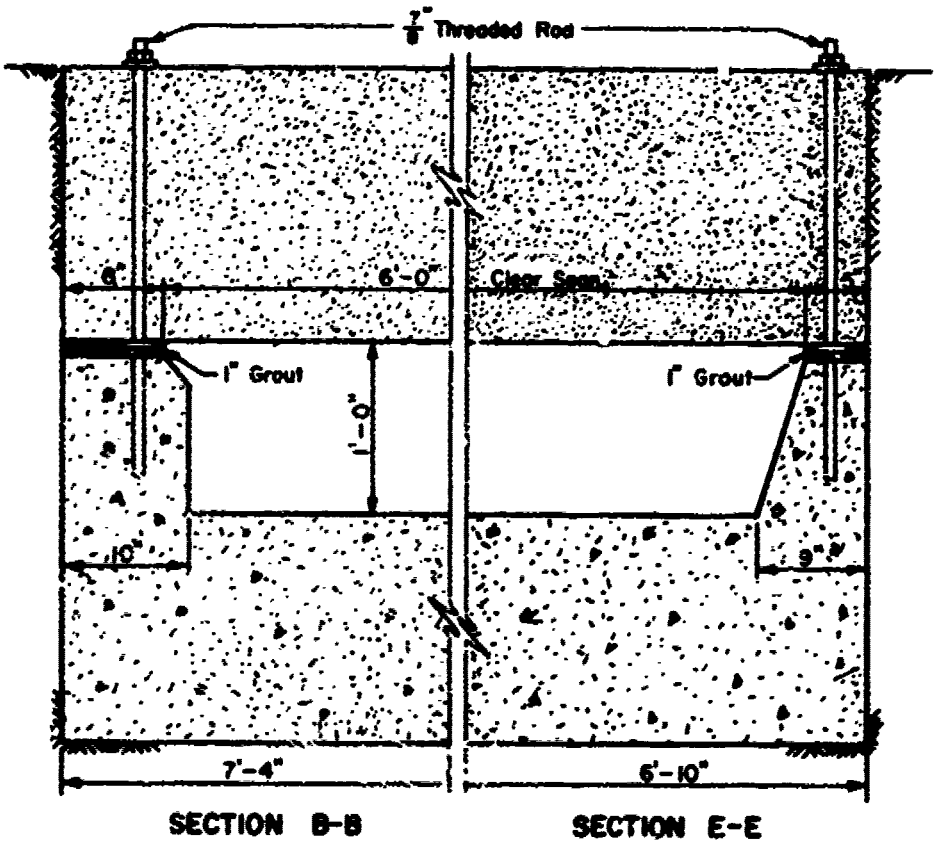

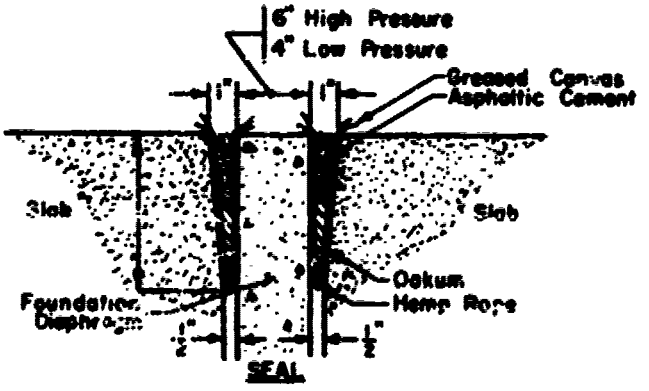

DETAIL C

Figure 2.4 One-way slab support details.

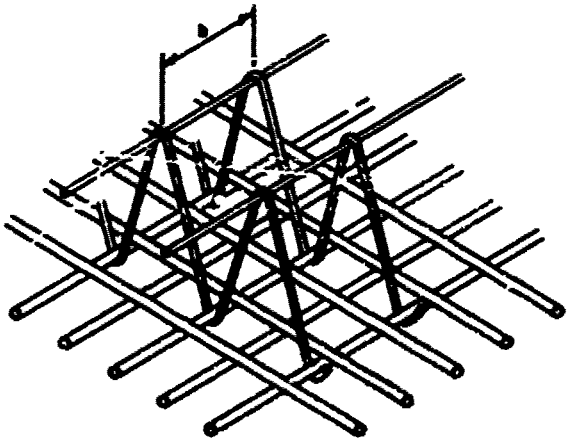

TYPICAL REINFORCEMENT DETAIL

Note: Reinforcement at depth d_2 occurs only on slab 30-1

TYPICAL CROSS SECTION

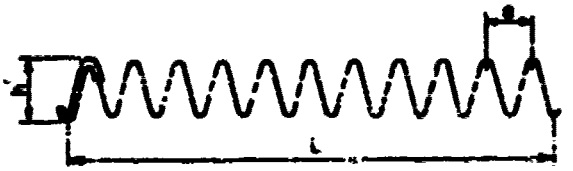

TYPICAL STIRRUP

Figure 2.5 Two-way slab details.

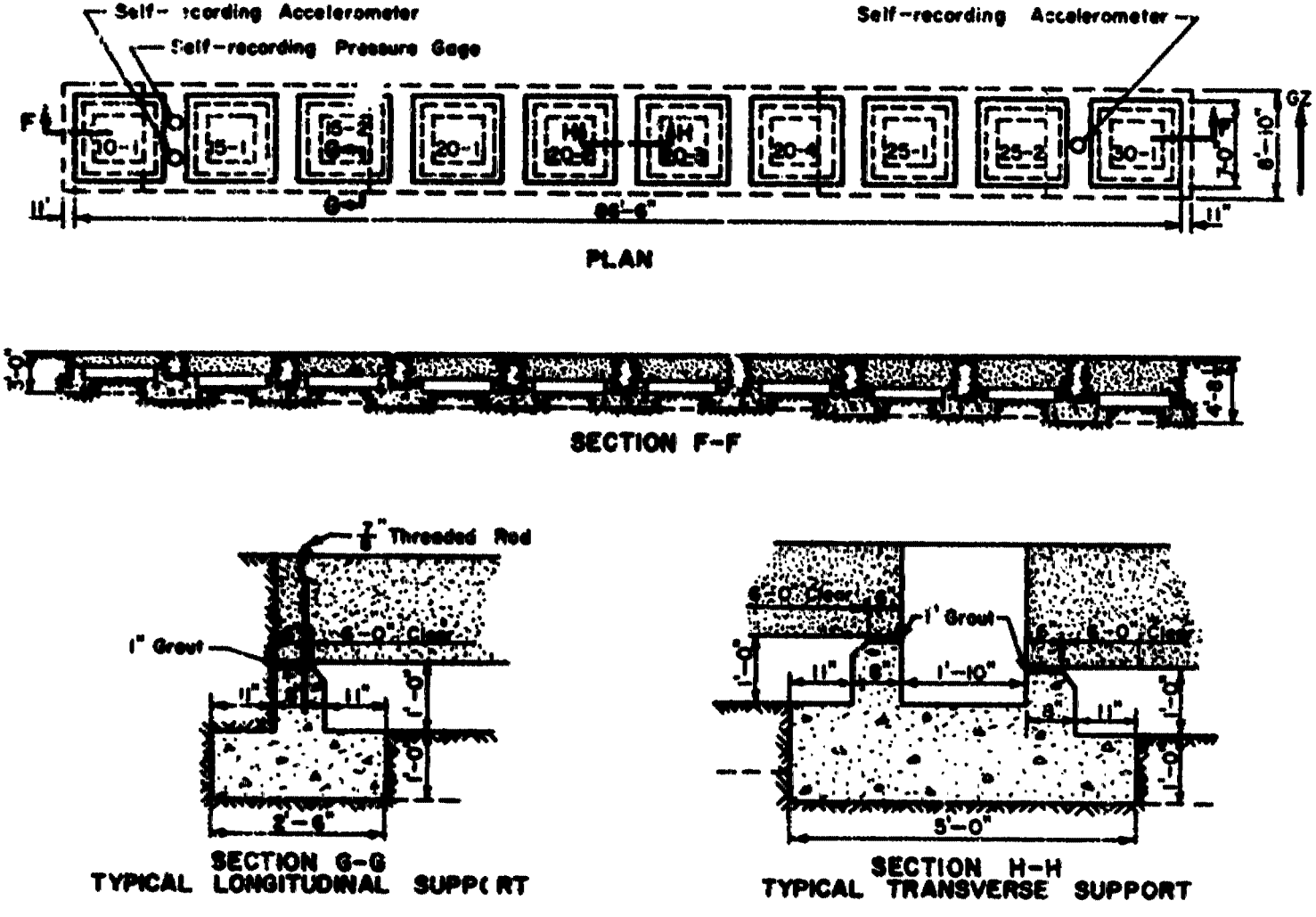

Figure 2.1 Two-way slab supports at Station 360.01.

Chapter 3

RESULTS

3.1 FREE-FIELD MEASUREMENTS

The free-field measurements consisted of surface overpressures at each of the test stations. These were recorded by self-recording gages furnished by BRL. In the test, some of the gage responses exceeded their calibrated ranges and had to be recalibrated before final reduction of the traces. The peak values on some of the records were difficult to identify definitely because of flaking of the recording-mirror surface in the vicinity of the peak value. Fortunately, the record needle scratches could be identified fairly well on the mirror glass itself.

From the three pressure gages installed at Station 360.01, ground range 1,830 feet, only two records were obtained. The other gage could not be found after the test. The pressure-time curves resulting from these records are reproduced in Figures 3.1 and 3.2. In order to rectify the wide variance in the time function evident in these two records, the surface overpressure-time record obtained by the Stanford Research Institute, Project 1.8, at ground range 2,000 feet, was consulted (Reference 7). This record is reproduced in Figure 3.3. It indicates that the pressure-time variation and peak-pressure value of Figure 3.1 is most probable for Station 360.01.

Relatively good records were obtained from all three pressure gages at Station 360.02, ground range 3,100 feet. These records (Figures 3.4, 3.5, and 3.6) indicate peak pressures of 171, 193, and 212 psi. For guidance in selection of a reasonable value of peak pressure for use in the analysis of the results, the surface overpressure-time record at ground range 3,144 feet was obtained (Reference 7). This record is reproduced in Figure 3.7. In spite of greater range, it shows a higher peak (239 psi) than any of the Station 360.02 records. For this reason it was considered that the best peak-pressure value at Station 360.02 was near the highest value for the three records. Therefore a value of 210 psi was selected as the effective peak pressure at Station 360.02.

3.2 SLAB FOUNDATION DISPLACEMENTS

Self-recording accelerometers were installed on the slab-supporting structures at both stations in an effort to obtain information concerning structure motions in high pressure regions. Unfortunately, the gage canisters did not prove to be watertight and the records were ruined. No acceleration data was obtained on this project.

The condition of the site after the test indicated that severe foundation displacements, and therefore, large accelerations occurred during the test. The changes in slab foundation elevations, as determined by posttest surveys, are given in Table 3.1. Inspection of Figure 3.12 indicates the ground displacements under the two-way slabs was not uniform. Slab 20-4, located in the middle of the foundation, was discovered to be about 1 foot below the level of the adjoining slabs. No posttest survey measurements are available for the two-way slabs.

3.3 BEHAVIOR OF SLABS

The preliminary incomplete data gained on the initial reentry indicated that the test specimens sustained only minor damage. Subsequent more complete study of the individual beams and slabs revealed that, while the damage was not severe, it was considerably greater than the earlier results indicated. Removal and inspection of the test specimens showed much more extensive cracking than was in evidence on the tops of specimens as they were viewed in place immediately after test. These more complete results are summarized in Tables 3.2 and 3.3. Supporting the verbal descriptions of the damage given in these tables are numerous photographs of the beams and slabs. Figures 3.8 to 3.14 are photographs of the stations before and after the test. Photographs of the slabs after the test appear as Figures 3.15 through 3.25 and are referenced in Tables 3.2 and 3.3 to the appropriate test specimen. Photographs are presented only when the cracks were sufficiently distinct to warrant it.

The most significant damage was observed in the one-way slabs at a range of 1,830 feet. Of the 15 test specimens, nine exhibited definite permanent evidence of damage. As would be expected on the basis of the predicted failure overpressures shown in Tables 3.2 and 3.3, most of the damage occurred in the form of vertical flexural cracking and diagonal cracking in the slabs. However, the extent of the damage observed was still small in comparison to that which would have been predicted on the basis of the measured overpressure of 1,100 psi.

The one-way slabs at a range of 3,100 feet showed only very slight damage. Since the one-way slabs at a range of 1,830 feet sustained no heavier damage than they did when subjected to a pressure of almost twice the nominal design value, it is not surprising that those at a range of 3,100 feet were virtually undamaged when loaded approximately with their design nominal pressure.

The two-way slabs at a range of 1,830 feet sustained very severe damage. However, the evidence available indicates that this damage resulted from foundation distortions and breakage rather than from applied surface loads. As indicated in Figures 3.11 and 3.12, this entire series of specimens appears to have been subjected to severe fissuring of the supporting subsoil. This contention is supported by the data of Table 3.3 wherein it is noted that the limited amount of damage to individual slabs that was in evidence occurred not on the weakest slabs but rather on those three that were in the area of most severe foundation damage. It is inconceivable that, except as influenced by the foundation distortions just mentioned, Slabs 20-3, 20-4, and 25-1 could have been damaged when Slabs 15-1, 15-2, 20-1, and 20-2 were not.

Because no data was obtained in this test that could be used in evaluating the response of deep two-way slabs to blast loads, no further discussion of the test results is made in this report. The meager static-load-resistance data available was consulted to obtain the expressions for the design of the two-way slabs developed in Chapter 4.

The permanent deflections recorded for each test specimen are also presented in Tables 3.2 and 3.3. The deflections given for the one-way slabs were obtained from post-test surveys performed by Holmes and Narver. Those for the two-way slabs were obtained in the initial reentry recovery effort by reading the center deflection from a straight-edge that spanned between reference points on the edges of the slabs. No permanent deflections were measured on those two-way slabs that sustained the only noticeable damage because, at the time of the initial reentry, they were completely buried in the area of the foundation failure. A change in the schedule of test events so restricted the time available for the final data recovery on this project as to make deflection surveys on these slabs after they were excavated impossible.

Little confidence can be placed in the deflection measurements as reported here. A study of these deflections reveals numerous inconsistencies resulting evidently from the fact that some of the studs installed in the slabs for profile measurements were lost during the test, thereby invalidating a comparison of pretest and posttest survey measurements. However, the deflections were, in general, so small as to be negligible.

TABLE A1 DISPLACEMENTS OF ONE-WAY SLAB FOUNDATIONS

Stud reference studs 1 and 3 are located near the edges of the foundation [illegible] Ranges in the principal foundation displacement. Stud 1 is on the [illegible] Stud 3 on the east side from ground zero. All measurements made in feet.

Reference Point Locations

Station 20+00, Ground Range 1,200 feet					Station 21+00, Ground Range 1,300 feet				
Slab	Stud	Pretest	Posttest	Change	Slab	Stud	[illegible]	[illegible]	[illegible]
[illegible]	[illegible]	11.019	[illegible]	[illegible]	[illegible]	[illegible]	[illegible]	[illegible]	[illegible]
	3	11.033	[illegible]	0.47		[illegible]	[illegible]	[illegible]	[illegible]
[illegible]	1	11.021	[illegible]	6.432	20-1	1	[illegible]	[illegible]	[illegible]
	3	11.023	[illegible]	6.515		3	[illegible]	[illegible]	[illegible]
[illegible]	1	11.025	[illegible]	6.471	20-2	1	[illegible]	[illegible]	[illegible]
	3	11.025	[illegible]	6.577		3	[illegible]	[illegible]	[illegible]
20-3	1	11.021	[illegible]	6.513	20-3	1	[illegible]	[illegible]	[illegible]
	3	11.023	[illegible]	6.589		3	[illegible]	[illegible]	[illegible]
[illegible]	1	11.025	[illegible]	-6.581	21-1	1	[illegible]	[illegible]	[illegible]
	3	11.021	[illegible]	6.633		3	[illegible]	[illegible]	[illegible]
[illegible]	1	11.029	[illegible]	-6.586	21-2	1	[illegible]	[illegible]	[illegible]
	3	11.029	[illegible]	-6.689		3	[illegible]	[illegible]	[illegible]
[illegible]	1	11.033	[illegible]	6.617	21-3	1	[illegible]	[illegible]	[illegible]
	3	11.031	[illegible]	6.728		3	[illegible]	[illegible]	[illegible]
[illegible]	1	11.015	[illegible]	6.660	21-4	1	[illegible]	[illegible]	[illegible]
	3	11.031	[illegible]	-6.802		3	[illegible]	[illegible]	[illegible]
20-5	1	11.025	[illegible]	6.701	21-5	1	[illegible]	[illegible]	[illegible]
	3	11.033	[illegible]	6.770		3	[illegible]	[illegible]	[illegible]
21-1	1	11.025	[illegible]	6.552	21-6	1	[illegible]	[illegible]	[illegible]
	3	11.015	[illegible]	-6.679		3	[illegible]	[illegible]	[illegible]
21-2	1	11.029	[illegible]	-6.594	26-1	1	[illegible]	[illegible]	[illegible]
	3	11.013	[illegible]	6.925		3	[illegible]	[illegible]	[illegible]
21-3	1	11.029	[illegible]	6.431	26-2	1	[illegible]	[illegible]	[illegible]
	3	11.029	[illegible]	6.937		3	[illegible]	[illegible]	[illegible]
[illegible]	1	11.029	[illegible]	6.449	26-3	1	[illegible]	[illegible]	[illegible]
	3	11.037	[illegible]	-6.849		3	[illegible]	[illegible]	[illegible]
26-1	1	11.025	[illegible]	6.922	71-1	1	[illegible]	[illegible]	[illegible]
	3	11.029	[illegible]	7.032		3	[illegible]	[illegible]	[illegible]
[illegible]	1	11.027	[illegible]	6.981	71-2	1	[illegible]	[illegible]	[illegible]
	3	11.035	[illegible]	7.122		3	[illegible]	[illegible]	[illegible]

SECRET

TABLE 3.2 SUMMARY OF TEST RESULTS (CONCRETE SLABS)

Slab*	Peak Pressure Pulse Characteristics			Observed Response	Permanent Deflection
	Overpressure psi	Impulse psi-sec	Diagonal Tension psi		inch
Station 30+00, Ground Range 1,470 feet, Effective Peak Pressure 1,100 psi					
20-1 (3.17)	960	320	660 to 970	Extensive midspan vertical cracking	0.25
20-2 (3.18)	970	660	800 to 1,000	Failure, possible shear failure at central and quarter point supports	0.20
20-3 (3.19)	1,000	640	665 to 965	Midspan vertical cracking, diagonal cracking near supports	0.10
20-4 (3.20)	990	660	800 to 1,000	Midspan vertical cracking, diagonal cracking near supports	0.11
20-5 (3.19)	1,150	1,130	970 to 995	Long curved crack from support region to midspan vertical crack near support	0.01
20-6	1,160	1,130	1,110 to 1,160	None	0
20-7 (3.20)	1,130	970	800 to 990	Long curved crack from support region to midspan	0.05
20-8	1,150	1,070	790 to 1,010	None	0.07
20-9 (3.21)	1,015	370	715 to 965	Midspan vertical cracking, diagonal cracking near supports	0.12
21-1	1,260	1,050	960 to 1,060	None	0.01
21-2	1,230	1,270	1,000 to 2,560	None	0.01
21-3 (3.22)	1,245	850	765 to 940	Midspan vertical cracking	0.02
21-4 (3.23)	1,250	420	600 to 900	Midspan vertical cracking, diagonal cracking near supports	0.07
26-1	1,420	1,370	2,850 to 3,410	None	0
26-2	1,410	1,370	1,130 to 2,510	None	0.03
Station 36+00, Ground Range 3,100 feet, Effective Peak Pressure 210 psi					
11-1	200	160	200 to 270	Light midspan vertical crack	0.02
16-1	110	225	150 to 255	None	0.00
16-2	120	335	145 to 195	None	0.01
16-3	115	235	225 to 315	Light midspan vertical crack	0.03
21-1	670	345	230 to 365	Light vertical cracks at midspan and quarter point.	0.01
21-2	395	285	350 to 470	None	0.01
21-3	640	195	200 to 315	Light vertical cracks at midspan and quarter point	0.03
21-4	610	195	155 to 295	Light vertical cracks at midspan and quarter point	0.05
21-5	550	600	500 to 715	Light vertical crack at midspan on one side only	0.01
21-6	530	290	235 to 315	Light vertical crack at midspan on one side only	0
26-1	990	440	675 to 900	None	0.02
26-2	710	295	230 to 365	None	0
26-3	625	390	365 to 405	None	0.02
31-1	810	420	740 to 995	Possible vertical crack at midspan on one side only	0
31-2	645	420	345 to 460	None	0

* Numbers in parenthesis refer to Figure Numbers.
Refer to Table 2.1.
† Measure relative to line between supports. Positive deflections are downward.

TABLE 2.5 SUMMARY OF TEST RESULTS ON TWO-WAY SLABS

Slab [illegible], ground range [illegible] feet, effective peak pressure, [illegible] psi.

Slab*	Revised Predicted Failure Overpressures†			Observed Damage	Permanent Center Deflection
	Pure Shear	Flexure	Diagonal Tension		
	psi	psi	psi		inches
10-1	875	294	140 to 145	Slab could not be found	—
15-1	[illegible]	706	650 to 670	None	0
15-2	720	706	225 to 280	None	1/32
20-1	1,250	625	[illegible] to 715	None	1/32
20-2	1,150	630	490 to 520	None	1/16
20-3	1,150	945	500 to 510	Roughly circular crack pattern on bottom	—
20-4 (8.24)	1,150	945	850 to 1,120	Straight line cracks running in both principal directions visible on bottom	—
25-1 (8.25)	1,610	925	460 to 615	Cracks visible in bottom near supports, curved cracks near one corner on sides	—
25-2	1,295	825	440 to 1,110	None	1/32
30-1	1,870	2,370	2,680 to 3,580	None	1/8

* Numbers in parentheses refer to figure numbers.

† Refer to Table 2.3.

‡ Permanent deflections relative to line between supports. Data from initial reentry straight-edge measurements. Positive deflections are downward.

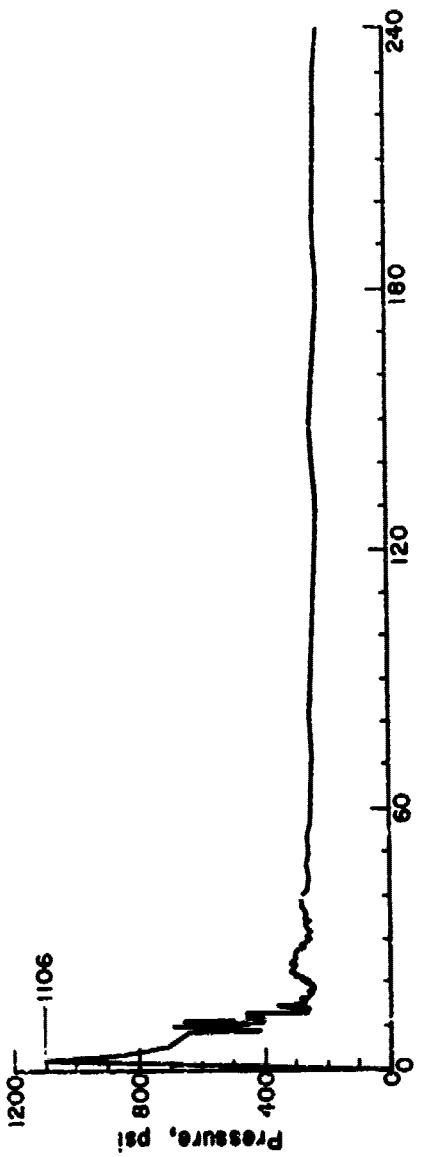

Figure 3.1 Pressure-time record 360.01 A at Station 360.01.

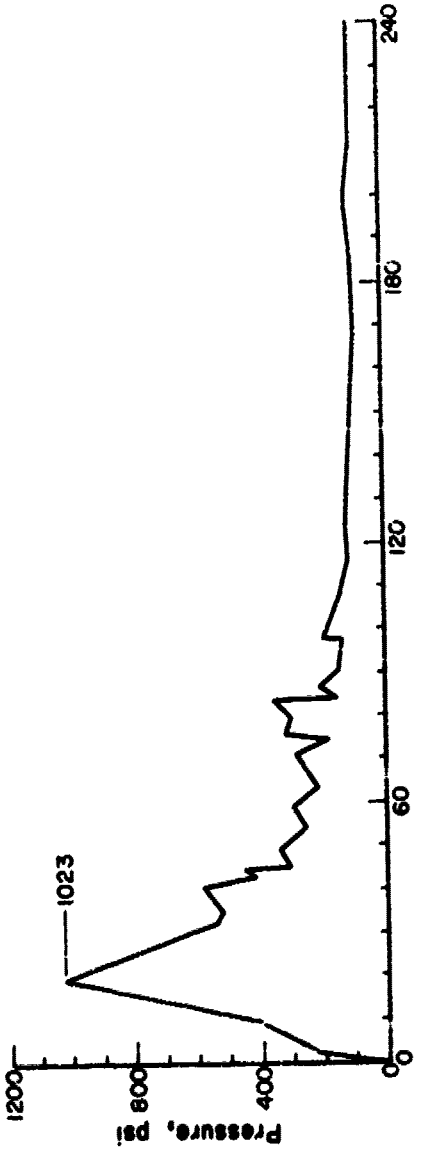

Figure 3.2 Pressure-time record 360.01 B at Station 360.01.

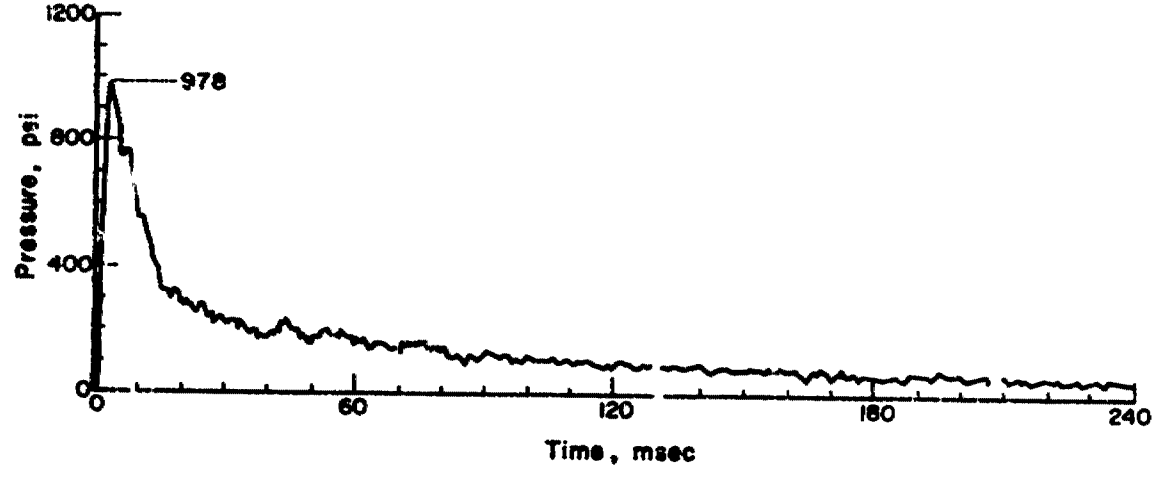

Figure 3.3 Pressure-time record 11 B at Station 180.01.

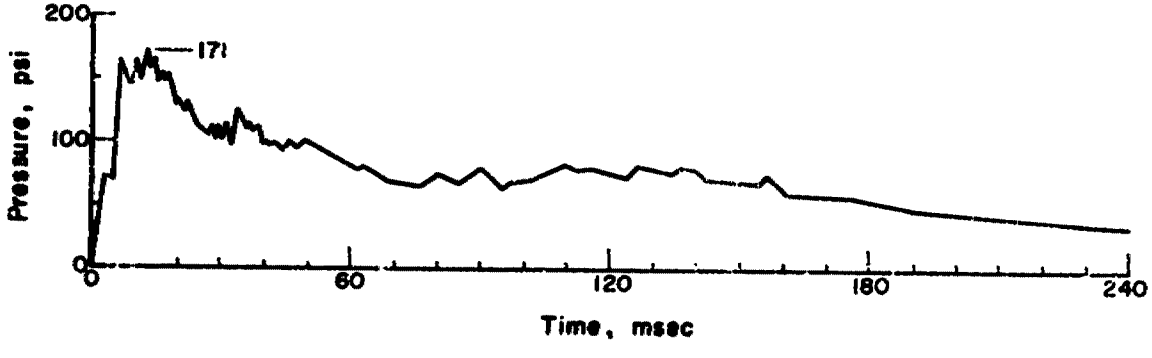

Figure 3.4 Pressure-time record 360.02 A at Station 360.02.

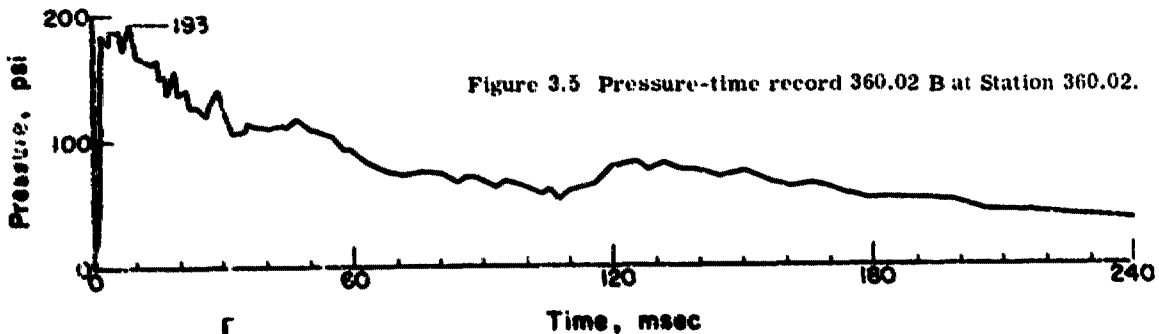

Figure 3.5 Pressure-time record 360.02 B at Station 360.02.

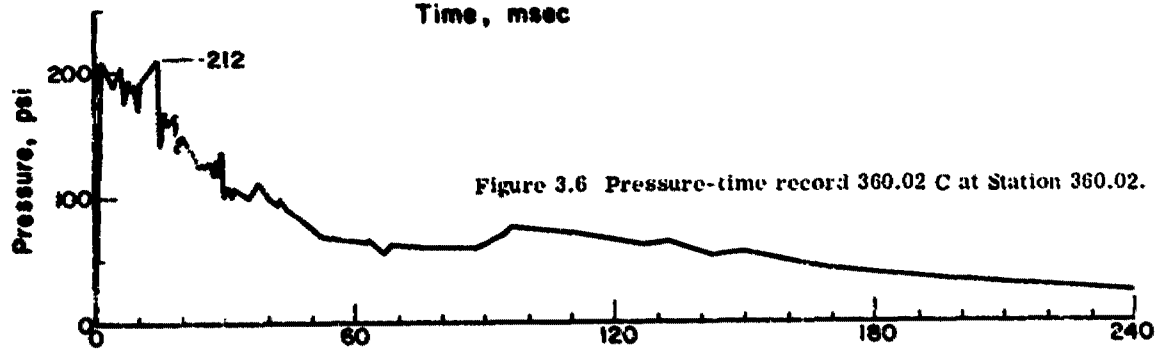

Figure 3.6 Pressure-time record 360.02 C at Station 360.02.

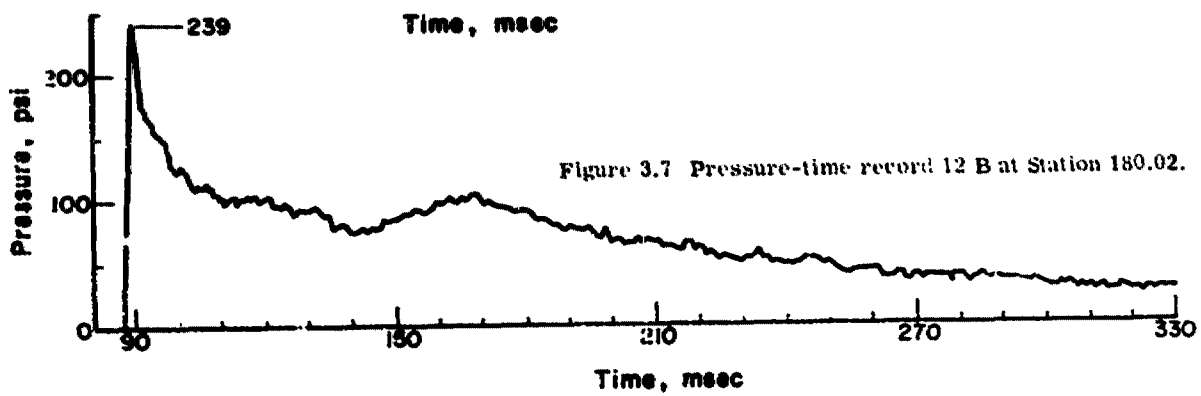

Figure 3.7 Pressure-time record 12 B at Station 180.02.

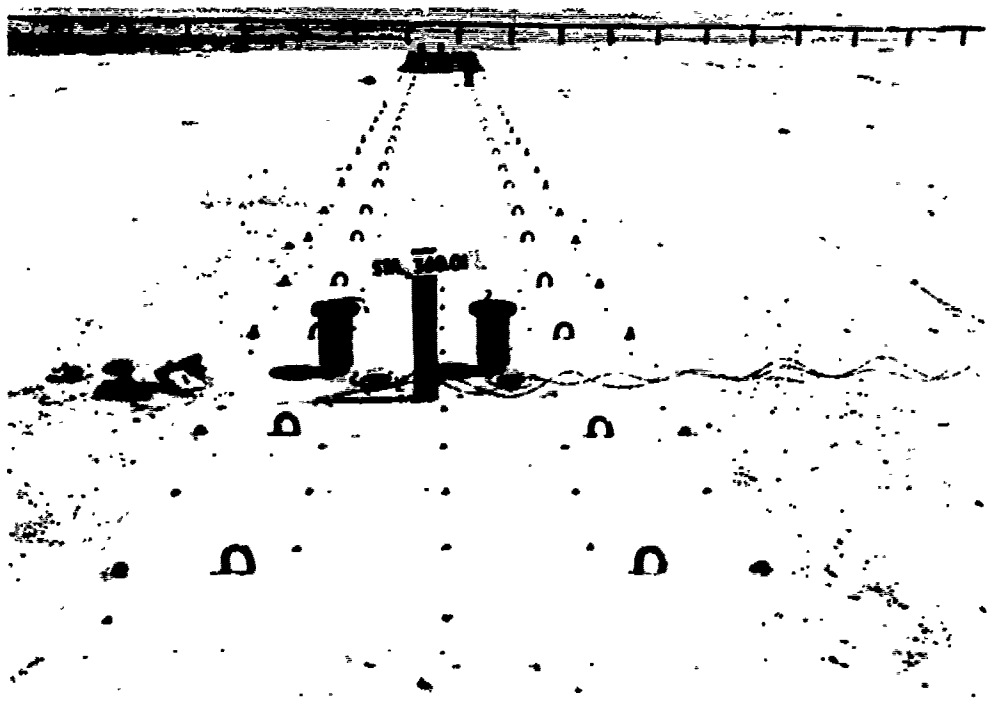

Figure 3.8 Pretest view of slabs at Station 360.01, range 1,830 feet. Two-way slabs are in foreground. One-way slabs are in background. Pressure gages and accelerometers are ready for installation flush with top of slabs. Ground zero is to the left.

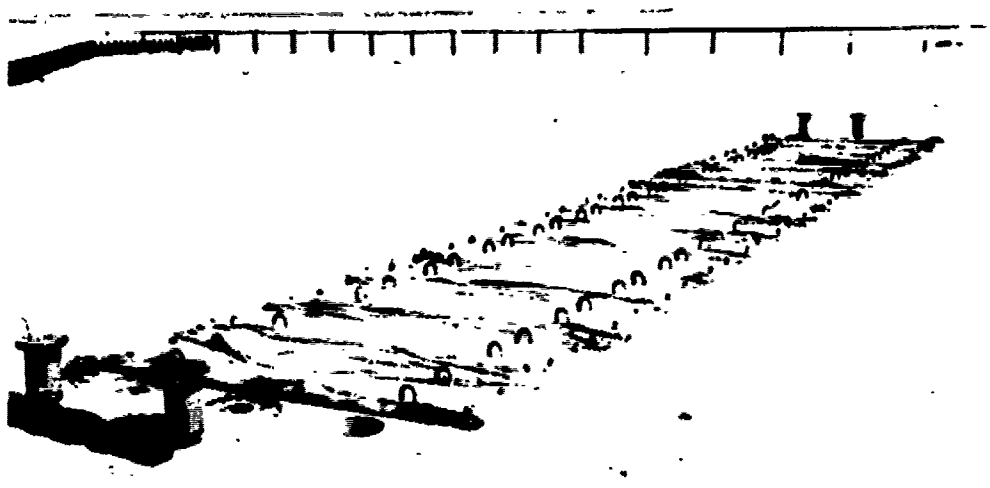

Figure 3.9 Pretest view of one-way slabs at Station 360.01, range 1,830 feet. Ground zero is to the left.

Figure 3.10 Pretest view of one-way slabs at Station 360.02, range 3,100 feet. Ground zero is to the left.

Figure 3.11 Posttest overall view of slabs at Station 360.01, range 1,830 feet. Note edge of crater adjacent to one-way slabs in rear. Ground zero is to the left.

Figure 3.12 Posttest view of two-way slabs at Station 360.01, range 1,830 feet, looking away from ground zero, showing evidence of foundation failure.

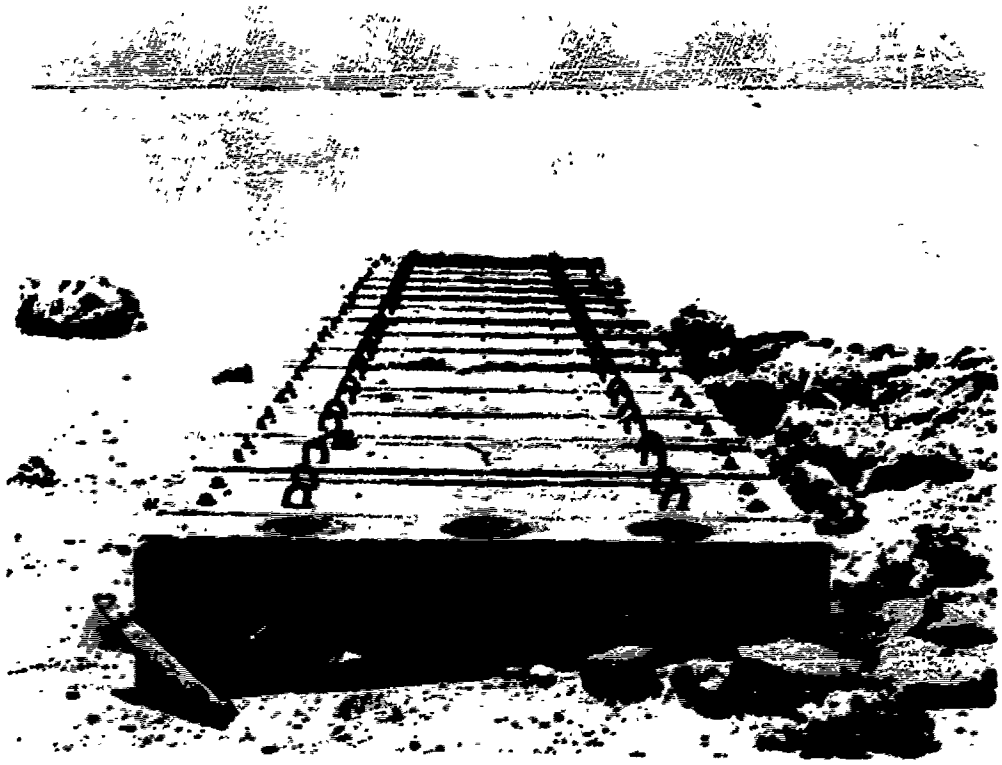

Figure 3.13 Posttest view of one-way slabs at Station 360.01, range 1,830 feet. Ground zero is to the left.

Figure 3.14 Posttest view of one-way slabs at Station 360.01, range 1,830 feet, looking at ground zero side of slabs.

Figure 3.1. Posttest side view of Beam 20-1. Beam is standing on end: top is at the right. Note flexural cracks near center of span.

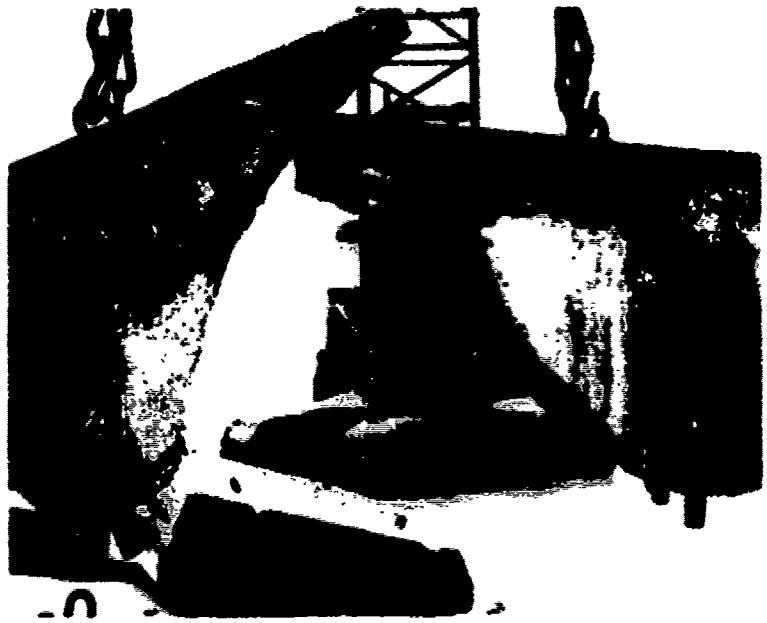

Figure 3.16 Posttest side view of Beam 28-1. Note complete failure, and that the tensile steel broke completely away from the upper portion of the slab.

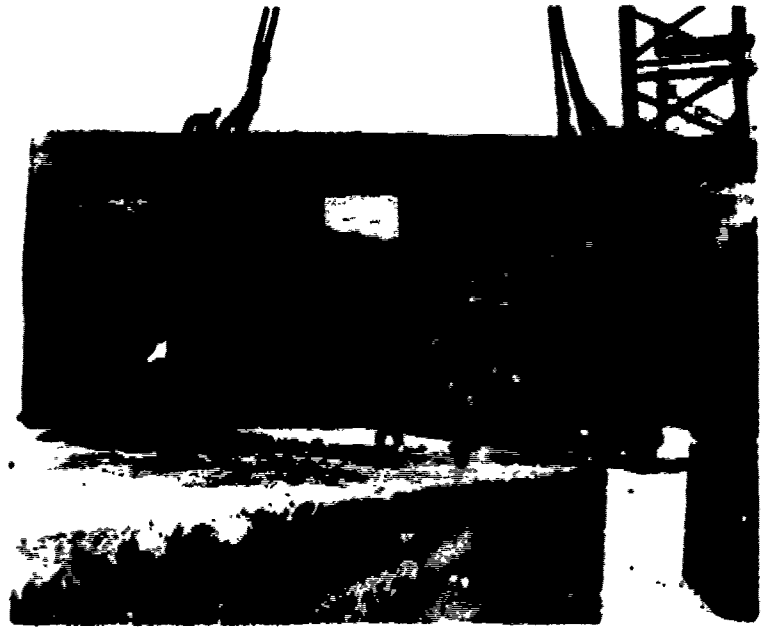

Figure 3.17 Posttest side view of Beam 28-2. Note flexural and diagonal tensile cracks.

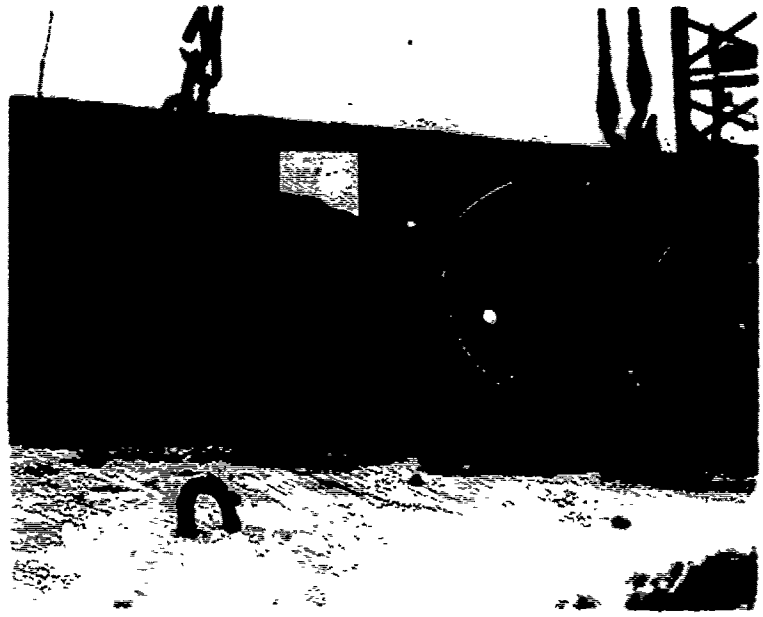

Figure 3.18 Posttest side view of Beam 28-2. Note flexural and diagonal tensile cracks.

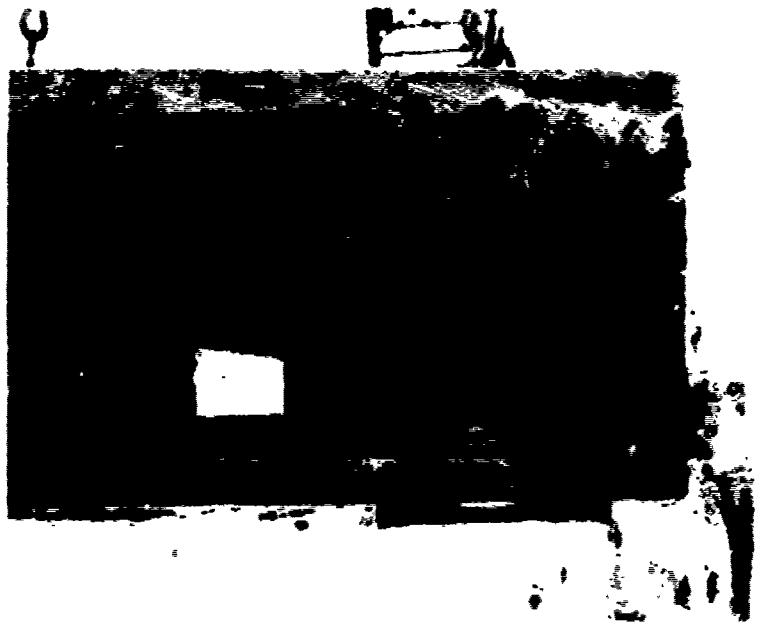

Figure 3.19 Posttest side view of Beam 36-1. Note distinct diagonal tensile crack.

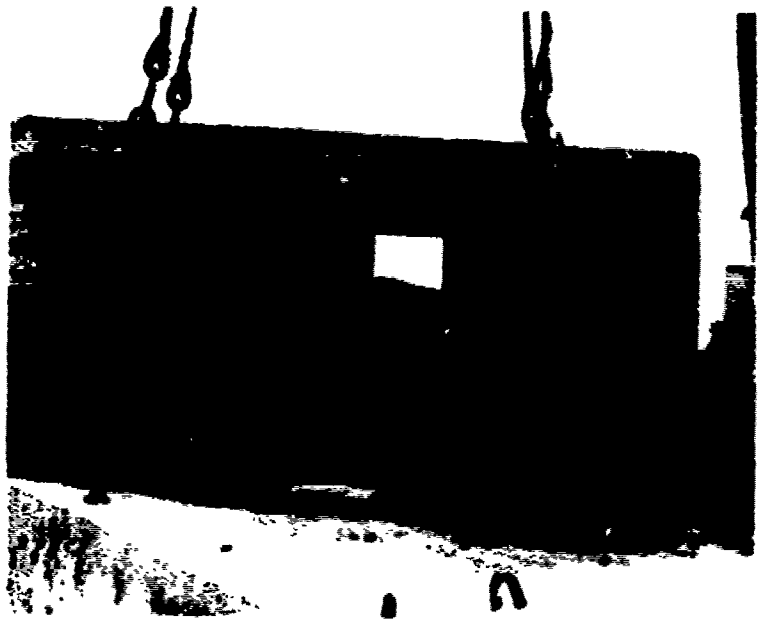

Figure 3.20 Posttest side view of Beam 36-3. Note diagonal tensile crack.

Figure 3.21 Posttest side view of Beam 36-5. Note flexural and diagonal tensile crack patterns.

Figure 3.22 Posttest side view of Beam 44-3. Note small midspan flexural crack.

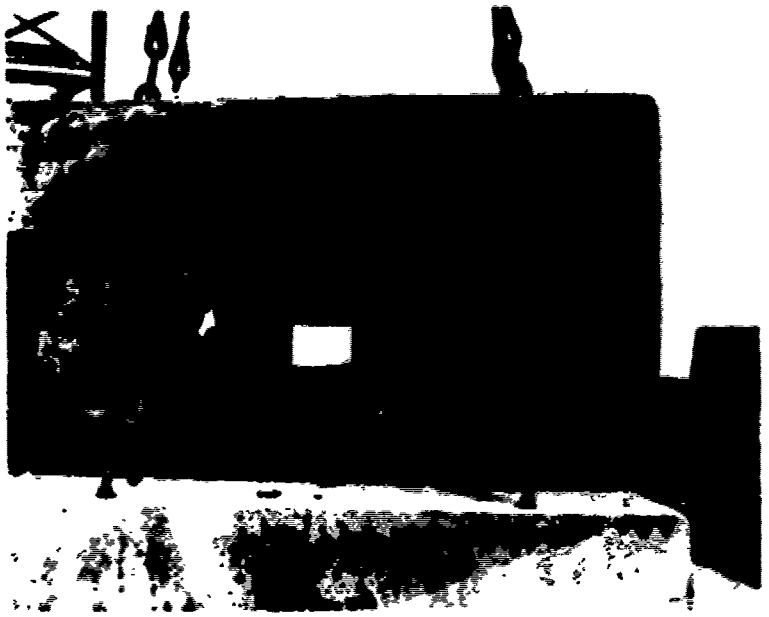

Figure 3.2.. Posttest side view of Beam 44-4. Note flexural cracking near center. Fine but distinct diagonal tensile crack is not visible in photograph.

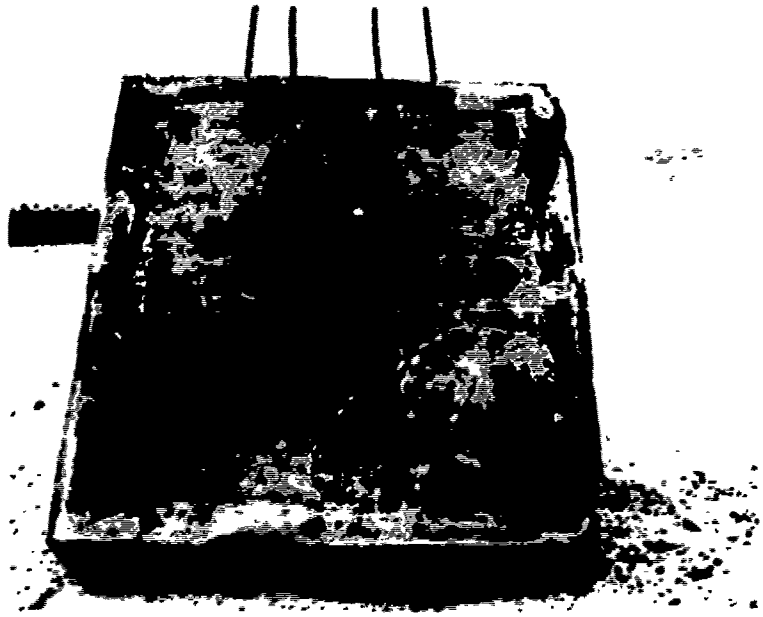

Figure 4.24 Posttest bottom view of Slab 20-4. Note cracking in both principal directions.

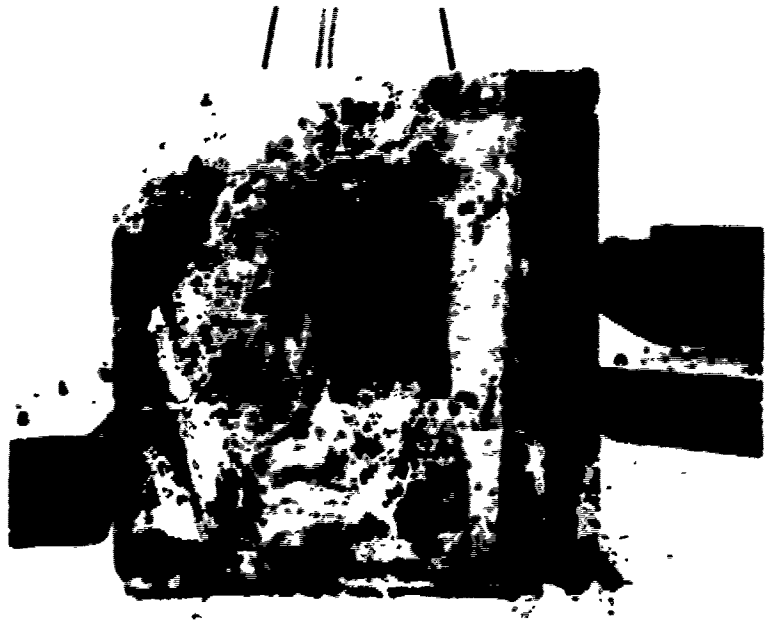

Figure 4.25 Posttest bottom view of Slab 25-1. Note extensive cracking in upper left corner; also parallel to right edge.

Chapter 4

DISCUSSION

4.1 STATIC BEHAVIOR OF DEEP ONE-WAY SLABS

4.1.1 Introduction. As indicated in Section 1.2, the design of reinforced-concrete beams and one-way slabs is based on empirical data obtained from tests of beams of normal proportions. Very few static tests have been conducted of beams with span-to-depth ratios as low as those of this series. Consequently, relatively little is known about the behavior of such members under static, much less dynamic, loading conditions. Thus, before taking up the response of deep members to dynamic loads, it is necessary to summarize what is known now about their behavior under static loads.

A thorough review of the literature pertaining to the behavior of deep structural members subjected to static loads has been published in References 2 and 8. The results of this survey can be summarized best by quoting from Reference 8. Figure 2.1 mentioned in the quotation is included as Figure 4.1 in this report.

> It has been found both theoretically and experimentally that the distributions of normal and shearing stresses in a typical very-deep beam depart radically from those given by the formulas of the ordinary theory of flexure for shallow members. The reason for the difference in stress distributions lies primarily in the fact that the vertical normal stresses, particularly those due to concentrated loads, and the shearing stresses are much larger than those in beams of ordinary depths and they produce a major effect on the state of stress and deformations throughout the whole beam.
>
> The rapid increase of load, bearing stresses, and shearing stresses with respect to flexural stresses as the depth of the beam is increased is demonstrated in Figure 2.1, in which are shown three simply supported reinforced-concrete beams with equal spans but different depths, acted upon by a uniform load of such magnitude as to produce constant maximum nominal flexural stresses assuming a fully cracked section and linear distribution of horizontal strains. The beams have one percent tensile reinforcement. It can be seen that the load and the bearing pressures increase in proportion to the square of the depth, and the maximum average shearing stress increases in direct proportion to the depth for constant steel and concrete flexural stresses, which in this case are taken as $f_s = 40{,}000$ psi and $f_c = 2{,}400$ psi.

Although no theoretical solutions considering the true properties (i.e., anisotropy, nonhomogeneity, etc.) of reinforced-concrete beams have ever been published, the simple considerations in the previous paragraph do predict qualitatively the change in behavior that takes place as a beam of a given span is increased in depth. Most obviously, the beam will support a greater load with increasing depth before failing and secondly, the mode of failure changes. These two predictions are confirmed by test data. Further, it is well known that the distribution of stresses in the vicinity of a concentrated load is different from those assumed (and computed) from the ordinary theory of flexure. In beams of

normal (l/d approximately 10 or more) dimensions, this departure is not significant, usually, and is often ignored. This is justified in most cases by St. Venant's principle. However, in the case of deep members, the span-depth relationship and the size of the area on which the boundary forces act are such that this departure cannot be ignored. This is illustrated in Figure 4.2 which shows qualitatively the trajectories of the principal stresses (tension and compression) in two simply supported beams of different span-depth ratios.

It is apparent that the change in the directions of the principal stress trajectories, occurring as the member becomes deeper, is gradual. Theoretical solutions indicate that the ordinary theory of flexure predicts the horizontal normal stresses at midspan of a simply supported, uniformly loaded rectangular beam reasonably well for span-depth ratios as small as 2.0. This is also predicted roughly by St. Venant's principle.

From a consideration of the changing pattern of principal stress trajectories, it might be expected that the response of the member changes from that of a beam to that of an arch as the span-depth ratio decreases. This predicted change in behavior has been confirmed by experiment, also.

4.1.2 Recent Tests. There have been two important series of tests subjecting prismatic beams of various span-depth ratios to uniformly distributed loads (References 2 and 9). Other tests of reinforced-concrete beams under uniformly distributed loads include tests of I-beams (References 10 and 11), which are not strictly comparable.

In Reference 9, tests of 18 prismatic, simply supported beams are reported. The loads were applied by 10 hydraulic jacks simulating a uniformly distributed load. The span-depth ratios for these beams varied from 15.49 to 6.07. As stated by the authors of that report, the general purpose of the investigation was to explore the behavior and strength in shear, i.e. shear-compression, of simply supported beams under uniform load. All were reinforced in tension only, without web reinforcement. The variables included span, steel percentage, and concrete strength. The objectives of the tests were divided into two groups:

1. A study of the behavior, up to failure by: (a) observation of the development of cracks; (b) investigation of the transition between shear and flexural failures; and (c) derivation of empirical equations for shear strength of such members.

2. An attempt to improve insight into the general problem of shear in reinforced concrete by: (a) determining from the measurement of strains in the steel the influence of diagonal-tension cracking on the distribution of stresses in the reinforcement; and (b) obtaining some indication of the actual strain distribution in the concrete, above and below the main diagonal-tension crack.

The results of these tests are summarized in Table 4.1. Note that a definite effort was made to obtain shear failures. This was accomplished by use of high-strength steels (in those beams with low steel percentages) and high steel percentages. The modes of failure observed were shear-compression and flexure. There were no diagonal-tension or shear-splitting failures, which frequently occur in beams subjected to concentrated loads. (See Section 4.1.4 for detailed discussion of modes of failure.)

It is believed that this can be explained adequately for shallower beams by consideration of the combined stress conditions in the concrete above the neutral axis. This matter will be discussed in detail later.

Tests of 14 prismatic beams under uniform static load were reported in Reference 2. The span-depth ratios of these members ranged from 7.2 to 1.5, concrete strengths from 2.14 ksi to 5.61 ksi, and the steel percentages from 1.00 to 2.20.

As stated by the authors, their investigation was exploratory in nature and covered a wide range of variables. No single phase of the problem was investigated comprehensively and few definite conclusions were drawn. However the tests do give insight into the behavior of deep beams.

The results are summarized in Table 4.2. Of the total, six beams failed in bearing, seven in flexure, and one failed in bearing and anchorage (shear splitting of concrete on a horizontal section above the tension steel at the support).

4.1.3 Behavior Under Uniform Load. There are similarities in the behavior of simply supported beams subjected to uniform load regardless of span-depth ratio. The development of flexure cracks with increasing load causes the usual redistribution of stresses, tension being transferred from the concrete to the steel. These flexural cracks start as vertical cracks at the bottom of the beam and remain vertical near midspan as they extend upward with increasing load. However, because of the pattern of principal stresses in the beam, cracks closer to the support start to bend over after reaching the level of the reinforcement.

The vertical cracks near midspan develop rapidly at first, but at a later stage, their progression almost stops and the inclined cracks develop more rapidly.

As noted in Reference 9 the existence of inclined cracks changes the behavior of the beam between the limits of the crack (Figure 4.3). Between the point at which the inclined crack crosses the reinforcement and the point at which the crack crosses the neutral axis of the beam, the stress in the tension steel must be constant as may be seen in Figure 4.3c. Between Sections A and B, the member is behaving as a tied arch. That is, because there can be no forces acting on the crack, the force in the steel (T) at Section A must be equal to the force in the steel at Section B. These stress conditions are exactly those in the tension tie of a tied arch; the stress in the tie is constant, regardless of the value of the applied moment at the section at which moments are taken.

After the crack rises above the neutral axis, between Sections B and C, the behavior of the member is a composite of arch and beam action. The stress in the steel increases with distance from the support but not linearly with increasing moment as required for purely flexural response. The increase in stress in the steel is due to the existence of a compressive force in the concrete below the crack. The existence of this compressive force has been established experimentally by means of strain gage measurements (Reference 9). Considering the equilibrium of the portion of the beam bounded by the inclined crack and section C, it was reasoned in Reference 9 that some force must act to counterbalance the moment exerted by the compression force C_2. The only internal force that could act on the body to resist the moment C_2d_2 is a shear force in the reinforcing steel, designated by V_2. It was then reasoned that a vertical force is now required to balance V_2 and this is evidently a shear force acting downward in the concrete below the crack at Section C. Thus, by statics

$$T_2 = C_2, \quad T_1 = \quad \text{and} \quad V = V_1 + V_2$$

Further, it was noted that if there is a limit on the shear V_2 that can be transferred by dowel action from the steel to the concrete, a limit is thus placed on the value of the compression force C_2. This accounts for the fact that the compressive strains below the diagonal tension crack remained practically constant after the development of the crack (Reference 9).

The existence of a compressive strain below the inclined crack was confirmed independently by others (Reference 12). Several reinforced concrete beams were tested

under concentrated loads to determine the validity of the usual assumptions that longitudinal reinforcement does not transmit vertical shear across an inclined crack and that the maximum compressive strain within the shear span (the portion of the beam from the support to the applied load) is developed at the extreme fiber. In Reference 12 it was concluded that the maximum compressive strains in the concrete occurred some distance below the extreme fiber (in the shear span) and that the longitudinal reinforcement carried considerable vertical shear across the crack at loads less than the ultimate.

Beyond the end of the crack, at Section C, the stress in the steel is proportional to the moment.

However, for members deeper than those reported in Reference 9, the inclined cracks from each support reach almost to midspan, while the slope of the crack is still steep. In some of the tests reported in Reference 2 these cracks crossed so that there was no portion of the member which exhibited beam properties. There is, probably, no portion of the very deep members in which composite beam-arch action occurs, because the neutral axis does not exist in the normal sense in these members. The only section at which the trajectories of principal tensile and compressive stresses are parallel is at midspan.

In shallower members under uniformly distributed load the crack rises steeply until it penetrates into the compression zone where it flattens, progressing toward midspan at a decreasing slope until it stops at a distance of approximately *l*/3 from the supports (Reference 9). This behavior may be explained by consideration of the combined stress conditions in the concrete. Noting that strain measurements in the steel indicate that the redistribution of stress in the steel, caused by the formation of the crack, is limited to the portion of the beam between the ends of the crack, it may be assumed that the crack is progressing into an area in the concrete where the stress distribution is unaffected by the existence of the crack.

If the extreme fiber stress in the concrete ahead of the crack is less than approximately 0.80 f'_c, the stress block may be assumed to be triangular. This is certainly justified for high strength concrete in which the stress-strain relationship is very nearly linear up to this point. With this assumption it is possible to arrive at the combined stress conditions in the concrete in compression as a function of the height above the neutral axis and distance from the support for a given load intensity, as shown in Appendix A.

The distribution of both shearing stresses and vertical normal stresses is uniquely determined by the horizontal normal stress distribution. For a simply supported beam subjected to uniformly distributed load with a triangular stress block in the compression zone, the variation of shearing stresses and vertical normal stresses with depth are as shown in Figure 4.4. Assuming that the crack is formed wherever the tensile stress (t) exceeds some limiting value, it is apparent that the crack will stop before it reaches the top of the beam. As it rises the shear stress decreases and the principal tensile stress approaches 0.

If a diagonal-tension failure is defined as one in which the inclined crack progresses to the top surface of the beam, resulting in a very sudden failure, it may be concluded that such a failure cannot occur in a simply supported rectangular beam subjected to uniformly distributed load. Such failures may be possible, however, in continuous beams and frames because the shear stress may be very high at a point of inflection where the horizontal normal stress is zero.

4.1.4 Summary of Resistance Criteria. In view of the preceding discussion, and References 2 and 9, it is concluded that the possible modes of failure of simply supported, prismatic members subjected to uniformly distributed static loads are: flexure, shear-compression, shear-anchorage, bond, and bearing.

Flexure. The yield and ultimate moments of such members with span-depth ratios from 1.64 to 15.47 may be predicted reasonably well by the standard expressions summarized in Reference 2:

$$M_y = f_y A_s jd \tag{4.1}$$

and

$$M_u = f_s A_s d (1 - k_2 k_u) \tag{4.2}$$

Where: M_y = yield-resisting moment

f_y = yield stress of the tensile reinforcement

A_s = area of the tensile reinforcement

jd = moment arm of the internal resisting couple as defined by the elastic theory of reinforced concrete behavior

M_u = ultimate resisting moment

f_s = stress in the tensile reinforcement at the strain corresponding to crushing of the concrete in compression

d = effective depth of the concrete

k_2 = coefficient expressing the location of the resultant compressive force as defined by the ultimate strength theory of reinforced concrete behavior

k_u = coefficient expressing the depth of the compression zone in the concrete at ultimate moment as defined by the ultimate strength theory $\left(k_u = \frac{\epsilon_u}{\epsilon_s + \epsilon_u}\right)$

None of the members with span-depth ratios of less than 2.32 failed in flexure, so the applicability of the expression for ultimate moment to such members has not been confirmed. On the average, the ultimate moments achieved in the test series (Reference 2) were somewhat higher than those computed by the above expression. It appears, therefore, that the expression is conservative when applied to deep beams but accurate enough to be useful.

Shear-Compression. A shear-compression failure is defined as one in which the concrete above the diagonal tension crack (and generally in the vicinity of the end of the crack) fails before failure occurs anywhere else, e.g., concrete crushes at midspan in flexure or at the support in bearing. Such a failure is generally more brittle than a flexural failure. The conditions for a shear-compression failure were stated by Reference 9 as follows: (1) Diagonal tension cracks must develop. This is a requirement for shear-compression failure but does not constitute failure of the beam. (2) The stresses induced by the bending moment in the reduced compression area above one of the diagonal tension cracks must cause failure by destruction of the concrete in that region.

The latter statement is not meant to imply that the area above the crack alone resists the entire compressive component of the bending couple (Figure 4.3). However, the existence of the crack obviates the necessity for the development of the ultimate stress block over the full depth of the compression concrete.

It would appear then that further conditions might be placed on shear-compression failures. The first of these is that the member must have a defined neutral axis. This

implies that the span-depth ratio must be greater than 2.0. As previously indicated in Figure 4.2, the trajectories of the principal tensile and compressive stresses are not parallel members with span-depth ratios less than 2.0. Thus the crack never crosses a defined neutral axis. Accepting the empirical determination that the critical section for a shear-compression failure is at $l/3$ (where l is the clear span); the location of the critical section must be in the portion of the beam at which the principal tensile and compressive stresses are parallel. This implies that the span-depth ratio must be equal to or greater than 3.

In Reference 2 it was noted that inclined cracks formed in the deep members at loads of about 35 to 55 percent of the yield load, and also, that using the expression developed in Reference 9, the shear-compression strengths of the beams tested were all greater than the theoretical ultimate flexural strengths. Reference 9 states: "It may also be noted in Table 5-9 that the maximum midspan moments developed in beams A-3, A-3-1, A-4, and A-6 exceeded the theoretical ultimate midspan moments, M's, for shear-compression failure. There is not enough data to determine whether an equation of the type of Equation (5-3) would apply to deep beams."

In view of the preceding considerations, it might be concluded that shear-compression failures as defined are not possible in members with span-depth ratios less than about 3.0, or, if possible, are hardly distinguishable from flexural failures. Further, although its applicability is in question, for lack of a better expression, the expression developed in Reference 9 should be used for members with span-depth ratios of 3 or greater. This expression is

$$M's = 1.52\, bd^2 f'_c\, k\, (0.57 - \frac{0.045\, f'_c}{1000}) \qquad (4.3)$$

Shear-Anchorage. A shear-anchorage failure is characterized by shear splitting of the concrete along a horizontal plane just above the level of the tensile steel over the supports. The concrete above the failure surface moves laterally away from midspan with respect to the concrete below the failure surfaces. This type of failure appears to be a direct shear failure.

In Reference 2 the following empirical expression was developed as a boundary between safe and failure regions as shown in Figure 4.5 (Figure 5-72 of Reference 2)

$$\frac{v_u}{f'_c} = 0.25 + \frac{f_{ba}}{10^4} \qquad (4.4)$$

Where: v_u - ultimate average shearing stress on the failure plane

f'_c = standard cylinder strength of the concrete

f_{ba} = average bearing stress at the failure plane

To use the above equation it is necessary to compute an anchorage shearing stress. Assuming that yield of the steel is defined as failure;

$$v_a = \frac{f_y A_s}{b\,(c + 0.5d')} \qquad (4.5)$$

Where: $(f_y A_s)$ - the total tensile force in the steel

$b\,(c + 0.5d')$ the nominal area of the concrete just above the level of the steel

That is, c = support width along the longitudinal axis of the member and d' is the distance from the top of the steel to the bottom of the beam. This formula is based on

the assumption that the inclined crack starts at the edge of the support and has a rise of twice the horizontal run.

The value thus obtained is compared with the value for v_u obtained by means of Equation 4.4. If it is greater than that obtained by Equation 4.4, the member will fail in shear anchorage before the tensile steel yields.

Bond. None of the members reported in Reference 2 appeared to have failed in bond, although the average bond stresses, u_a, at failure for all members even without special anchorage were extraordinarily high, ranging from 0.19 f'_c to 0.74f'_c. The authors of that report believe that this may be explained by two factors: high compressive stresses normal to the steel in the vicinity of the supports, and restraint against expansion provided by the bearing plates.

A nominal value of the average bond stresses at the anchorage may be computed as follows:

$$u_a \quad \frac{f_s A_s}{\Sigma_o \, l} \tag{4.6}$$

Where: $f_s A_s$ - the total tensile force in the steel

Σ_o = the total perimeter of the reinforcing steel

l = the length of embedment. For deep beams l may be taken as approximately equal to c, the support width.

This formula may be used in a manner similar to Equation 4.4, assuming some limiting value such as

$$u_u - 0.30 \, f'_c$$

However, there have been no adequate theoretical or empirical investigations upon which to base an anchorage bond criterion for deep members.

Bearing. It has been noted (Reference 8) that bearing failures have been common in tests of deep reinforced concrete members. The results of previous work on the bearing strength of such members is summarized in Section 5.6.1 of Reference 2 and an analysis of additional tests is presented in Paragraph 5.6.2 of the same reference.

Three end conditions were used in the tests of Reference 2: plain ends; ends with side plates clamped on to prevent lateral expansion; and ends with vertical reinforcing to help carry the reaction. The results of the tests on members with plain ends confirmed results obtained previously in Reference 13; that is, bearing failures occurred at average bearing stresses of 0.84 to 1.0 f'_c, or, about 0.91 f'_c.

However, as reported in Reference 2, others obtained bearing failures with lower average bearing stresses; one series at 0.76 f'_c and another at stresses on the order of one-half the cylinder strength. The latter were explained as follows: "Breton suggests that the low bearing strength developed in his beams was due to the arrangement of the longitudinal reinforcement which was bent sharply at both ends through an angle of 90° and extended vertically to the top."

That explanation may be perfectly valid, but it is well to remember that unless the supports are on rockers, the flexural deformation of the members will result in stress concentrations at the inside edges of the supports which might well reduce the average bearing stress required for failure. In the tests of Project 3.6, the supports were not free to rotate with the member.

The results of the tests of members with plates clamped on the sides indicate that this restraint increased the bearing capacity by about 40 percent to 1.28 f'_c which also, is in good agreement with previous test results.

As stated in Reference 2, the Portland Cement Association (PCA) manual (Reference 14) suggests that the bearing capacity of a deep beam may be increased by the use of vertical reinforcement at the supports. This was confirmed, but there was considerable scatter in the data. In two of four specimens, the introduction of vertical reinforcement did not appear to raise the bearing strength at all. In the other two, the vertical steel had an appreciable effect on the bearing capacity. No detailed explanation of this difference in behavior was offered.

Increases in bearing capacities of approximately 50 percent were obtained by means of cagelike local reinforcement to restrain the transverse expansion of the concrete (Reference 13). Further, the bearing capacities of wide beams or one-way slabs should be appreciably greater than those of narrow members because of the lateral restraint provided by the concrete itself.

In view of these considerations conservative values for the average bearing failure stresses under static load may be defined as

Plain ends	f_b	$0.76\ f'_c$	
Clamped ends	f_b	$1.06\ f'_c$	(4.7)
Cage reinforced	f_b	$1.11\ f'_c$	

4.1.5 Yield Load-Deflection Relationship. The deflection of a shallow beam under uniformly distributed load at initial yielding of the reinforcing steel may be predicted reasonably well by the expression (Reference 2)

$$\delta_y = \frac{5}{48} \frac{\epsilon_y l^2}{(1-k)\,d} \tag{4.8}$$

Where: δ_y = the deflection at midspan

ϵ_y = strain at which the reinforcing steel yields

$k = \sqrt{2pn + \overline{pn}^2} - pn$

d = the effective depth of the member

Equation 4.8 is based on the following assumptions (Reference 2): (1) the variation of curvature along the length of the beam is parabolic; (2) the concrete is assumed to be elastic but unable to resist tension; (3) the maximum curvature (at midspan) is assumed to be equal to the initial steel yield strain divided by the distance from the centroid of the steel area to the neutral axis, as in the ordinary theory of flexure; and (4) shear distortions and vertical deformations are neglected (i.e., a plane section before bending is a plane section after bending).

When the problem of predicting the deflections of a deep member is considered, two basic defects in the ordinary method of computation of beam deflection become apparent. First, in a beam of homogeneous material, as the span-depth ratio decreases, the effects of vertical and shearing stresses on deformation cease to be negligible. Second, a reinforced-concrete beam is far from homogeneous; therefore, serious difficulties arise in selecting appropriate values for properties of the section (such as moment of inertia and area effective in resisting shear) to use in equations for deflections. Thus, even if consideration is given to deformation produced by shear stresses and vertical stresses, equations for the deflection so developed are of doubtful reliability.

Fortunately, at the time of preparation of this report, the first extensive series of laboratory tests of deep reinforced-concrete members was under way at the University

of Illinois Reference 2). The load-deflection measurements made in this work provided an opportunity to evaluate existing deflection equations, and to develop expressions which would predict the observed results.

The deflections at yield of the beams in the C and D series tested as described in Reference 2 were compared with the deflections computed for these beams under the same load using ordinary flexural theory. The assumptions made in the computations are indicated in Figure 4.6 and the results of the comparison are tabulated in Table 4.3. It is evident that this method of computation is considerably in error except for the shallowest beam with $l/d = 6$. For the deeper members actual deflection can be as much as twice that calculated by flexural theory.

A study of the steel strains measured in the laboratory tests of the deep beams indicated that the beams responded as tied arches, even for loads well below yield. Arch action is indicated when the distribution of steel strain is more nearly uniform than parabolic. As a result of these observations, a semirational expression was developed based on arch-type response (Figure 4.7). The test results were used to evaluate various constants in the expression. The equation which expresses center deflection at the top of the member is;

$$\delta_c = \frac{M_c}{\frac{1}{4} A_s E_s \alpha} \left(\frac{l}{d}\right)^2 \qquad (4.9)$$

Where: δ_c = center deflection in inches

M_c = moment at the center, inch-pounds

A_s = area of the tensile steel, inches

E_s = modulus of elasticity of tensile steel, lb/in

α = a constant proportion of the depth

l = span of the member, inches

d = depth of the member, inches

The derivation of Equation 4.9 does not take into consideration the deflection due to compressive deformation caused by vertical stresses in the concrete between the supports and the center of the member at the top; that is, the compressive deformation in the rib of the arch. However, as shown subsequently, this deformation is accounted for empirically in the determination of the value of the constant α.

An expression for α was developed consistent with the properties of the members and the measured load-deflection history. It appears to be a function of the span-depth ratio and the steel percentage, primarily. There was no discernible effect of concrete strength over a range of strength from 2,500 to 6,500 psi. The resulting expression for α is:

$$\alpha = \frac{-0.01 (l/d)^2 + 0.22 l/d + 0.17}{\phi^{\frac{1}{4}}} \qquad (4.10)$$

Where: ϕ = percentage of tensile steel reinforcement

l = effective span of member, inches

d = effective depth of member, inches

A comparison of measured deflections with those computed using Equation 4.9 is shown in Table 4.4. Relatively good agreement is obtained for a wide range of span-depth

ratios and steel percentages. Two of the beams tabulated had compressive reinforcement and the expression appears to hold for them as well.

A number of tests of deep members were conducted under Series A and B described in Reference 2. The actual deflections of these members cannot be checked against deflections computed by Equation 4.9 because the deflections were measured with respect to a deflecting datum. However, though difficult to interpret, these measured deflections gave no indication that the equations presented above were less applicable to these members than they were to those of Series C and D.

4.1.6 Ultimate Load-Deflection Relationship in Flexure. Expressions for ultimate deflection were developed by setting up rational expressions for the deflection, considering the beams to respond as tied arches, and using the test data obtained in Reference 2 to evaluate the constants in the expressions.

The yield deflection (δ_y) is considered to consist of two components, the deflection due to deformation in the concrete (δ_{cy}), and the deflection due to deformation in the tensile steel (δ_{sy}).

$$\delta_y = \delta_{cy} + \delta_{sy}$$

The ultimate deflection (δ_u) (deflection at maximum resisting moment) is also considered to consist of two such components.

$$\delta_u = \delta_{cu} + \delta_{su}$$

The test data indicate that the deflections after yield are largely due to deformations in the yielding tensile steel so the term δ_{cu} is considered to be equal to δ_{cy}. Thus, the ratio between the ultimate deflection and the yield deflection can be approximated as

$$\frac{\delta_u}{\delta_y} = \frac{\delta_{cu} + \delta_{su}}{\delta_{cy} + \delta_{sy}} \approx \frac{\delta_{cy} + \delta_{su}}{\delta_{cy} + \delta_{sy}}$$

If the deflection due to steel deformation is expressed as $\beta \epsilon_s$, when ϵ_s is the steel strain at midspan, the expression for δ_u/δ_y becomes

$$\frac{\delta_u}{\delta_y} = 1 + \frac{\beta (\epsilon_{su} - \epsilon_{sy})}{\delta_y} \tag{4.11}$$

δ_y can be determined from the Equation 4.9. In terms of the tied-arch model shown in Figure 4.7, it will be noted that β can be expressed as

$$\beta = \frac{l}{4d} \lambda l \tag{4.12}$$

where λ expresses the effect of the distribution of steel strains along the span and the effective height coefficient α of the tied-arch model. The test data indicating the effect of steel deformation on center deflection was studied, and it was determined that λ had an average value of 0.8 with no regular variation apparent with either l/d or ϕ. Thus, the value for β becomes:

$$\beta = 0.2 \frac{l^2}{d} \tag{4.13}$$

The resulting expression for ultimate deflection is then:

$$\phi_u = \phi_y + 0.2 \frac{l^2}{d} (\epsilon_{su} - \epsilon_{sy}) \quad (4.14)$$

The value of ϵ_{sy} is known from the properties of the reinforcing steel. The value of ϵ_{su} is less well defined but, if a calculation is made for the ultimate moment resistance of the member, a value of ϵ_{su} consistent with the assumptions made for ultimate concrete strain and the character of the ultimate concrete stress block can be readily determined.

$$\epsilon_{su} = \frac{d - a}{a} \epsilon_u \quad (4.15)$$

Where: ϵ_u - the ultimate concrete strain

d the effective depth of the beam

a the depth of the concrete stress block

The determination of ϕ_u with the above equations requires a relatively complete knowledge of the properties of the reinforcing steel, just as does the determination of ultimate moment resistance. If a more hasty analysis is desired, the expression for ductility factor given in Reference 1 gives relatively good results.

$$\frac{\phi_u}{\phi_y} = \frac{10}{\phi - \phi'} \text{ but less than 20} \quad (4.16)$$

Table 4.5 compares the measured factors ϕ_u/ϕ_y (Reference 3) with the corresponding ratios computed from Equation 4.11 and 4.16. The method of loading used in the tests described in Reference 2 confined the concrete in the compression zones of the beams so that ultimate concrete strains far in excess of the accepted average 0.004 in/in were measured before failure. Thus the factors ϕ_u/ϕ_y are computed for ϵ_u of 0.008 in the concrete, a value recommended by the test personnel, as well as for the more usual 0.004. It is unlikely that a strain of 0.008 is safe to use for airblast or earth-pressure loadings, but dynamic effects may permit a value higher than 0.004. It must be cautioned that these relationships apply to flexural mode failures alone and will be unsafe if the member fails in another mode at a value of resisting moment lower than that for flexural failure.

4.1.7 Effects of Axial Loads. In the laboratory, considerable effort is expended to eliminate unwanted variables. One of these is friction at the supports of a simply-supported beam. However, this was not practicable in the field test of the slabs tested under this project.

Brief consideration of the behavior of deep reinforced-concrete members will indicate that there is a tendency toward outward translational motion of the member at the supports. This tendency is obvious if the member is considered to behave as a tied arch. That is, there must be an outward lateral motion at the supports for stress to develop in the tension tie. This stress can be shown to exist if it is assumed that the member is responding in pure flexure, so long as the elastic neutral axis is above the geometric centroid of the concrete.

In addition, the slabs tested under this project were set flush with the surface of the ground so that the soil (sand) came into contact with the ends of the slabs. As the shock wave passed over the target area it loaded the soil surrounding the structures as well as the structures themselves. These pressures, undoubtedly, were transmitted through the soil loading the test members axially.

Thus, the slabs of Project 3.6 experienced loading similar to that indicated in Figure 4.8, where the supports are represented as concentrated loads. Consideration will be given to the effect of finite support dimensions later.

The exact nature of the lateral pressure exerted as a function of depth in the soil is not known. The load distribution shown in Figure 4.8 is only an assumed distribution which is based on the following reasoning. The soil adjacent to the ends of the slab is highly compressible relative to the slab and its supports, and it is envisioned that there was a relative motion of the soil down with respect to the end of the slab, permitting the overpressure to act against the end of the slab at the top. This, of course, would result in relatively higher pressure acting against the end of the slab on the side toward ground zero and relatively less on the side away from ground zero due to reflections in the one case and vortices in the other. However, because the depth of the slab exposed by this motion is not great these differences have been ignored.

In previous DOD tests it has been established that, for depths of cover up to about 10 feet in most soils, there is some attenuation of vertical pressure with depth for long-duration pulses (Reference 15). Because the depths of interest here are less than 10 feet and because the lateral pressure developed by the weight of the soil is insignificant compared to the overpressure, it has been assumed that the lateral earth pressure at the depth of the foundation is a constant function of the instantaneous value of the overpressure at the surface of the ground. In previous tests, the lateral earth pressures at such depths were found to be as low as 15 percent of the surface pressure in dry, well-compacted, silty soils and as high as 100 percent for porous, well-saturated soils. For purposes of computation later in this report, it will be assumed that the value of the lateral pressure acting at the depth of the footings is 35 percent of the surface pressure.

The manner in which the lateral pressure varies with depth from a value equal to the side-on overpressure at the top of the slab to 35 percent of that value at the bottom of the slab is unknown. A linear variation with depth has been assumed.

Flexure. In practice, the effect of combined bending and axial loads, whether concentric or eccentric, on the flexural strength of reinforced concrete members is best determined by means of an interaction diagram. Such a diagram, Figure 4.9(a) for an elastic, homogeneous, isotropic material is based on the equation of superposition:

$$f = \frac{P}{A} + \frac{Pe}{Z} \qquad (4.17)$$

Where: f the stress in the extreme fiber

P the value of the axial load

A the area of the member

Pe moment of the section being analyzed

Z the section modulus at that section

If the axial load is concentric and there are no other moment-producing loads applied to the member:

$$P_o = A f$$

Conversely, if there is no axial load applied:

$$m_o = Z f$$

Dividing Equation 4.17 by f

$$1 = \frac{P}{P_o} + \frac{M}{M_o} \qquad (4.18)$$

Thus, the interaction diagram for a member of an ideal material is a straight line. Notice that, as shown, the diagram is dimensionless.

If the material were anisotropic, such that its strength in tension were half its strength in compression, the interaction diagram would be as shown in Figure 4.9(b). See Reference 16 for further discussion.

Two interaction expressions for the flexural capacities of under-reinforced concrete members subjected to axial load and bending were developed in Reference 17. That for yield moment is only approximate and is conservative as indicated in Figure 4.10. The theoretical interaction line for yield moment, shown as a dashed line, intersects the line for ultimate moment at the balance point. The expression for ultimate moment capacity is exact if the values of the constants k_1, k_2, k_3, and k_u are known exactly for a given section. These expressions are:

For yield moment,

$$\frac{M_y}{bd^2 f'_c} = \frac{M_{y_o}}{bd^2 f'_c} + \left(1 - \lambda - 2q\,\frac{k_2}{k_1 k_3}\right)\left(\frac{N}{bd\,f'_c}\right) - \left(\frac{k_2}{k_1 k_3}\right)\left(\frac{N}{bd\,f'_c}\right)^2 \qquad (4.19)$$

For ultimate moment

$$\frac{M_f}{bd^2 f'_c} = \frac{M_o}{bd^2 f'_c} + \left(1 - \lambda - 2q\,\frac{k_2}{k_1 k_3}\right)\left(\frac{N}{bd\,f'_c}\right) - \frac{k_2}{k_1 k_3}\left(\frac{N}{bd\,f'_c}\right)^2 \qquad (4.20)$$

Where: M_f = ultimate flexural resisting capacity

M_y = flexural yield capacity

M_o = ultimate flexural capacity with no axial load

M_{y_o} = flexural yield capacity with no axial load

N = axial load

f'_c = compressive strength of the concrete

f_y = yield-point stress of tensile reinforcement

b = width of section

d = effective depth of tensile reinforcement

λd = distance from mid-depth of the member to the centroid of the tensile steel

k_1 = ratio of area of the concrete stress block to area of the enclosing rectangle

k_2 = fraction of depth of the compressive zone to the resultant of the compressive forces in the concrete

k_3 = ratio of maximum compressive stress in the concrete to the cylinder strength f'_c

k_u = ratio of depth of compression zone to effective depth

q = reinforcing index $\left(\frac{\rho}{100}\,\frac{f_y}{f'_c}\right)$

Typical interaction diagrams for members tested under Project 3.6 are shown in Figure 4.11. Note that these diagrams are not dimensionless, and that the increase in moment-resisting capacity with increasing axial load is very large for the deeper member which has a relatively low percentage of reinforcing steel.

For these two diagrams the compression failure line from P_o to P_b was assumed to be a straight line because the flexural failure line from P_b to M_y is of primary interest. In fact, the compression failure line would be slightly convex upward. Both were prepared taking moments at the geometric centroid of the concrete, using static values for the strengths of the material.

Shear-Compression. Relatively little is known about the effect of axial loads on the shear-compression strength of reinforced-concrete beams even under static loading. In Reference 17, tests of 20 simply supported beams under a single concentrated load are reported, 10 without axial load and 10 with an axial load. Those beams tested with axial loads were identical to those without, except for minor variations in concrete strength. The variables were span length and steel percentage; only two were used, 0.0190 and 0.0333. The span lengths ranged from 52 to 132 inches. It was noted that the axial load increased the shear-compression strength more than the diagonal-tension strength. The increase in strength was larger for shorter beams than for longer ones.

Tests of 24 frame members under combined uniform lateral loads and axial loads are reported in Reference 18. The variables were span length, depth, steel percentage, and concrete strength. These tests were a continuation of a long-range program to determine the effect of an axial load on the strength in shear of reinforced-concrete members. Reference 18 states that an attempt was made to interpret the results of these and previous tests by means of a semirational approach using principal stress theories but that, owing to the complexity of the problem and the inherent uncertainties involved, an empirical approach was used instead. It was recognized that the emperical approach has the disadvantage that the derived expressions may not be applicable for values of variables outside of the range of those from which the expressions were derived.

Further, it was decided to use the cracking load as a measure of the useful capacity of a given member. Several reasons were given for this decision (Reference 17):

1. Many of the members tested, especially those having the larger spans, failed at the cracking load (defined as the load at which inclined cracks are formed).

2. Although some members were able to carry appreciable loads beyond the cracking load, it was not possible to develop reliable methods of predicting this additional capacity.

3. In all cases, the degree of damage to the member, as judged by its appearance and the nature and width of the inclined cracks, was considerable when the cracking load was reached, even though additional capacity might be available.

4. The use of ultimate rather than cracking load would require the use of different expressions for shear capacity for members failing in shear-compression and diagonal tension.

As previously noted, deeper members subjected to uniformly distributed loads have considerable capacity beyond the cracking load, and do not fail in diagonal tension. Thus the use of the expressions derived would be very conservative when applied to the slabs tested in Project 3.6. Further, while the third and fourth reasons above are logical when applied to the conventional structures for which they were developed, the amount of damage acceptable in protective construction might be considerably greater than that considered acceptable for normal structures. Under these circumstances the development of a specific expression for the shear compression strength of a deep member subjected to axial load would be highly desirable.

In any event, the expressions derived in Reference 18 for the cracking loads are useful and are given below.

For members under uniform load:

$$v_c = \frac{8V_c}{7bd} = 11{,}000 \frac{(0.046 + \phi/100)(12 + N/V_c)}{(19 + l'/d)} \sqrt{\frac{f'_c}{4{,}000}} \qquad (4.21)$$

For members under concentrated load:

$$v_c = \frac{8V_c}{7bd} = 11{,}000 \frac{(0.046 + \phi/100)(12 + N/V_c)}{(25 + 4.7\,a/d)} \frac{f'_c}{4{,}000} \qquad (4.22)$$

Where: v_c = the nominal unit shearing stress computed at the supports for simply supported members and at the point of contraflexure for framed members

V_c = value of the reaction at the cracking load

b = width of the beam

d = effective depth of the beam

ϕ = percentage of tensile reinforcement

N = axial load

a = shear span

Equations 4.21 and 4.22 hold for a considerable range of values of the variables: concrete strengths from 2,500 to 6,600 psi; steel ratios from 0.67 to 3.36; ratios of simply supported span length to effective depth from 3.2 to 15.5 (in Equation 4.21); and ratios of shear span to effective depth of 2.0 to 6.0 (in Equation 4.22).

In summary, the existence of an axial load increases the shear-compression strength of deep members of reinforced concrete. This increase is probably due to the lowering of the neutral axis and consequently the lowering of the ultimate height of the inclined crack. However, no definitive expression for this increase in strength has been developed.

Expressions have been developed for the cracking load which are useful primarily because the existence of an inclined crack is required for both shear-compression and shear-anchorage failures.

Shear-Anchorage. The effect of the lateral pressure transmitted through the soil on the shear-anchorage strength of a deep member may be evaluated roughly from Figure 4.12(a). Taking the sum of the horizontal forces on either free body formed by a failure plane just above the level of the reinforcing steel, the average shearing stress on the failure plane may be computed to be

$$v_a = \frac{C - P}{b(c + 0.5d')} = \frac{T}{b(c + 0.5d')} \qquad (4.23)$$

This expression is essentially the same as Equation 4.5. Thus, because the vertical load required to produce a given stress in the steel is increased by the axial load, the vertical load required to produce a shear-anchorage failure would be increased accordingly.

From Figure 4.12(b), the effect of friction at the supports on the shear-anchorage strength of a deep member would appear to be negligible. Taking the sum of the horizontal forces on the free body above the failure plane it is apparent that the value of the average shearing stress on the section is determined by the value of the compressive

force C. The value of this force produced by the vertically applied loads is only slightly reduced by the existence of the friction force due to a slight increase in the lever arm of the internal resisting couple (i.e., the centroid of the two forces T and $c_f V$ is below T).

This approach is obviously oversimplified in that no consideration was given to the effect of the axial loads on the cracking strength of the member or to the effect of the axial loads on the location of the crack. Equations 4.21 and 4.22 may be used, as appropriate, to determine whether inclined cracks would have formed at some critical moment such as the yield moment. If so, then the member may be analyzed for its shear-anchorage strength as previously indicated.

Bond. From consideration of Equation 4.6 and the basic phenomenon of bond it would appear that the effect of axial loads on the bond strength of a member is directly related to the total value of the axial load. Whether the member is considered a beam or a tied arch the expression $T = C - P - c_f V$ is applicable. Thus the total force in the steel (T) is reduced by the existence of axial loads increasing the vertical load required to produce bond failure proportionally.

Bearing. From statics, the existence of axial loads would appear to have no effect on the bearing strength of the member. That is, the nominal unit compressive stress in the concrete below the reinforcing steel is unaffected by the existence of an axial load. However, the lateral pressure would serve to confine the concrete at the support in that direction and might raise the bearing strength of the member thereby. Most bearing failures in static tests consist of a spalling or shearing off of the corner of the member at the support. The failure plane is roughly diagonal and does not intersect the tension steel. The exact contribution of the confining pressure cannot be determined from the data available from this test program but may be considerable (Reference 19).

4.1.8 Effect of Finite Support Dimensions. Normally, when computing the moment at a section in a simply supported member, the supports are assumed to be point supports. In a laboratory the supports are designed so that this assumption is valid. That is, the bearing plates are supported on rockers or rollers and the effective span is the distance between the lines of contact between the bearing plates and the rockers or rollers.

In actual structures, the effective span of a simply supported member is often assumed to be the clear span. However, this assumption is not strictly correct. Ignoring the effect of the deflections on the distribution of stresses at the supports, the effect of the finite support dimension on the moment at any section may be determined by consideration of Figure 4.13. Taking moments at midspan, the moment at the center neglecting the support dimension is:

$$M' = \frac{1}{8} pb l^2$$

The correction due to the dimension of the support is:

$$\Delta M = pb \left(1 + \frac{l}{2c}\right) \frac{c^2}{2} - pbc \left(\frac{c}{2}\right) = pb \frac{cl}{4}$$

Thus the total moment at the center is:

$$M_c = M' + \Delta M = pb \left(\frac{l^2}{8} + \frac{cl}{4}\right) = \frac{1}{8} pb (l^2 + 2cl)$$

However, if an effective span of $l' = l + c$ is assumed:

$$M_c = \frac{1}{8} pb (l')^2 = \frac{1}{8} pb (l^2 + 2cl + c^2) \qquad (4.24)$$

If it is assumed that the distribution of bearing stress is uniform, the error in M_c using Equation 4.24 is:

For $c = \frac{1}{10}l = \frac{l}{10}$

$$\text{Error} = 100\,\frac{\left(l^2 + \frac{2l^2}{10} + \frac{l^2}{100} - l^2 - \frac{2l^2}{10}\right)}{l^2 + \frac{2l^2}{10}} = 0.8 \text{ percent}$$

Whereas for the same assumptions the error involved in using the clear span is:

$$\text{Error} = 100\,\frac{l^2 - \left(l^2 + \frac{2l^2}{10}\right)}{l^2 + \frac{2l^2}{10}} = -16.7 \text{ percent}$$

The error involved in using the clear span is not only much greater but is also on the unsafe side.

4.2 EFFECTS OF RATE OF LOADING ON MATERIALS PROPERTIES

4.2.1 Reinforcing Steel. A series of tests, both static and dynamic, was made to determine the physical properties of the reinforcing steel used in project slabs. The details of these tests and an evaluation of the results obtained from them may be found in Appendix B.

In the dynamic, or high-load-rate series of tests, efforts were made to use a loading function (stress versus time) which was similar to that which acted on the reinforcing in the field-test slabs. It is believed that this objective was achieved. Four specimens were tested, for which yield occurred in 4 to 5 msec from the beginning of loading, with the loading increasing while the yield was occurring. Dynamic analyses of the field-test slabs indicate that the yield point of the steel in these slabs was achieved, for those which yielded, in times ranging from about 1.5 to 3 msecs. It is believed that the laboratory test data can be reliably extrapolated for this limited range.

The measured upper yield stress versus time from start of loading to yield is plotted in Figure 4.14. Because the data on the response obtained from the field tests are extremely limited, it seemed reasonable, on the basis of the laboratory tests, to use a uniform dynamic-yield level of 63 ksi for all computations of the resistance of the field-test slabs.

4.2.2 Concrete. It is well known that concrete displays a time-dependent response. Within the usual range of so-called static strain rates, the strength and elastic properties of concrete are only slightly sensitive to variations in the rate of straining; however, a large increase in strain rate may double the compressive strength.

The effect of the strain rate on the compressive strengths of concrete cylinders is shown in Figure 4.15 (Figure 2 of Reference 20). Reference 20 notes that the data of three separate investigations are presented in the figure, but a really satisfactory base for comparison is lacking because of differences in cylinder sizes and methods of determining straining rates. However, these latter differences are of little significance in comparing the effects of greatly different straining rates. For some computations, the effect of the stressing rate on the compressive strength of concrete may be used more conveniently. The results of work done by several investigators is summarized in Figure

1 of Reference 20, which is reproduced as Figure 4.16 in this report.

The question remains as to whether this data is applicable to the compressive strength of concrete in flexures. There is little published data on the effect of the rate of loading on the flexural strength of concrete, and it deals with unreinforced beams which failed in tension. The data indicates that, over the range of stressing rates applied, the effect of stressing rate on the tensile strength of concrete in flexure is the same as the effect of stressing rate on the compressive strength of concrete cylinders. Specifically, in the range of stressing rates of 1 to 1,000 psi/sec, the compressive strength and modulus of rupture both vary directly with the logarithm of the rate of stressing. However, the rate of stressing of interest is on the order of 10^6 psi/sec. The effect of the rate of stressing on the compressive strengths of cylinders deviates from this logarithmic relationship beyond that point, but there is no data on the effect of the rate of stressing on the modulus of rupture for stressing rates in excess of 1,000 psi/sec.

For purposes of analysis in this report, it is assumed that Figures 4.15 and 4.16 define the effect of straining and stressing rates on both the compressive and tensile strengths of concrete in flexure as well as on the strength of the beams in bearing.

The effect of straining rate on the modulus of elasticity of concrete has been investigated extensively in Reference 21, in the range of straining rates of from less than 1 in./in-sec to more than 10^6 in./in-sec. In impact tests described in Reference 21 it was found that the "modulus of elasticity of each of the concretes increased significantly with the rate of application of the load. The secant values of the dynamic (impact) moduli were 12 to 47 percent greater than the static values for weak concrete and 7 to 33 percent greater for strong concrete." The secant moduli for both static and dynamic tests were determined using 0.9 f'_c and 0.5 to 0.6 f'_c. Reference 20 states: "The higher rates of stressing produced a greater increase in the modulus at loads of 0.9 f'_c than at 0.5 to 0.6 f'_c, due probably to greater creep during the static test at the higher load."

If it is assumed that the strain at which failure occurs (in uniaxial compression tests of cylinders) is constant regardless of the straining rate, and that the shape of the stress-strain curve is the same for static and dynamic loading, it can be shown that the effect of straining rate on the compressive strength and the modulus of elasticity should be the same. However, this is not the case. The effect of straining rate on the compressive strength of the concrete is greater than the effect of the straining rate on the modulus of elasticity, indicating that the shape of the stress-strain curve is different under different rates of loading.

The probable change in shape of the stress-strain curve is indicated in Figure 4.17. The value of the modulus of elasticity probably approaches the value of the initial tangent modulus as the straining rate is increased, resulting in a linear relationship between stress and strain up to the maximum compressive stress attained for very rapidly applied strain. The shape of the compressive-stress block at the ultimate moment in a beam failing in flexure would be determined approximately by that value of strain which maximizes the ratio of the area under the stress-strain curve to the area of the enclosing rectangle.

Too little is known about the properties of concrete under various strain rates to permit the determination of the value of ultimate concrete strain in dynamic flexure. Thus, for purposes of analysis, it was assumed that the ultimate strain in compression is a constant (0.004 in./in) and that the value of the compressive force (C) is defined by the expression (see Reference 2):

$$C = k_1 k_3 f'_c b k_u d \qquad (4.25)$$

Where: k_1 a coefficient expressing the ratio of the area of the stress block to that of the enclosing rectangle

k_3 - a factor depending on the stressing or straining rate and obtained from Figure 4.14 or 4.15

f'_c the standard cylinder strength

b width of the compression zone

k_u $\frac{\epsilon_u}{\epsilon_u + \epsilon_s}$

4.3 DYNAMIC BEHAVIOR OF DEEP ONE-WAY SLABS

4.3.1 Natural Period of Vibration. For the same reasons that caused the deflections predicted by normal-beam theory to be in error for deep concrete members (the high value of vertical stresses relative to the horizontal bending stresses and the inapplicability of the normal assumptions such as plane sections remaining plane), the usual equations for beams cannot be expected to yield correct values of natural periods of vibration for deep concrete members. The deflection (S) and the natural period (T) can be related in a form of the following expression:

$$T = 2\pi C \sqrt{\delta_s / g}$$

Where: δ_s the deflection of a specified point in the beam under the action of the dead-mass loads acting on the beam

C = an arbitary constant depending on the location of the point at which deflection is measured

g gravity constant

It should be noted that the error in period is less severe than the error in deflection, because the period is a function of the square root of the deflection.

For the reasons stated above, it was decided that the best period values for the deep one-way slabs could be determined by use of the yield-deflection expression developed from the tests of deep concrete members (Reference 2). This expression was developed in Reference 2 and is repeated below for convenience:

$$\text{Center deflection} \quad \frac{M_c}{4E_s A_s \alpha} (l'/d)^2$$

Where $\alpha = \frac{-0.01 (l'/d)^2 + 0.22 l'/d + 0.17}{\phi^{2/3}}$

These expressions were used to define the stiffness of each member for computation of the longest natural period by Rayleigh's method (Reference 22).

For free vibration of an undamped system, the maximum potential energy must equal the maximum kinetic energy. PE max = KE max. The potential and kinetic energies were computed by assuming the deflected shape to be the deflection due to the distributed weight of the beam, and δ_{gc} and δ_{sq} to be the center deflection and quarter point deflection respectively under this load. From use of Simpson's rule for approximate integration,

$$PE\,max = w/' 12 (\delta_{sc} + 4\delta_{sq})$$

$$KE\,max = (2\pi/T)^2 w/g\ l' 12 (\delta^2_{sc} + 4\delta^2_{sq})$$

By equating PE max to KE max, the equation for the longest natural period becomes

$$T = 2\pi \sqrt{\frac{\delta_{sc}^2 + 4\delta_{sq}^2}{g(\delta_{sc} + 4\delta_{sq})}} \tag{4.26}$$

An evaluation of the deflection data obtained from the C series of Reference 3 revealed that the quarter-point deflection was approximately 0.56 of the center deflection. There was no consistent variation in this relationship with l', d, ϕ, or f'_c. Thus, equation 4.26 can be written as;

$$T = 2\pi \sqrt{\frac{0.696\delta_{sc}}{g}} \tag{4.27}$$

A reasonable lower limit for the ratio of the quarter-point deflection to the center deflection is 0.5, and a reasonable upper limit, 57/80. The difference between the periods computed using these two limits is less than 10 percent. Therefore, Equation 4.27 was used to determine the fundamental period of the one-way slabs tested under this project.

As an indication of the error involved in defining the deflection curve by means of center and quarter-point deflections only, consider a simply supported, prismatic beam vibrating in the flexural mode. The quarter-point deflection is (57/80) δ_{wc}. Therefore, from Equation 4.26:

$$T = 2\pi \sqrt{\frac{0.787\delta_{sc}}{g}}$$

whereas, the exact expression for fundamental period of such a beam is:

$$T = 2\pi \sqrt{\frac{0.788\,\delta_{sc}}{g}}$$

Thus, the error resulting from the assumption that the deflected shape may be defined by the center and quarter-point deflections only is not great.

4.3.2 Equivalent Single-Degree-of-Freedom System. The equation of motion for an undamped single-degree-of-freedom (SDF) system like that shown in Figure 4.18 can be found by solution of the dynamic equilibrium equation:

$$m\ddot{y} + k(y - x) = p \tag{4.28}$$

Where: m = the mass of the system assuming the spring to be massless

$\ddot{y}$ = the acceleration of the mass

k = the stiffness of the spring

y = the displacement of the mass

x = the displacement of the foundation

p = external force applied to the mass

Subtracting $m\ddot{x}$ from each side and denoting $u - x$ by x, yields

$$m\ddot{u} + ku = p - m\ddot{x} \tag{4.29}$$

Setting $T = 2\pi\sqrt{m/k}$ and assuming that p and $\ddot{x}$ are single-valued functions of time, the solution of Equation 4.29 is

$$u = \frac{A}{k}\sin\left(\frac{2\pi}{T}t + \alpha\right) + \frac{p}{k} - \frac{m\ddot{x}}{k} \tag{4.30}$$

Where: $A = \sqrt{\left[r_0 - p_0 + m\ddot{x}_0\right]^2 + \left(\frac{r_0 - p_0 + m\ddot{x}_0}{2\pi/T}\right)^2}$

$\alpha = \frac{2\pi}{T}t_0 - \sin^{-1}\left(\frac{r_0 - p_0 + m\ddot{x}_0}{A}\right)$

t_0 = initial time

r_0 = initial resistance, ku_0

$\dot{r}_0$ = $k\dot{u}_0$ or k times the initial relative velocity

The solution may be expressed in terms of resistance also as:

$$r = A\sin(2\pi/T\ t + \alpha) + p - m\ddot{x} \tag{4.31}$$

where $r = ku$ and the other terms are as previously defined.

To use an equivalent SDF system for the test slabs, the mass, resistance, load, spring constant, displacement, and stored energy of the SDF system must be expressed as functions of the mass, resistance, applied load, spring constant, displacement, and stored energy of the slab. The dynamic characteristics of the two systems must be the same. This is accomplished by equating the periods of the slab and the SDF system.

The selection of parameters of the SDF systems used for dynamic analysis of the project slabs was as follows:

SDF System	Slab
Period, $T = 2\pi\sqrt{\frac{m_e}{k}}$	$T = 2\pi\sqrt{\frac{1}{g}\frac{\dot{o}^2_{sc} + 4\dot{o}^2_{sq}}{\dot{o}_{sc} + 4\dot{o}_{sq}}}$
Resistance, $r = ku$	$r = \frac{8M_c}{b(l')^2}$
Forcing function, P	p = incident overpressure
Deflection, u = c	cc = center deflection relative to supports
Base disturbance, $\ddot{x}$ = $\ddot{x}$ of slab footings	$\ddot{x}$ = acceleration of slab footings
Mass, $m_e = \frac{\dot{o}_c^2 + 4\dot{o}_q^2}{\dot{o}_c + 4\dot{o}_q}m$	m = mass of slab/unit area
Kinetic energy, $KE_e = 1/2\ m_e(\dot{u})^2$	$KE = 1/12\ mb^2(\dot{o}_c^2 + 4\dot{o}_q^2)$
Potential energy, $PE_e = 1/2\ ru$	$PE = 1/12\ rb^2(\dot{o}_c + 4\dot{o}_q)$

(The subscript e denotes an equivalent parameter.)

With the use of these relations, the deflection or resistance of the SDF system at any time can be converted into corresponding slab deflections or center moment.

One important stress function of the slab is not described by the SDF model, this is the slab reaction. It is not consistent with the remainder of the analysis to use 1/2 rb/ as the value for the slab reaction. Considering the forces shown acting on the slab in Figure 4.19 the value of the Reaction V can be determined by taking moments about the centroid of the inertia-force distribution. For a trapezoidal distribution of inertia forces with $\sigma_q = 0.56\sigma_c$, the location of the centroid, $\bar{x}$, is 0.33l'. For a second-degree parabolic distribution, $\bar{x}$ is 0.31l'. Taking $\bar{x}$ as 0.33l', the equation for V becomes:

$$V = b/'(0.12p + 0.38r) \qquad (4.32)$$

In order to represent slab behavior after yield some modification of the SDF system is required. The factor of primary importance is the change in moment-deflection ratio for the slab which requires a change in k, the spring stiffness, for the SDF system. Because r for the slab converts directly to r for the SDF system, and σ_c for the slab is equal to u for the SDF system, the conversion of the k value is simple to accomplish. The value of m_e, equivalent mass, of the SDF system might also be altered to account for the change in the deflected shape of the slab in passing from the elastic range to the yield range However, because the change of m_e, will not be great, it is convenient to neglect it and thus be able to make direct use of response charts and rapid computational methods such as those outlined in Reference 23.

4.3.3 Response to Applied Vertical Loading Only. To evaluate the order of magnitude of the possible effect of the axial load and friction at the supports on the response of the test slabs, each was analyzed first as though the only external force applied was the side-on blast overpressure on the top surface of the slab. The original design calculations and response predictions for these slabs were based on this assumption.

The forcing function for each station was obtained by considering the pressure records for that station, pressure records obtained at nearby Stanford Research Institute stations, and the theoretical pressure-time curves of References 24 and 25, for the value of the peak overpressure experienced at each station. Because the duration of the applied load was quite long compared to the fundamental period of the slabs, the slope of the decay of pressure with time was represented by a straight line which appeared to fit the measured pressure-time history best at the early stages of decay (initial tangent approximation).

Representations of the measured pressure-time curves for Stations 360.01 and 360.02 are shown in Figures 3.1 to 3.7. The simplified forcing functions used in all subsequent computations are shown in Figure 4.20.

Resistance functions defining the flexural response of each slab were determined as follows:

1. Yield moments were computed using Equation 4.1. A yield stress in the steel of 63 ksi was assumed, for reasons stated in Section 4.2.1. Because the ultimate strength of the concrete is raised also by the rapid stressing rate, it was assumed that the distribution of compressive stress in the concrete was linear at yield. Therefore, the moment arm of the internal resisting couple is assumed to be that computed from the elastic theory.

2. Yield deflections were computed from Equation 4.9 using the yield moment computed above for M_c (Tables 4.6 and 4.7).

3. Ultimate moments, i.e., that moment at which the concrete crushes in compression

or the steel ruptures, were computed from Equation 4.2 after computing f_s by an iterative method (Table 4.8). The effects of the rapid loading on the strengths of the steel and the concrete, and strain hardening in the steel, were taken into consideration. The stress-strain relationship for the steel was assumed to be bilinear as shown in Figure 4.21. This assumption is believed to be justified by the fact that most of the slabs had multiple layers of tension steel. A more refined assumption does not appear to be warranted, because the different layers of steel undoubtedly experienced different stress states at the same time.

4. Ultimate center deflections were computed using Equation 4.14. The dynamic yield strain ($\epsilon_{s,y}$) was assumed to be 0.0021 in./in. This is consistent with a dynamic yield stress of 63 ksi and was based on the assumption that rapid loading has no effect on the modulus of elasticity of the steel. Values for the ultimate strain in the steel were obtained from the computations fro the ultimate moment.

5. Finally, the resistance function was assumed to be linear between the three points defined by the origin, the yield resistance, and the ultimate resistance, as indicated in Figure 4.22.

The flexural yield resistance of a given slab is given by the expression:

$$r_y = \frac{8M_y}{b(l')^2} \tag{4.33}$$

Where: r_y = the yield resistance, psi

M_y = the yield moment as previously computed, inch-pounds

b = width of the slab, inches

l' = the effective span length, inches

The effective span length for all computations was assumed to be the clear span plus one support width.

Similarly, the flexural ultimate resistance may be computed as follows:

$$r_u = \frac{8M_u}{b(l')^2} \tag{4.34}$$

The slabs were analyzed by the rapid computational methods of Reference 23, using the method outlined in Section 2.2.2 of the reference to account for strain-hardening of the resistance function. The results of these calculations are shown in Tables 4.9 and 4.10, for Stations 360.01 and 360.02, respectively, and are compared with observed crack patterns. From these tables it is apparent that the computed response assuming only a vertically applied blast load was far more sever in each case than the actual response of the slabs. At Station 360.01, the computations indicate that 7 of the 15 slabs should have failed and the remainder should have exhibited considerably more permanent deflection and cracking than they did.

No slab at Station 360.01 with a computed maximum response of less than 4.4 times the yield deflection was cracked. Slab 36-1, which did not have vertical reinforcing, suffered light inclined cracking, whereas its companion Slab 36-2, with vertical stirrups, did not crack, though it had the same computed response of 6.5 yield deflections.

At Station 360.02, only Slab 11-1 (the shallowest) was computed to have failed, and it suffered light cracking at midspan. Of those with computed responses of less than 6.6, 5 of 12 were very lightly cracked. Two with computed responses of 14 yield deflections showed only light vertical cracking at midspan.

To summarize briefly, the observed response at each station was much less than that computed by assuming that the only external force applied to each slab was the side-on

overpressure on the top surface. This may be due, in part, to the assumption that the ultimate strength of the reinforcing steel was not increased by rapid loading. However, in the range of response of less than 5 yield deflections, the effect of this assumption is negligible. Thus, a slab having a predicted failure should have shown at least signs of extensive yielding in the reinforcing steel and a residual deflection of 5 or more yield deflections.

4.3.4 Response to Axial Loads. As discussed under Section 4.1.7, it is believed that the ends of the slabs were subjected to lateral earth pressure and that a friction force directed toward midspan was generated by the tendency of the bottom of the slab to move outward at the supports. It is not possible to determine the value of either force exactly. The assumption made under Section 4.1.7 regarding the distribution of the soil-transmitted pressure will be used here.

The support friction is even more complex, but for purposes of analysis it is assumed that the force can be represented as the product of a coefficient of friction and the slab reaction. Further, it is assumed that the coefficient of friction is a constant. Several references give the static coefficient of friction of concrete on concrete as 0.6 to 0.70. This is a limiting value—kinetic friction is slightly less than static friction and decreases with time and the relative velocity. Because the exact value of the coefficient is unknown and because the previously mentioned values represent an upper limit, it was assumed that the coefficient of friction at the supports was 0.5.

As indicated in Equation 4.32 the slab reaction is a function of two variables: the instantaneous overpressure, and the resistance (which was assumed to be a function of deflection only). However, when axial loads are introduced, the force-deformation relationship for a reinforced-concrete member is altered, as discussed under Section 4.1.7. The moment-resisting capacity is increased significantly. Enough experimental data is available on tests of beam-columns to make some rational allowance for the influence of these forces on members of normal dimensions, i.e., span-depth ratios of about 10. It is assumed that the same methods of analysis are applicable to these deep members. That is, it is assumed that the forces involved may be resolved into an axial force and a resisting moment at midspan, and that the resisting moment in the section is defined by assuming a linear distribution of strain with depth at midspan (Figure 4.23).

The classic definition of moment on a section is that moment taken about the centroid or neutral axis of the section. In a member of reinforced concrete, the transformed area of the section changes with axial load. It is impossible to develop analytically a closed-form expression for the moment about a changing axis; when the stress-strain relationship for the material changes, the axial load changes with the moment and the moment varies with time.

If the member were made of a homogeneous, isotropic, elastic material, the resisting moment taken at middepth would be a function of the deflection (or rotation of a plane section) at midspan, regardless of the value of the axial force. This is implied in the equation for superposition (4.17). But, obviously, this is not so for reinforced-concrete members; there is no depth at which the moment is a function of the angle change alone regardless of the value of the axial load, because a change in axial load changes the cracked-section moment of inertia. As shown in Figure 4.24, the distance between the centroids of the compressive and tensile forces changes with the axial load, even though the angle change may be constant. This change in the moment arm is due to inelastic behavior of the concrete and the fact that the location of the centroid of the tensile forces remains constant. Therefore, the resisting moment computed at middepth decreases

gradually with increasing axial load for the same angle change at the section. For purposes of these computations, however, it will be assumed that the resisting moment M_r (Figure 4.23) is a function of the deflection only and that it is defined by taking moments at the geometric centroid of the concrete, that is, at a depth of 0.5h.

The existence of axial forces also affects the frequency of vibration of a beam-column. Assuming a span-depth ratio of about six or more so that the vibration of the member is primarily flexural, and rewriting Equation (d), page 375 of Reference 26, it can be shown that

$$\omega_a = \omega \left(1 - \frac{N}{N_{cr}}\right)^{1/2} \tag{4.35}$$

Where: ω_a = circular natural frequency of beam-column in fundamental mode

ω = circular natural frequency of member in fundamental mode with no axial force acting

N = axial force

N_{cr} = critical buckling load in first mode

From equation 4.35 it is apparent that a compressive axial force decreases the natural frequency of the member. However, a simple computation indicates that N_{cr} is about 100 times the axial load at the balance point for these test members. Thus the effect of the axial load as expressed in Equation 4.35 is negligible.

An axial load also affects the frequency of flexural vibration of a reinforced-concrete member by inhibiting cracking and thus stiffening the member. Consider the term ω from Equation 4.35:

$$\omega = \frac{\pi^2}{l'^2} \sqrt{\frac{EI}{\mu}} \tag{4.36}$$

Where: l' = effective span

E = modulus of elasticity

I = moment of inertia about the bending axis

μ = mass per unit length

Under axial load the cracked moment of inertia of a reinforced concrete beam is increased while all other terms of Equation 4.36 remain essentially constant. Calculations for members of this test series indicate that the increase in cracked moment of inertia due to an axial load equivalent to that at the balance point for each member is on the order of 50 percent. Thus, the maximum possible effect consistent with flexural response increases the natural circular frequency of the member about 22 percent.

While the preceding expressions apply only to members with span-depth ratios of about six or more, the indications are that the effect of the axial loads on the periods of vibration may be ignored without introducing a very large error. This would be especially true if the maximum value of the axial force were small compared to the value of the axial load at the balance point. For values of axial loads subsequently computed, the effect is to increase the periods by less than 10 percent.

The frequencies of the members tested, as computed by Equation 4.27, quite probably are not accurate to within ± 10 percent, so modifications of them based on the preceding considerations are not warranted.

Also, the rise time of the applied pressure pulse is only about 0.16 to 0.4 of the computed periods. Consideration of the spectra of maximum displacement (Figure 4.19 of Reference 22) resulting from forcing functions of the type shown in Figure 4.20 leads to the conclusion that period changes on the order of ±10 percent do not significantly change the maximum response of the structure.

In view of all the preceding considerations, it was decided that analyses of the response of the slabs would be based on the following simplifying assumptions: (1) vertical forcing functions were as shown in Figure 4.20, (2) earth-transmitted axial force was as shown in Figure 4.8, that is, the shape of the force was trapezoidal, with the pressure a function of the instantaneous side-on overpressure at the surface, (3) friction force at the supports was equal to half of the instantaneous value of the reaction; (4) internal resisting moment in the slab was a function of the deflection at midspan only; and (5) effect of the axial loads on the periods of vibration of the slabs was negligible.

Referring to Figure 4.23, it is now possible to define the elastic behavior of the slab. Ignoring rotatory inertia;

$$N = c_f V + P \tag{4.37}$$

Taking moments at the intersection of centroid of the inertial forces and the friction force $c_f V$, and assuming elastic deflections are so small that they do not affect the moment arms of the forces involved:

$$V = \frac{b\left(l'^2 (0.25\, r + 0.04\, p) - 0.08\, Ph\right)}{(0.33\, l' - 0.25\, h)} \tag{4.38}$$

Where: b = width of slab, inches

l' = effective length of slab, inches

r = instantaneous value of resistance, psi

p = instantaneous value of the overpressure, psi

P = instantaneous value of the axial load due to lateral earth pressure $\left(P = \frac{0.35p}{2}\right) bh$; pounds

h = depth of slab, inches

The instantaneous value of the resistance of the slab, r, may be determined from a solution of the differential equation of motion of the equivalent SDF system under the appropriate forcing function. For example, ignoring the base disturbance and assuming an undamped system, the equation of motion for the one-way slabs at Station 369.02 is

$$m_e \ddot{y} + ky = p_m - p_m \frac{t}{t_d}, \quad (\text{For } o \leq t \leq t_d) \tag{4.39}$$

Where: m_e = equivalent mass of the system

$\ddot{y}$ = mass acceleration

k = equivalent spring stiffness

y = mass displacement

p_m = peak overpressure

t_d duration of pressure pulse

Solving Equation 4.39 for the deflection of the slab while the force is acting on the structures:

$$y = y_s \left[1 - \frac{t}{t_d} \cdot \sqrt{1 + \frac{1}{(2\pi t_d / T)^2}} \sin\left(2\pi \frac{t}{T} + \alpha\right) \right] \qquad (4.40)$$

Where: y center deflection of the slab, inches

y_s center deflection of slab under p_m acting as a static load, inches

t_d duration of pressure pulse, seconds

T fundamental period of slab, seconds

$$\alpha = -\sin^{-1} \frac{1}{\sqrt{1 + (\frac{1}{2\pi t_d/T})^2}}$$

To obtain r, it is necessary only to multiply both sides of Equation 4.40 by k. Thus:

$$r = p_m \left[1 - \frac{t}{t_d} \cdot \sqrt{1 + \frac{1}{(2\pi t_d/T)^2}} \sin\left(2\pi t/T + \alpha\right) \right] \qquad (4.41)$$

Solving Equations 4.41, 4.38, and 4.37 at discrete intervals of time, it is possible to obtain instantaneous values for M_r and N which may be plotted on an interaction diagram. The yield moment M_{ya} is then obtained from the intersection of the trace of these values with the yield line of the interaction diagram. In the preparation of the interaction diagrams for this step of the analysis, the effect of the rapid loading rate on the strengths of the concrete and the tensile steel were taken into consideration as discussed under Section 4.2. Specifically, the yield point of the steel was assumed to be 63 ksi, the ultimate strain in the concrete was assumed to be 0.004, and the value of the compressive force in the concrete was computed by Equation 4.25.

Typical results of these computations are shown in Figures 4.25 and 4.26. The computations indicate that the tensile steel would not have yielded in most of the members under the assumed loading conditions. For Slab 44-4, which was computed to have failed if vertical loads only were acting (Table 4.9), Figure 4.26 shows that the effect of the axial load (under the assumptions listed above) would be so great as to prevent yielding of the tension steel at midspan.

New resistance functions were prepared for each slab with values of yield moments obtained from the graphical solutions. Again, assuming that the axial forces do not affect the stiffnesses of the members, yield deflections were computed by multiplying the yield deflection obtained from Equation 4.9 by the ratio of the yield moment obtained from the interaction diagram to the yield moment computed by Equation 4.1.

A new ultimate moment may be obtained from the interaction diagram, also. However, because the yield moment approaches the ultimate moment as the axial load is increased, the new resistance functions were assumed to be plastic beyond the yield point. The response of each slab was again computed by rapid techniques. The results of these computations are shown in Tables 4.11 and 4.12.

As previously discussed, many assumptions were made to permit these analyses. There were no experimental data obtained to confirm or deny the validity of the assumptions. The only response data obtained consisted of the word and picture descriptions of the visible crack patterns and the residual deflection data, which were not conclusive

at all. However, the results of the computations indicate that the effect of axial loads, if they existed, would be to increase the strengths of the slabs markedly.

If the effect of the axial forces on the yield resistances of the slabs is ignored and it is assumed that the periods of the slabs at Station 360.01 were equal to the rise time of the applied pressure pulse (reducing the amplification factor for maximum response to 1.0), 11 of the slabs still should have exceeded their respective yield deflections and 6 of these would have failed in flexure. Thus, errors in period computations alone cannot account for the discrepancies that exist between predicted and observed response.

A brief study of Tables 4.11 and 4.12 reveals that the effects of an earth-transmitted axial force and friction at the supports tend to bring the computed and observed response into line except for Slabs 20-1, 28-1, -2, and -3 at Station 360.01 and Slab 11-1 at Station 360.02. In these cases, the periods of the slabs are greater and the depths of the foundations less than the others at the same station. Any ground motion induced by the airblast passing over the surface would undoubtedly have had a greater effect on the initial response of these slabs than on the others. The effect of base disturbances in general is discussed under Section 4.3.5.

4.3.5 Effects of Base Disturbance. The posttest conditions at Stations 360.01 and 360.02 indicate that large vertical ground accelerations must have occurred during the passage of the shock wave. The final elevation of the ground surface at Station 360.01 was 7 feet below the preshot elevation while that at Station 360.02 was 1/2 foot lower than the preshot elevation. The fact that a base disturbance may have a significant effect on the response of a structure is well known, but it cannot be clearly established what that effect might be without detailed knowledge of the acceleration as a function of time.

This fact was recognized during the planning stages of this project. Provisions were made for the installation of accelerometers on the slab foundations. Unfortunately, the records from these accelerometers were completely obliterated through leakage of seawater into the gages. As a result, the only indications available of the acceleration-time behavior of the slab foundations came from the Project 1.8 records of accelerations at Stations 180.01 and 180.02.

The data available from Project 1.8 include horizontal and vertical accelerations in the soil at a depth of 10 feet and vertical accelerations at a depth of 1-foot in the soil. Station 180.01 was located at a range of about 170 feet greater than Station 360.01, and Station 180.02 was located at a range of about 44 feet greater than station 360.02. It is believed that this data does not justify detailed computations of the effects of base disturbance on the slabs. The Project 1.8 data shows a considerable attenuation of the acceleration peaks from the 1-foot depth to the 10-foot depth and a change in the times of the peak upward and downward acceleration with reference to airblast arrival. The accelerations of the slab foundations are not deducible from this earth acceleration data, either in magnitude of peaks or in time variation. The appearance of the test site and the two-way slab foundations at Station 360.01 after the test indicated considerable localized variations in ground movements. Thus, only order of magnitude estimates can be made of the effect of ground movements on the response of the Project 3.6 slabs, using pulses of an acceleration-time variation conforming to the range appearing in the Project 1.8 data for vertical accelerations at 1- and 10-foot depths.

The highly simplified acceleration-time function shown in Figure 4.27 was derived from the Project 1.8 data. The peak acceleration values and time variation are somewhat arbitrary. Values which seemed reasonable were chosen for the peak accelerations at the average depth of the slab foundations by using an exponential interpolation between the two gage depths (1 foot and 10 feet). The time variation was established to give downward

and upward acceleration spikes representing velocity changes intermediate between the velocity changes at the 1-foot and 10-foot depths.

The acceleration pulses were applied in conjunction with the pressure pulses to Slabs 36-4 and 21-2, which showed no signs of yielding in the actual test, in order to estimate the possible effects of the base disturbance. The method of analysis is covered in Section 4.3.2. In the calculations of response, the slabs were assumed to remain elastic and the resistances required in the positive direction and in rebound were evaluated. Because estimates of order of magnitude were sought, it was believed unnecessary to include the effect on the required rebound resistance of the change in stiffness for the slab in rebound. As discussed in the section on rebound behavior which follows, neglecting the change of stiffness gives low values for required rebound resistance. However, damping is also neglected, and, under the conditions of loading, maximum rebound did not occur until several cycles of vibration had taken place. Thus, the required rebound resistance values given are considered to be significant more in their differences than in their magnitudes. The results of the analysis of response are given in Table 4.13. These results indicate that the ground displacements could have had considerable effect upon the resistance required to prevent yielding and therefore on the slab response also. The comparison between Cases 1 and 2 indicates the beneficial effect resulting from a favorable timing of the ground disturbance, whereas a comparison of Cases 1 and 3 indicates the unfavorable effects of a delayed commencement of the base disturbance. It is obvious that the timing of the ground disturbance relative to the overpressure-time function is of primary importance.

The consideration of the data available on ground disturbances during the test of the Project 3.6 slabs indicates that such disturbances, judging from the intensities and time variations of accelerations measured in the soil at nearby Project 1.8 stations, could be responsible for either a significant apparent increase or decrease in the slab resistance, depending on the time variation of the acceleration. The order of magnitude of the apparent change in resistance is dependent upon the value of the peak accelerations, and is thus unknown, but rough calculations indicate the effect could have been as much ±50 percent of the predicted resistance. It seems probable that the foundation accelerations began coincidentally with the arrival of the airblast pressure, that is, that the slab foundations did not show the delay in commencement of acceleration indicated by the Project 1.8 data. If this time sequence is correct, the base disturbances were likely to have been responsible for a significant portion of the apparently higher-than-predicted resistance of the Project 3.6 slabs.

4.3.6 Elastic Rebound. A negative displacement or rebound can occur after the slabs undergo their maximum positive displacement. Rebound displacement results in stresses of the opposite sense to those produced during the normal positive displacement. The magnitudes of the rebound displacements, and the rebound stresses, are influenced by the time history of the overpressure loading as well as the peak value of the overpressure. If the loading is a pure impulse, for a slab that remains elastic throughout the loading history, the magnitude of the negative or rebound displacement will be equal to that of the positive displacement. Conversely, if the loading is of infinite constant duration, no rebound will occur; the oscillations of the system with respect to the unloaded equilibrium position will never proceed into the negative range. The analysis of rebound magnitude becomes more complex when inelastic response of the slab occurs, but the simple cases stated bound the range of possible rebound response of a slab with identical stiffness in positive and negative response.

The analysis of rebound response is further complicated by the changed dynamic behavior

of reinforced-concrete slabs in the region of negative displacement. The slabs had no longitudinal compression reinforcement; therefore, in rebound response, they were essentially unreinforced-concrete members. Thus, the load deflection relations, and therefore the natural frequencies of the slabs, would change as they deflected upward beyond the unloaded equilibrium position.

A rapid procedure for computation of required rebound resistance has been developed and was published in Reference 27. This procedure was developed for an equivalent SDF system and considers the system to have the same dynamic characteristics during normal response and rebound. It is, therefore, not exact for reinforced-concrete structures which may not be reinforced identically for positive and negative displacements. The charts available for this procedure will give results that are conservative when the assumptions made in the analytical development are satisfied, because the charts are prepared to correspond an envelope containing the peak rebound values.

A comparison of the moments of inertia for the one-way project slabs in normal deflection (I of the cracked transformed section by normal elastic therory) and in rebound (I of the gross concrete sections assuming effective homogeniety) indicates the moment of inertia in rebound will be greater than that in normal deflection—from two times as great in the shallower slabs to over four times as great in the deeper slabs. This variation of moment of inertia in turn indicates that the periods in rebound will run from less than 50 to 79 percent of the periods in normal deflection. The effect of this change in stiffness as the slab begins to deform into the negative range is to increase the required rebound resistance over that which would be required if the stiffness were the same in the two directions of response. The factor of amplification appears to be in the neighborhood of $\sqrt{I_r/I}$ where I_r is the moment of inertia in rebound and I is the moment of inertia of the cracked elastic transformed section. Thus the rebound response charts prepared in Reference 27 would appear to be on the unsafe side for use with the Project 3.6 slabs.

The rebound stress that the slabs can resist is limited by the resistance of the slabs to bending in the rebound direction. It is not possible to give exact values for this resistance. The slab concrete was not tested in tension, and little is known concerning dynamic effects on the tensile strength of concrete. In order to estimate the rebound resistance of the slabs, it was assumed that the modulus of rupture for the concrete in tension was 0.15 f'_c (0.10 f'_c is a normal static rule-of-thumb value for the modulus of rupture, and 0.15 f'_c was chozen to allow for dynamic effects). The rebound resistance is expressed as the equivalent pressure in psi on the slab surface that would develop the modulus of rupture on the tensile surface. The values of rebound resistance r_r are tabulated in Table 4.14.

An estimate of r'_r, the required rebound resistance to preclude cracking in rebound, can be made from the rebound charts in Reference 27. The value of σ_{max}/δ_y used to enter the charts is that determined as described in Section 4.3.3 considering only normal loadings to act on the slabs. Because the yield resistance is higher when axial loads are considered, calculations assuming no axial load to act will lead to somewhat low values for required rebound resistance. This is due to the fact that the maximum elastic deflection is somewhat greater when axial loads act. As discussed previously, the values of required rebound resistance taken from the chart are increased by the factor $\sqrt{I_r/I}$ to allow for the effect of changed stiffness in rebound.

The conditions of the slab installation place another limit on the rebound stress that can be developed. The only positive resistance to the lifting of the slabs from their supports was provided by two 7/8-inch diameter threaded anchor bolts at each end. Thus the maximum end shear in rebound is limited to the yield resistance of these anchor bolts.

The yield stress under rapid loading conditions for these bolts is not known, but the value of 63 ksi used for the yield stress of the intermediate grade reinforcing might be slightly high, because the steel was probably similar to a hot-rolled SAE 1015 type. The end shear in rebound that the bolts could develop was assumed to be approximately 53 kips; a value computed using the area at the roots of the two 7/8-inch diameter threads and a stress of 63 ksi. Approximating r_a (the rebound stress as limited by anchorage resistance) as equivalent pressure on the slab surface:

$$r_a = \frac{2V_a}{bl_a} = \frac{2\ (53{,}000)}{24\ (75.75)} \qquad 58 \text{ psi}$$

when l_a is the span between anchor bolts. The expression for r_a is in error, because the end shear is not precisely half the total slab resistance in the dynamic case.

The above-computed value is much smaller in most cases than the rebound response calculated for an end anchorage assumed to be sufficient to prevent end displacement. However, the end shear that can be developed in rebound can be greater than the yield load of the anchor bolts because of friction between the soil and the ends of the slabs. It is not possible to state confidently a value for this friction force. However, for order-of-magnitude estimates, the friction force can be considered to be a unit shear of one-fourth the overpressure value (average normal pressure on end of slab is assumed to be roughly one-half the overpressure, and coefficient of friction between slab and sand backfill to be 0.50). At the time of maximum rebound the overpressure at Station 360.01 would have been in the neighborhood of 400 psi, and at Station 360.02, in the neighborhood of 150 psi. Taking r_s to be the uniform pressure on the slab surface that would statically develop a unit shear at the slab ends equal to one-fourth the above surface overpressure levels

$$r_s = \frac{0.50\ p(t)}{l_s}$$

Where: h = slab height in inches

p (t) = 400 psi at 360.01, 150 psi at 360.02

l_s = length of slab = 88 inches at 360.01, 82 inches at 360.02

The pressure values expressing rebound stress attributable to anchor-bolt stress r_a, and to soil friction r_s have been converted to the pressures r'_a and r'_s respectively which will give the same values of center moments on the span (center to center of supports). This span was used for computation of the rebound resistance r_r; thus, the values r'_a and r'_s can be used for comparison with r_r.

In Table 4.15 the values of r'_a, r'_s, $r'_a + r'_s$, and r_r are tabulated for each slab. The observed response in rebound is also indicated by a statement as to whether tensile cracking at the top of the slab was noted.

It must be emphasized that the values set upon the quantities discussed (available rebound resistance r_r, required rebound resistance for no cracking assuming adequate anchorage r'_r, and the rebound resistance which could be developed by anchorage $r'_a + r'_s$) are approximate, because the computations for these quantities required the estimation of poorly defined parameters such as the dynamic modulus of rupture of the concrete and the period of the slabs in rebound. At the best, these quantities carry about one significant figure, and r'_r, which is very sensitive to the precise time history of the dynamic response and loading function, is certainly only an order-of-magnitude quantity.

Certain conclusions can be drawn with reliability from the results summarized in

Table 4.15. The low degree of rebound response noted in the project slabs is probably due to the weak uplift anchorage which existed. The calculations indicate that with strong anchorage against uplift, negative moment of a magnitude sufficient to crack the top of the slab would have occurred in most slabs. Thus, in a location where such slabs will be firmly held down, reinforcing steel will be required to aid in carrying the rebound stresses, if cracking in rebound is to be prevented. It appears from the test results that the weak anchorage used was adequate to prevent permanent displacement of the slabs from their supports; where such anchorage techniques are permissible, they appear to offer good protection against rebound failures.

Considerations other than available anchorage resistance limit the accuracy of the technique used to compute r'_r, the rebound resistance required to prevent cracking. Assuming that the natural periods in normal and rebound response were known, it would still be impossible to predict precisely the maximum positive response because of the limited reliability of the resistance function for the slabs and the additional forces of doubtful magnitude acting on the slab through soil pressure at the ends and friction at the supports. The required rebound resistance varys markedly for slight changes in time of maximum positive response because of the change of overpressure with time. In the calculations for r'_r, no attempt was made to take careful account of the overpressure-time variation since the time of maximum response is poorly defined. At both stations, the overpressure decayed very slowly beyond a pressure of about one-third the peak value. The weaker slabs, which underwent large nonelastic positive deflections, may have rebounded in this time region. If such is the case, the r'_r values for these slabs are quite excessive since the value of r'_r becomes significantly reduced when $\dot{o}_m \dot{o}_y$ passes 2.0 and t_d/T exceeds 5.0. The use of the amplification factor $\sqrt{I_r/I}$ (on the values obtained from the charts in Reference 27 for r_r) to account for the change in period of the slabs in rebound is an approximation strictly correct only for response to an impulse loading. The analyses for r'_r do not consider the effects of damping, which would limit rebound. Damping could be particularly significant in cracked slabs.

The values of r_r, available rebound resistance, were computed using a rule-of-thumb $0.15 f'_c$ for the modulus of rupture of the concrete and assuming a homogeneous section of the full cross-sectional area of the slab to be effective. Slabs that yielded during positive deflection and cracked in the region above their midheight would have reduced areas available for carrying tensile stresses and thus a reduced r_r.

Ground movements, depending on their amplitude and timing, could have a major effect on the rebound response—the effects could be detrimental or beneficial, and quite logically different for slabs at the same station. No adequate information is available for determining the effects of ground motion on individual slabs. A general discussion on the possible magnitude of ground-motion effects is given in Section 4.3.5.

4.4 EVALUATION OF RESISTANCE TO OTHER MODES OF FAILURE

4.4.1 General Approach. The evaluation of the strengths of these members in other modes is basically dependent on the analysis of their response in flexure. As in the static case, the desired mode of response is flexure, because the member is far more ductile in this mode than in shear compression, shear anchorage, bond and/or bearing. Also, as in the static case, the objective in the analysis is to determine whether the member should have failed in one of these less desirable modes before reaching its computed flexural strength.

4.4.2 Cracking Strength. As stated in Section 4.1.4, diagonal tension cracks must develop before a member can fail in shear compression or shear anchorage. For that reason the cracking strength of each member was determined, using Equation 4.21. The use of this expression implies two assumptions in the dynamic case: (1) the effect of rapid stress or strain rate on the cracking strength may be accounted for by allowing for an increase in concrete strength only, and (2) if crack formation is a time-dependent phenomenon, sufficient time elapsed during the response of the member to permit the crack to form. These same assumptions are implied in the application of the formulas for shear-compression shear-anchorage, bond and bearing strengths.

The ratio of N to V (axial force to shear at the supports) varies with time as the slab responds. For a first approximation, values for N were obtained from the interaction diagrams for those members that were computed to have yielded under the combined loading condition. Values for V corresponding to the yield moment were obtained from the dynamic-response computations. For those members that did not yield, the maximum values of N and V attained during elastic response were obtained from the response computations. A consistent set of values of N and V may be obtained by iteration, using the value of N corresponding to the computed value of the reaction in each successive computation.

Initially, no allowance was made for an increase in the strength of the concrete due to rapid stress rate, because it is not clear what stress or strain rate is applicable. If an increase in strength of 50 percent is assumed, the cracking strength would be increased by only 22.4 percent, because the cracking strength is expressed as a function of the square root of the concrete strength in Equation 4.21.

The results of these computations shown in Tables 4.16 and 4.17 indicate that inclined cracks should have developed in all members at both stations even if a considerable increase in concrete strength were allowed. However, it should be noted that most of the slabs had span-depth ratios beyond the range for which the expression was stated to be applicable. Even for those slabs whose span-depth ratios were greater than 3.2 the expression appears to be conservative, if it is applicable at all to dynamic response.

4.4.3 Shear-Compression Strength. Equation 4.3 was used to compute the static shear compression strength of each member, recognizing that the validity of the expression has not been established for deep members even under static loads. The effect of the rapid strain rate was computed by using the time to yield or time to maximum elastic deflection, whichever is applicable. It was assumed that if the slab were going to fail in shear compression, the strain in the concrete above the crack must be 0.004 in./in. at the time of yield (or maximum elastic deflection) or earlier. This reasoning led to strain rates of approximately 2 in./in.-sec. From Figure 4.15, the effect of such a straining rate is to increase the strength of the concrete approximately 50 percent.

The computed shear-compression strengths of the members are compared with various computed flexural strengths in Tables 4.18 and 4.19. Note that the computed static shear-compression strength is greater than the computed dynamic yield and ultimate moments (assuming no axial forces acting) with the single exception of Slab 56-4 at Station 560.01. This slab did not appear to be cracked at all and thus could not have failed in shear-compression.

The estimated dynamic shear-compression strengths of the members are greater than the estimated maximum resisting moments attained, except for Slab 44-4. The estimated maximum resisting moment attained is the dynamic yield moment obtained from the interaction diagram for those members that were computed to have yielded under the combined loads, and the maximum elastic resisting moment obtained from the response computations

for those that did not yield under the combined loading.

In these computations, no consideration was given to the effect of the axial loads on the shear-compression strengths of the members, although it is quite likely that the axial loads would increase the shear-compression strengths, as previously discussed. Thus, if Equation 4.3 were applicable to deep beams under dynamic loads, at all it would be conservative when applied to deep members under the loading conditions encountered in these tests.

4.4.1 Shear-Anchorage Analysis. If rotary inertial forces are ignored, the average shear stress on the failure plane at the yield moment (Figure 4.25) may be computed from the following expression:

$$v_a = \frac{T_y - c_f V_y - 0.3 p_y bd'}{b(c + 0.5d')} \qquad (4.42)$$

Where: v_a = average shear stress on the failure plane, psi

T_y = tensile force in the steel at yield, pounds

c_f = coefficient of friction between slab and support, assumed to be 0.5 for these computations

V_y = instantaneous value of the reaction at the yield moment, pounds

b = width of slab, inches

c = width of support, inches

d' = distance from the centroid of the tensile steel to the bottom of the slab, inches

p_y = instananeous value of the overpressure at the surface at the time of yield, psi

Equation 4.42 above ignores the slight increase in pressure assumed to exist between the bottom of the slab and the level of the tensile steel. However, the contribution of the lateral pressure is so small (on the order of 100 psi for the deepest members) that the last term of the numerator may be ignored entirely without seriously affecting the results.

The shear-anchorage capacity of the member may be determined by means of the following expression obtained from Equation 4.4:

$$v_u = kf'_c \left(0.25 + \frac{fb_y}{10^4}\right) \qquad (4.43)$$

Where: v_u = maximum shearing stress capacity of the member, psi

k = a constant expressing the ratio of the strength of the concrete at the rapid stressing rate to the cylinder strength under standard test conditions

f'_c = concrete cylinder strength under standard test conditions, psi

fb_y = instananeous value of the bearing stress at yield, psi

The value of the constant k was determined by computing the rate of stressing in bearing at the supports. It was assumed that there is a linear relationship between shear strength of the concrete at a given stressing rate, and the compressive strength obtained from tests of cylinders at the same stressing rate. Further, it was assumed that the concrete at the failure plane was subjected to the same stressing rate as the concrete at the supports.

The results of these computations are compared with observed response in Tables 4.20 and 4.21. Slabs in the 21, 26, 31, 44, and 56 series did not reach the yield moment under the combined loading according to previous computations. For these slabs, the tensile force in the steel was assumed to be T_d for computation of the shear-anchorage stress by Equation 4.42, and the maximum computed value of the bearing stress was used in Equation 4.43 for computation of v_u. Thus the computed shear-anchorage stresses for these members are probably higher than the stresses attained, whereas the computed capacities are the maximum shear-anchorage stress capacities the members could have attained during response.

According to these computations, none of the slabs should have failed in shear-anchorage, but Slab 28-1 may have done so. When the slab was removed, the concrete below the shear-anchorage failure plane and the principal inclined cracks remained in place on the foundation. Some of the slabs contained vertical web reinforcement, which undoubtedly helped to resist shearing forces at the anchorage. However, the following slabs had no vertical reinforcement and are therefore comparable to 28-1, 36-1, 36-3, 36-4, 44-1, 44-3, and 56-2. Of these, 36-1 and 36-3 developed inclined cracks (at one end only) but did not fail in shear-anchorage. For both, the ratio of the computed average shearing stress attained to the computed shearing-stress capacity was slightly less than for Slab 28-1, but this may not be significant.

The fact that no inclined cracks developed in the other slabs without vertical steel is significant, however, because the development of an inclined crack is a necessary condition for shear-anchorage failure. As previously discussed, it is quite probable that the existence of axial forces prevented inclined crack formation in those members.

In view of these considerations, it is not clear whether Slab 28-1 happened to be weak in shear-anchorage or whether the equations used to analyze the members are not applicable to the dynamic case. It is possible that the failure described occurred during rebound and is not a shear-anchorage failure at all.

The data contained in Table 4.21 for Station 360.02 contains little information of value. With the possible exception of Slab 21-1, none of these members developed inclined cracks.

4.4.5 Bond-Stress Analysis. The average bond stress developed at the anchorage when the tensile steel reaches yield may be computed from the following expression:

$$u_a = \frac{Ty_d}{\Sigma_0 c} \qquad (4.44)$$

Where: u_a = average bond stress, psi

Ty_d = total tensile force in the steel when the dynamic yield point is reached, pounds

Σ_0 = sum of the perimeters of the reinforcing bars, inches

c = support dimension, inches

In addition to assuming that the dynamic yield point was attained in the tensile steel, the above expression presumes the formation of inclined cracks near the supports. While most of the members tested did not exhibit such cracks, some did. By comparing stresses computed in those members which developed inclined cracks (and in which the dynamic yield point may have been reached in the tensile steel) with stresses computed in those members which did not crack, it may be possible to determine whether the latter would have failed in bond before the flexural yield resistance was attained despite the lack of an adequate criterion.

It is not clear whether an allowance should be made for an increase in bond strength because of the rapid stressing rate. Brief consideration of the state of stress in the concrete at the level of the steel above the supports leads to the conclusion that friction between the concrete and the steel may play an important role in determining bond strength. As noted under Section 4.1.4, the stress conditions around the steel in the tests upon which present bond-strength criteria are based are not similar to those encountered at the anchorage in tests of deep members. In view of the foregoing, the stresses computed by Equation 4.44 were compared to the static concrete strengths obtained from standard cylinder tests. The results of these computations are compared with the observed response in Tables 4.22 and 4.23, for members at Stations 360.01 and 360.02, respectively. None of the members showed signs of bond failure at the anchorage.

Because none of the members at Station 360.02 developed inclined cracks, nothing definite can be learned from those computations. However, at Station 360.01 a number of the test slabs did develop inclined cracks. The highest ratio of computed average bond stress to static cylinder strength attained in such a member was 0.273 for Slab 20-1. Because the computed average bearing stress at yield was less for this member than for the others, it is probable that none of the members that did not attain flexural yield resistance would have failed in anchorage. This statement is based on the assumptions that the value of the compressive stress in the concrete at the level of the steel is approximately the same as at the support and that the anchorage bond strength of a member is affected by the value of vertical compressive stress in the concrete at the level of the steel.

4.4.6 Bearing-Stress Analysis. The average value of the bearing stress at any time may be computed by dividing the instantaneous value of the reaction by the area of support. For a member with a elastoplastic resistance function, the reaction is that corresponding to the yield moment. If the yield moment is not attained, then the maximum value of the reaction may be obtained from the dynamic-response computations.

For purposes of comparision with bearing strengths, computed as outlined below, three sets of bearing stresses were computed; those corresponding to the yield moment assuming that the member was subjected to vertically applied forces only (f_{by}), those corresponding to the yield moment assuming the member was subjected to the previously assumed combined loading condition (f_{by_a}), and those corresponding to the maximum value of the reaction assuming the members remained elastic ($f_{b_{max}}$).

For determination of the bearing strengths, it was assumed that the static bearing strength of each member was equal to the concrete cylinder strength for that member. In this manner some allowance was made for the unknown effect of confinement by lateral earth pressure. The stressing rate was computed by dividing the bearing stress by the time required to attain that stress, that is, either the time to yield or the time to maximum elastic deflection. And finally a stress-rate factor was obtained from Figure 4.15.

Note that the stressing rate computed is the average stressing rate during response. A number of investigators have noted that the rate at which the last 50 percent of the load is applied determines the compressive strength of concrete cylinders. Because the stress-time relationship at the support has the general shape of a cosine curve, the use of the average stressing rate may underestimate or overestimate the effect of the dynamic loading on the bearing strength in some cases. However, in view of other unknowns involved in the analysis a more refined determination of the stressing rate hardly seems warranted.

The results of these computations are compared with the observed response in Tables 4.24 and 4.25 for Stations 360.01 and 360.02 respectively. The computed bearing strengths

of the slabs at Station 360.02 were greater than the computed bearing stresses for each of the bases assumed, and there was no evidence of bearing failure or incipient bearing failure. Thus, the computations and the observed response are in relative agreement at Station 360.02.

At Station 360.01, five slabs (36-1, 36-2, 36-3, 36-4, and 44-4) showed evidence of bearing failure or some sign of distress over the support, such as a vertical crack. The computed bearing strengths (Column 5 of Table 4.24) are much greater than the computed bearing stresses assuming vertical loading only (Column 2 of Table 4.24). However, the computed bearing stresses achieved under the assumed combined loading (Column 3 of Table 4.24) are approximately equal to or greater than the computed bearing strengths for Slabs 36-1, 36-2, 36-3, and 36-4 which were cracked at or over the supports. For Slabs 20-1, 28-1, 28-2, 28-3, and 36-5, which showed no signs of cracking at the supports, the computed bearing stresses were lower than the computed bearing strengths. Thus, for these nine members, very good correlation was obtained.

According to previous computations based on the assumed combined loadings, none of the slabs in the 44- and 56-inch series yielded. Therefore, the bearing stresses tabulated in Column 4 of Table 4.24 would apply to those slabs. For those members, the computed maximum bearing stresses were greater than the computed bearing strengths, whereas only Slab 44-4 showed any sign of incipient bearing failure. There are many possible explanations for this discrepancy, including the fact that errors in computing the natural periods for these members would have a greater effect on the value of the maximum reaction than for those slabs with longer periods. The computed periods for slabs in the 44- and 56-inch series are closer to the value of the rise time of the pressure pulse.

It is interesting to note that in the cases of Slabs 36-1 through 36-4 and 44-4, the computed bearing stresses assuming vertical loading only (f_{by}) were considerably less than the static bearing strengths of their respective cylinders. For the computed bearing stresses to be equal to the computed dynamic bearing strengths, the yield resistances of these members would have had to be increased considerably (2 to 5 times). Although base acceleration may account in part for an apparent increase in the flexural resistance of the slabs, it cannot account for the development of higher bearing stresses at the same time. Thus, it can be concluded that: (1) the yield resistances of these members were probably increased by the existence of axial forces, or (2) the cracking observed at the supports was not indicative of high bearing stresses. The cracks must be attributed to some other cause, and Conclusion (1) is more probably correct, because other causes undoubtedly would have resulted in cracks above the supports of some other members as well.

4.4.7 Pure Shear — It is recognized that the state of stress on the vertical section adjacent to the support is not one of pure shear. That term has been used to describe the stress on that section because the internal moment is theoretically zero at that point. In fact, the state of stress on a unit element at any depth in the section is quite complex, which is apparent from consideration of Figure 4.2. The existence of axial loads and inclined cracks further complicates the stress state.

Owing to the complexity of the problem, past effort has been directed toward establishing empirical criteria based on the average shearing stress on the section. Reference 28 recommends that the following expression be used to determine the ultimate average shearing stress at the section, recognizing that it is conservative:

$$v_{su} = 0.135\, f'_c \qquad (4.45)$$

Where: v_{su} = ultimate average shearing stress on the section

f'_c = concrete strength as determined by standard cylinder test

However, as indicated in Table 5-11 of Reference 2, average shearing stresses as high as $0.13\, f'_c$ were developed at the vertical section adjacent to the support of simply supported deep members subjected to uniformly distributed static load without resulting in shear failure.

The average shearing stress on that section at yield was computed by the following expression, which neglects axial load effects, for the one-way slabs tested under Project 5.6:

$$v_{sy} = \frac{l}{d}(0.12\, p_y + 0.38\, r_y) \qquad (4.46)$$

Where: v_{sy} = average shearing stress on the vertical section adjacent to the support when yield stress is reached in the tensile steel

l = clear span

d = effective depth

p_y = instantaneous value of the overpressure on the slab when yield occurs

r_y = yield resistance

The results of these computations are compared with the ultimate stress computed by Equation 4.45, and observed response in Tables 4.26 and 4.27 for Stations 360.01 and 360.02 respectively. Two cases were computed: one assuming the member to be subjected to vertical loading only, and the other assuming the member to be subjected to the combined loading conditions defined in Section 4.3.4. Note that none of the slabs failed in pure shear.

At Station 360.02 none of the computed shearing stresses at yield reached the ultimate average shearing stresses computed by Equation 4.45. However, at Station 360.01 the computed average shearing stress exceeded the computed ultimate average shearing stress in several members even for the case of vertical loading only, as shown in Table 4.26 for Slabs 26-1, 36-1, 36-2, 36-4, 44-1, and 44-2. For the case of the combined loading condition, all of the computed average shearing stresses exceeded the computed ultimate — some by a factor of 2.0.

Slabs in the 44- and 56-inch series did not reach yield according to the previous computations. For these members, the average shearing stress on the section adjacent to the support was computed using the maximum value of the reaction attained during elastic response in the following expression:

$$v_{sm} = \frac{l}{l'}\,\frac{V_{max}}{bd} \qquad (4.47)$$

Where: v_{sm} = maximum value of average shear stress attained during elastic response

l = clear span

l' = effective span (center to center of the supports)

V_{max} = maximum value of the reaction (obtained from elastic response calculations)

b width of slab

d effective depth of slab

It is apparent from these computations that Equation 4.45 is very conservative, if the effect of the axial loads on the flexural yield resistance is accepted. As discussed in Section 4.4.6, there is some evidence to indicate that the yield resistances of these members were increased as indicated.

Further, it is noted that no consideration is given, in Equation 4.45, to the effect of rapid stressing on the strength of the concrete. Assuming that the effect of the stressing rate on the shear strength is proportional to the effect of the stressing rate on the compressive strength of a concrete cylinder, the average shearing stress can be expressed as a function of the dynamic compressive strength. The maximum value obtained for the ratio of the average shearing stress at the support to the dynamic compressive strength of the concrete, in Table 4.26, is 0.203 (Slab 44-3).

In view of the results of the analysis of recent static tests of deep beams of reinforced concrete subjected to uniformly distributed load, the results of these computations, and brief consideration of the effect of the stressing rate, it is believed that the allowable ultimate average shearing stress should be increased for deep slabs or beams subjected to dynamic loads. Although the value of the average stress at which a vertical shear failure will occur has not been established, the available evidence indicates that the present criterion is too conservative.

TABLE 4.1 MEASURED CAPACITY OF BEAMS FROM REFERENCE 9

Beam	Span Depth	f'_c psi	Percentage Reinforcement	Cracking Moment inch-kips	Yield Moment inch-kips	Ultimate Moment inch-kips	Mode of Failure *
D-15	8.85	3,860	1.01	336	371	466	S
D-14	8.85	4,650	1.01	350	395	487	S
D-16	8.85	5,760	1.01	364	480	571	S
D-13	11.07	2,780	1.01	342	330	367	S
D-12	11.07	4,160	1.01	--	489	490	F
D-17	11.07	5,970	1.01	370	--	447	S
D-5	6.64	3,710	1.35	315	442	498	S
D-4	8.85	3,020	1.21	178	510	631	F
D-9	8.85	2,790	3.36	413	--	566	S
D-10	8.85	3,540	3.36	456		625	S
D-11	8.85	5,840	3.36	578	--	795	S
D-7	11.07	2,700	3.36	527	630	632	S
D-6	11.07	3,150	3.36	529	-	702	S
D-1	11.07	4,470	3.36	513	--	626	S
D-2	11.07	5,590	3.36	564	--	744	S
D-8	11.07	6,600	3.36	591	--	829	S
D-3	13.28	4,820	3.36	698	698	761	S
D-18	15.49	4,210	3.36	645		621	S

* S denotes shear compression failure; F denotes flexural failure.

TABLE 4.2 MEASURED CAPACITY OF BEAMS FROM REFERENCE 2

Beam	Span Depth	f'_c psi	Percentage Reinforcement	Cracking Moment inch-kips	Yield Moment inch-kips	Ultimate Moment inch-kips	Mode of [illegible] *
A-1	1.60	3,650	1.10	683	--	1,025	B
A-8-1	1.24	3,130	1.03	600	--	859	B
A-2	1.64	3,100	1.00	273	-	911	B
A-2-2	1.64	3,260	1.00	400	920	921	B
A-2-3	1.64	3,740	2.00	720	--	851	B
A-3	2.32	2,740	1.00	198	370	638	B, A
A-3-1	2.32	3,470	1.00	265	524	638	F
A-3-2	2.32	5,610	1.00	210	480	650	F
A-3-3	2.32	3,160	1.94	400	--	600	B
A-4	3.60	2,110†	1.00	78	204	265	F
A-4-2	3.60	4,400	1.00	91	177	293	F
A-4-3	3.60	2,820	2.20	136	301	327	F
A-5	1.65	3,640	1.00	37	120	133	F
A-6	7.20	2,620	1.00	27	39	66	F

* F denotes flexural failure. B denotes bearing failure. A denotes anchorage failure.
† Cylinder strength estimated.

TABLE 4.3 COMPARISON OF ACTUAL DEFLECTIONS OF DEEP BEAMS WITH DEFLECTIONS COMPUTED BY FLEXURAL THEORY

Beam	Span Depth	Percentage Reinforcement	Yield Load kips	Measured Yield Deflection inch	Computed Yield Deflection inch	Ratio Computed/ Measured
C-1	3.00	1.15	64.5	0.060	0.0679	0.88
C-2	3.00	1.15	61.0	0.056	0.0615	0.91
C-3	3.00	1.15	66.0	0.048	0.0507	0.94
C-4	3.16	1.99	93.5	0.047	0.0428	1.10
C-5	3.16	1.99	93.5	0.091	0.0428	0.47
C-6	3.16	1.99	98.2	0.078	0.0419	0.54
C-7	3.32	2.09	98.6	0.064	0.0419	0.65
D-10	1.00	0.246	12*	0.011	0.0099	0.91
D-12	1.20	0.369	15*	0.025	0.0151	0.60
D-15	1.50	0.513	18*	0.030	0.0176	0.59
D-20	2.00	0.765	36	0.032	0.0218	0.68
D-20-1	2.00	1.43	39*	0.058	0.0257	0.44
D-20	2.00	1.15	39	0.072*	0.0289	0.40
D-40	4.00	0.994	32.5	0.071	0.0145	0.20
D-60	6.00	0.415	12.5	0.066	0.0067	0.10

* Believed to be high, defective gage.

TABLE 4.4 COMPARISON OF ACTUAL DEFLECTIONS WITH COMPUTED DEFLECTIONS USING EQUATION 4.9

Beam	Span Depth	Percentage Tensile Reinforcement	f'_c psi	Yield Load* kips	Computed Yield Deflection † inch	Measured Yield Deflection inch	Ratio Computed/ Measured	Remarks
C-1	3.00	1.15	3,970	64.5	0.058	0.060	0.97	
C-2	3.00	1.15	3,250	61.0	0.055	0.056	0.98	Web reinforcement
C-3	3.00	1.15	3,520	66.0	0.051	0.048	1.13	Web reinforcement
C-4	3.00	1.99	3,650	93.5	0.043	0.047	0.92	
C-5	3.00	1.99	3,060	93.5	0.038	0.091	0.46	Web reinforcement
C-6	3.00	1.99	3,520	98.2	0.035	0.078	0.45	Web reinforcement
C-7	3.00	2.09	3,140	98.6	0.036	0.064	0.62	
D-10	1.00	0.246	4,021	12*	0.011	0.011	1.00	
D-12	1.20	0.439	4,257	15*	0.022	0.025	0.96	
D-15	1.50	0.575	3,548	18*	0.030	0.030	1.00	
D-20	2.00	0.765	2,900	36	0.038	0.032	1.19	
D-20-1	2.00	1.43	4,240	39*	0.067	0.058	1.15	
D-20-2	2.00	0.765	3,026	39	0.038	0.052	1.19	Compression reinforcement
D-20	2.00	1.15	3,650	39	0.053	0.072	0.74	
D-20-1	2.00	1.15	3,979	41	0.055	0.052	1.06	Compression reinforcement
D-40	4.00	0.994	3,731	32.5	0.040	0.071	0.56	
D-60	6.00	0.415	3,106	12.5	0.067	0.066	0.99	

* Ultimate moment in inch-kips equals 9 times the load.

† Relations for computing deflections.

$$\Delta = \int_0^{M_u} \phi \, dM$$

where $\phi = 0.01 + P/b^2 \ldots$ 0.17

TABLE 4.3 COMPARISON OF COMPUTED AND MEASURED CENTER DEFLECTIONS AT ULTIMATE LOAD IN FLEXURE

Beam	Span Depth	Percentage Tension Reinforcement ϕ	Percentage Compressive Reinforcement ϕ'	Yield Load*	Ultimate Load*	Measured Deflection Yield	Measured Deflection Ultimate	Measured Ductility Factor	Computed Ductility Factor Method 1	Computed Ductility Factor Method 1 1	Computed Ductility Factor Method 2 †
				kips	kips	inch	inches				
C1	3.00	1.13	--	64.5	76.2	0.080	0.475	14.6	7.1	11.8	8.7
C2	3.00	1.13	--	61.0	80.2	0.056	0.828	14.8	8.0	12.0	8.7
C3	3.00	1.13	--	60.0	94.2	0.048	0.823	17.1	9.5	16	8.7
C4	3.16	1.19	--	89.5	102.0	0.087	0.412	4.7	3.2	6.0	5.0
C5	3.16	1.19	--	93.8	100.0	0.091	0.512	5.6	2.9	5.3	5.0
C6	3.16	1.19	--	98.2	102.6	0.078	0.350	4.5	3.9	6.3	5.0
C7	3.22	2.19	-	90.6	93.0	0.084	0.352	4.2	3.2	5.3	4.8
D10	1.00	0.246	--	128	253	0.044	0.706	30.5	43	81	20
D20	2.00	0.765	---	96	153	0.033	0.865	26.2	11	24	13.1
D20-2	2.00	0.765	0.493	97	187	0.032	1.855	58	27	42	20
D30-1	3.00	1.15	0.740	61	89	0.052	1.297	24.9	18	28	20
D40	4.00	0.788	---	33	36	0.075	0.604	8.1	7.9	13	10.1
D60	6.00	1.15	-	13	16	0.068	0.602	10.2	14	25	12.3

* Center moment in inch-kips is 5 times the load.

† Method 1 $\mu = \frac{\omega}{\omega_1} + \frac{0.2\,(d')^2}{d}\,(\epsilon_{su} - \epsilon_y)$

Ultimate concrete strain taken at 0.004 in./in. ϵ_y taken as measured yield deflection.

‡ Method 1 Above equation

Ultimate concrete strain taken at 0.008 in./in. ϵ_y taken as measured value.

‡ Method 2 $\mu = \frac{\epsilon_u}{\epsilon_y}\,\frac{10}{\phi - \phi'}$ but less than 20.

TABLE 4.6 COMPUTATIONS OF ULTIMATE AND YIELD DEFLECTIONS IN FLEXURAL RESPONSE UNDER VERTICAL LOADING: MONTE STATION 36+61 ONE-WAY SLABS

f'_c taken as 30×10^6 psi ε_{sy} taken as 0.0021 in/in for f_y 63 ksi.

Slab	Span l' inches	Span Depth l'/d	Area Reinforcement A_s in^2	Percentage Reinforcement ρ	α	Yield Moment M_y 10^6 in-lb	Yield Deflection δ_y inches	Ultimate Moment M_u 10^6 in-lb	Steel Strain at Ultimate Moment ε_{su}	$\varepsilon_{cu} l'/d$ inches	Ultimate Deflection δ_u inches	Ductility Factor μ
20-1	80	4.0	5.97	1.5	0.68	7.859	0.2 8	8.4 8	0.0254	61	1.71	7.8
28-1	80	2.86	.63	1.0	0.72	10.358	0.151	12.059	0.0189	43.8	2.31	15.3
28-2	80	2.86	5.63	1.0	0.72	10.358	0.151	12.117	0.0517	43.8	2.32	16.0
28-3	80	2.86	5.63	1.0	0.72	10.358	0.151	12.076	0.0191	43.8	2.30	15.2
36-1	80	2.22	8.84	1.0	0.61	18.023	0.137	20.736	0.0195	33.5	1.82	13.3
36-2	80	2.22	8.84	1.0	0.61	18.023	0.137	20.790	0.0508	33.5	1.87	13.7
36-3	80	2.22	5.63	0.65	0.71	13.084	0.114	16.005	0.0059	33.5	2.37	20.8
36-4	80	2.22	12.82	1.5	0.47	25.646	0.175	29.099	0.0301	33.5	1.17	6.7
36-5	80	2.22	1.12	0.3	0.97	9.161	0.088	11.102	0.0912	33.5	2.25	37.0
44-1	80	1.82	10.61	1.0	0.54	20.435	0.127	30.225	0.0462	29.1	1.11	11.3
44-2	80	1.82	7.956	0.75	0.65	20.068	0.107	23.358	0.0077	29.1	2.02	18.9
44-3	80	1.82	5.304	0.50	0.85	13.602	0.083	16.306	0.0925	29.1	2.70	32.5
44-4	80	1.82	2.652	0.25	1.36	6.948	0.053	9.070	0.1500 *	29.1	4.05	88.0
56-1	80	1.43	6.63	0.50	0.74	21.660	0.075	26.276	0.1013	22.8	2.33	31.1
56-2	80	1.43	6.63	0.50	0.74	21.660	0.075	26.170	0.0975	22.8	2.15	28.7

* Steel at rupture.

TABLE 3.3 COMPUTATIONS OF ULTIMATE AND YIELD DEFLECTIONS IN FLEXURAL RESPONSE UNDER VERTICAL LOADING ALONE: STATION 760.02 ONE-WAY SLABS

E_s taken as 30 $\times 10^6$ psi ε_{sy} taken as 0.0021 in/in for f_y = 63 ksi.

Slab	Span ℓ' inches	Span Depth ℓ'/d	Area Reinforcement A_s in²	Percentage Reinforcement ρ	α	Yield Moment M_y $\times 10^6$ in-lb	Yield Deflection δ_y inches	Ultimate Moment M_u $\times 10^6$ in-lb	Steel Strain at Ultimate Moment ε_{su}	Ultimate Deflection δ_u inches	Ductility Factor μ
11-1	77	7.00	3.078	1.3	0.93	2.425	0.207	2.684	0.0252	2.737	10.33
16-1	77	4.82	3.078	1.0	1.00	3.302	0.175	4.038	0.0370	2.766	15.84
16-2	77	4.82	5.746	1.3	0.76	5.056	0.226	5.649	0.0257	1.978	8.75
16-3	77	4.82	5.746	1.3	0.76	5.086	0.226	5.642	0.0253	1.948	8.62
21-1	77	3.67	4.862	1.0	0.84	5.807	0.159	6.695	0.0540	3.092	19.44
21-2	77	3.67	4.862	1.0	0.84	5.807	0.159	6.651	0.0478	2.742	17.24
21-3	77	3.67	2.652	0.5	1.31	3.240	0.102	3.859	0.0363	3.687	36.87
21-4	77	3.67	2.652	0.5	1.31	3.240	0.102	3.837	0.0361	3.650	37.55
21-5	77	3.67	7.311	1.5	0.61	8.751	0.204	9.750	0.0274	4.054	8.01
21-6	77	3.67	3.078	0.75	1.02	4.775	0.119	5.472	0.0522	3.913	26.75
26-1	77	2.96	4.862	0.75	0.89	7.242	0.122	8.438	0.0628	4.837	11.69
26-2	77	2.96	3.091	0.5	1.07	4.684	0.103	5.578	0.0869	3.966	38.53
26-3	77	2.96	6.188	1.0	0.73	9.095	0.147	10.290	0.0379	1.779	12.10
31-1	77	2.48	3.536	0.5	1.04	6.393	0.089	7.643	0.0905	3.477	39.07
31-2	77	2.48	3.536	0.5	1.04	6.399	0.089	7.710	0.1081	4.137	46.48

TABLE 4.8 COMPUTATIONS FOR ULTIMATE MOMENT IN FLEXURE UNDER UNIFORM VERTICAL LOADING ALONE FOR ONE-WAY SLABS

Ultimate compressive strain of concrete ϵ_u 0.004 in in

k_1 0.85 k_2 0.42 $\epsilon_s \quad \frac{0.004\ (k_1\ k_2\ f'_c - p\ f_s)}{p\ f_s}$

f_s 90 ϵ_s · 62.82

k_3 taken from Figure 4.15, using a strain rate obtained by assuming ϵ_u to be attained in one quarter the slab period.

Slab	Period T	Reinforcement Ratio p A_s /bd	k_3	f'_c	f_s	k_u ϵ_u ϵ_u · ϵ_s	Ultimate Moment M_u $f_s A_s d$ (1 − k_2 k_u)
	10^{-3} sec			psi	ksi		10^6 in-lb
20-1	8.5	0.0147	1.53	5,410	65.11	0.136	8.498
28-1	7.1	0.0098	1.54	6,679	67.22	0.076	12.079
28-2	7.1	0.0098	1.54	6,900	67.37	0.072	12.147
28-3	7.1	0.0098	1.54	6,571	67.15	0.077	12.076
36-1	5.9	0.0102	1.55	6,845	67.19	0.075	20.736
36-2	5.9	0.0102	1.55	7,020	67.30	0.0729	20.790
36-3	6.2	0.0077	1.55	6,832	68.56	0.057	16.005
36-4	5.5	0.0148	1.57	6,180	65.52	0.0904	29.099
36-5	6.6	0.0051	1.54	6,310	70.63	0.0421	11.102
44-1	5.2	0.0100	1.57	6,208	66.91	0.0796	30.225
44-2	5.5	0.0075	1.57	6,744	68.72	0.0558	23.558
44-3	5.9	0.0050	1.55	6,238	70.76	0.0432	16.306
44-4	6.6	0.0025	1.54	6,614	Rupture	0.0227	9.050
56-1	4.9	0.0049	1.58	6,586	71.43	0.0394	26.266
56-2	4.9	0.0049	1.58	6,328	71.13	0.0410	26.130
11-1	12.3	0.0150	1.49	5,628	65.09	0.137	2.6[illegible]
16-1	10.1	0.0104	1.51	5,443	66.11	0.0975	4.038
16-2	9.45	0.015	1.52	5,609	65.13	0.1346	5.649
16-3	9.45	0.015	1.52	5,535	65.10	0.1365	5.642
21 1	8.3	0.0093	1.53	6,882	67.57	0.0740	6.695
21-2	8.3	0.0093	1.53	6,117	67.04	0.0773	6.654
21-3	9.3	0.0053	1.52	6,587	70.55	0.0424	3.859
21-4	9.3	0.0053	1.52	6,273	70.22	0.0444	3.847
21-5	7.7	0.0149	1.54	5,821	65.28	0.1274	9.750
21-6	8.7	0.0079	1.52	5 654	67.42	0.0713	5.[illegible]
26-1	7.4	0.0078	1.54	6,688	68.35	0.0596	8.438
26-2	8.3	0.0050	1.53	5,932	70.29	0.0440	5.578
26 3	7.1	0.0099	1.54	5,203	66.20	0.0557	10.229
31-1	6.9	0.0048	1.54	5,917	70.59	0.0422	7.645
31-2	6.9	0.0048	1.54	6,692	72.52	0.0357	7.710

TABLE 4.9 COMPARISONS OF COMPUTED FLEXURAL RESPONSE UNDER VERTICAL LOADING ALONE WITH OBSERVED RESPONSE: STATION 360.01 ONE-WAY SLABS

Slab	Computed Parameters: Yield Resistance r_y	Computed Parameters: Ultimate Resistance r_u	Computed Parameters: Ductility Factor μ	Computed Response: Maximum Deflection / Yield Deflection δ_m/δ_y	Observed Response	Residual Deflection* / Yield Deflection
	psi	psi				
20-1	408	442	7.8	Failure	Extensive vertical cracks	1.1
28-1	549	628	15.5	Failure	Failure, not in flexure	N A
28-2	549	633	16.0	Failure	Midspan vertical cracking	0.7
28-3	549	628	15.2	Failure	Midspan vertical cracking	0.7
36-1	940	1,080	13.3	6.5	Inclined cracking No center vertical cracking	0.3
36-2	940	1,082	13.7	6.5	No cracking	0
36-3	712	835	20.8	Failure	Inclined cracking No center vertical cracking	0.3
36-4	1,337	1,515	6.7	1.8	No cracking	0.1
36-5	477	575	37.0	Failure	Midspan vertical cracking	1.4
44-1	1,379	1,573	11.1	1.6	No cracking	−0.3
44-2	1,043	1,228	15.9	4.4	No cracking	−0.1
44-3	710	850	32.5	26	Midspan vertical cracking	0.2
44-4	362	471	88.0	Failure	Midspan vertical cracking	1.3
56-1	1,130	1,368	31.1	3.7	No cracking	0
56-2	1,139	1,360	[illegible]	3.7	No cracking	−0.4

* From posttest survey data.

TABLE 4.10 COMPARISONS OF COMPUTED FLEXURAL RESPONSE UNDER VERTICAL LOADING ALONE WITH OBSERVED RESPONSE: STATION 360.01 ONE-WAY SLABS

Slab	Computed Parameters: Yield Resistance r_y	Computed Parameters: Ultimate Resistance r_u	Computed Parameters: Ductility Factor μ	Computed Response: Maximum Deflection / Yield Deflection δ_m/δ_y	Observed Response	Residual Deflection* / Yield Deflection
	psi	psi				
11-1	136	151	10.3	Failure	Light midspan crack	+0.1
16-1	202	227	15.8	6.6	No cracking	−0.1
16-2	286	317	8.8	1.8	No cracking	+0.3
16-5	286	317	8.4	1.8	Light midspan vertical crack	+0.1
21-1	326	376	19.4	1.3	Light vertical cracking	−0.1
21-2	326	374	17.2	1 3	No cracking	+0.1
21 3	182	217	49.8	14	Light vertical cracking	+0.3
21-4	182	217	47.6	14	Light vertical cracking	+0.3
21-5	492	547	8.0	No yield	Slight vertical crack, one side	+0.05
21-6	268	307	26.8	2.2	Slight vertical crack, one side	0
26-1	407	474	41.7	1.05	No cracking	+0.3
26-2	263	313	38.5	2.2	No cracking	0
26-3	510	579	12.1	No yield	No cracking	−0.2
31-1	359	429	39.1	1.15	Possibly cracked, one side	+0.2
31-2	359	433	46.5	1.15	No cracking	−0.2

* From posttest survey data.

TABLE 4.11 COMPARISON OF COMPUTED FLEXURAL RESPONSE, UNDER COMBINED BENDING AND AXIAL LOADS, WITH OBSERVED RESPONSE: STATION 360.01 ONE WAY SLABS

Slab	Yield * Resistance r_y psi	Computed Response θ_m/θ_y	Observed Response	Residual Deflection † / Yield Deflection θ_m/θ_y
20-1	583	Failure	Extensive vertical cracking	1.1
28-1	990	6.5	Shear-anchorage failure	N.A
28-2	990	6.5	Inclined and vertical cracking	0.7
28-3	990	6.5	Inclined and vertical cracking	0.7
36-1	1,833	1.1	Inclined cracking, one end	0.3
36-2	1,833	1.1	Corner cracked, one support	0
36-3	1,677	1.25	Inclined cracking, one end	0.3
36-4	1,901	1.1	No visible cracks	0.1
36-5	1,526	1.5	Inclined and vertical cracking	1.4
44-1		No yield	No visible cracks	−0.3
44-2		No yield	No visible cracks	−0.1
44-3		No yield	One crack at midspan	0.2
44-4		No yield	Fine inclined and vertical cracking	1.3
56-1		No yield	No visible cracks	0
56-2		No yield	No visible cracks	−0.4

* From interaction diagrams. † From posttest survey data.

TABLE 4.12 COMPARISON OF COMPUTED FLEXURAL RESPONSE, UNDER COMBINED BENDING AND AXIAL LOAD, WITH OBSERVED RESPONSE: STATION 360.02 ONE-WAY SLABS

Slab	Yield * Resistance r_y psi	Computed Response θ_m/θ_y	Observed Response	Residual Deflection † / Yield Deflection
11-1	164	Failure	One light midspan crack	0.1
16-1	298	1.6	No visible cracks	−0.1
16-2	354	1.2	No visible cracks	−0.3
16-3	354	1.2	One light midspan crack	0.1
21-1	—	No yield	Very light vertical cracking	−0.1
21-2	—	No yield	No visible cracks	0.1
21-3	354	1.2	Light vertical cracking	−0.3
21-4	354	1.2	Light vertical cracking	0.3
21-5	—	No yield	Short vertical crack, one side	0.03
21-6	—	No yield	Short vertical crack, one side	0
26-1	—	No yield	No visible cracks	0.3
26-2	—	No yield	No visible cracks	0
26-3	—	No yield	No visible cracks	−0.2
31-1	—	No yield	Possibly cracked, one side	0.2
31-2	—	No yield	No visible cracks	−0.2

* From interaction diagrams. † From posttest survey data.

TABLE 4.13 THE EFFECTS OF FOUNDATION ACCELERATION UPON THE SLAB RESISTANCE REQUIRED TO MAINTAIN ELASTICITY

All measurements in psi.

Station	Slab	Case *	Required Positive Resistance + r	Required Negative Resistance − r	Available Positive Resistance + r	Available Negative Resistance − r
360.01	36-4	1	1,970	−970	1,337	−300
		2	1,330	−150	1,337	−300
		3	2,450	−1,350	1,337	−300
360.02	21-2	1	108	−210	326	−115
		2	332	−112	326	−115
		3	620	−106	326	−115

* Case 1: Station pressure pulse, no acceleration pulse. Case 2: Station pressure pulse and acceleration pulse beginning at airblast arrival. Case 3: Station pressure pulse and acceleration pulse beginning 2×10^{-3} second after airblast arrival.

TABLE 4.14 REBOUND RESISTANCE OF PROJECT SLABS

f_r modulus of rupture $= 0.15\ f'_c$, psi; h height of slab, inches; b width of slab, inches; I_r moment of inertia in rebound $= \frac{1}{12} bh^3$ in^4; r_r rebound resistance $= 16\ I_r/bh\ l^2 = 0.15\ f'_c$, psi.

360.01 slabs

b Slab	24 inches h in	f'_c psi	l 80 inches I_r in^4	r_r psi
20-1	22.5	5,410	22,800	85
28-1	30.5	6,679	56,800	194
28-2	30.5	6,900	56,800	200
28-3	30.5	6,571	56,800	191
36-1	39.5	6,845	123,000	332
36-2	39.5	7,020	123,000	341
36-3	39.5	6,832	123,000	332
36-4	39.5	6,180	123,000	300
36-5	39.5	6,425	123,000	312
44-1	47.5	6,510	214,000	444
44-2	47.5	6,208	214,000	426
44-3	47.5	6,744	214,000	474
44-4	47.5	6,238	214,000	445
56-1	58.5	6,614	400,000	706
56-2	58.5	6,586	400,000	704

360.02 slabs

b Slab	24 inches h in	f'_c psi	l 77 inches I_r in^4	r_r psi
11-1	12.5	5,628	3,900	30
16-1	18.5	5,443	12,600	63
16-2	18.5	5,609	12,600	65
16-3	18.5	5,535	12,600	64
21-1	23.5	6,882	26,000	129
21-2	23.5	6,117	26,000	115
21-3	23.5	6,587	26,000	123
21-4	23.5	6,273	26,000	117
21-5	23.5	5,327	26,000	100
21-6	23.5	5,634	26,000	106
26-1	28.5	6,658	46,300	184
26-2	28.5	5,973	46,300	167
26-3	28.5	5,203	46,300	145
31-1	32.5	5,917	68,600	211
31-2	32.5	6,692	68,600	238

TABLE III-6 COMPARISONS OF AVAILABLE REBOUND RESISTANCE AND REQUIRED REBOUND RESISTANCE FOR ONE-WAY SLABS

All resistance measurements in psi.

Slab	Available Resistance *	Required Resistance r'_f †	r'_a ‡	r'_s §	r'_a	r'_s ¶	Observed Rebound Response**	Web Reinforcement	Cracked Above Midheight	Remarks
Station 360.01 One-Way Slabs										
20-1	87	260	55	61	116		Yes	Yes	Yes	
28-1	191	440	55	84	139		Yes	Yes	Yes	
28-2	200	450	55	84	139		Yes	Yes	Yes	
28-3	191	470	55	84	139		Yes	Yes	Yes	
36-1	332	640	55	108	163		No	No	Yes	
36	311	640	55	108	163		No	Yes	No	One anchor bolt loosened at foundation
36-3	332	650	55	108	163		No	No	Yes	
36-4	306	750	55	108	163		No	No	No	Two anchor bolts loosened at foundation
36-5	307	920	55	108	163		Yes	Yes	Yes	
44-1	411	1,370	55	130	185		No	No	No	
44-2	430	650	55	130	185		No	Yes	No	
44-3	471	900	55	130	185		No	No	Yes	
44-4	445	1,030	55	130	185		No	Yes	Yes	
56-1	706	800	55	162	217		No	Yes	No	
56-2	704	800	55	162	217		No	No	No	
Station 360.02 One-Way Slabs										
11-1	30	60	59	12	71		No	Yes	Yes	
16-1	63	85	59	20	79		No	Yes	No	
16-2	65	150	59	20	79		No	No	No	
16-3	64	150	59	20	79		No	Yes	No	
21-1	129	250	59	24	83		No	No	Yes	
21-2	115	250	59	24	83		No	Yes	No	
21-3	123	190	59	24	83		No	Yes	Yes	
21-4	117	280	59	24	83		No	No	No	
21-5	109	420	59	24	83		No	No	No	
21-6	105	170	59	24	83		No	Yes	No	
26-1	184	410	59	30	89		No	Yes	No	
26-2	163	200	59	30	89		No	No	No	
26-3	143	470	59	30	89		No	No	No	
31-1	211	360	59	34	93		No	Yes	No	
31-2	238	360	59	34	93		No	No	No	

* Available resistance to rebound of slab, r_f.

† Required rebound resistance for slab fully anchored against uplift from supports, r'_f.

‡ Required rebound resistance for slab anchored against uplift from supports by anchor bolts alone, r'_a.

§ Required rebound resistance for slab anchored against uplift from supports by soil friction alone, r'_s.

¶ Required rebound resistance for slab anchored against uplift from support by anchor bolts and soil friction, $r'_a + r'_s$.

** Observed rebound response, slab cracked at top.

TABLE [illegible] COMPARISON OF COMPUTED CRACKING STRENGTH WITH OBSERVED RESPONSE: STATION 360,01 ONE-WAY SLABS

Slab	Static Cracking Strength V_c [illegible]	Maximum Reaction V 10^3 lb	Cracking Strength / Maximum Reaction	Observed Response
[illegible]	1,987	7.41	0.27	Inclined crack, one end only
28-1	2,780	11.10	0.25	Inclined cracks, both ends
28-2	2,780	11.10	0.25	Inclined cracks, both ends
28-3	2,780	11.10	0.25	Inclined cracks, both ends
36-1	3,682	16.9	0.22	Inclined crack, one end only
36-2	3,720	16.9	0.22	No inclined cracking
36-3	3,523	16.1	0.22	Inclined crack, one end only
36-4	3,803	17.2	0.22	No cracking
36-5	3,243	15.4	0.21	Inclined cracks, both ends
41-1	4,417	18.9	0.23	No cracking
41-2	4,176	18.9	0.22	No cracking
41-3	4,149	19.0	0.22	No inclined cracking
41-4	3,798	20.2	0.19	Inclined cracks, both ends
56-1	5,363	20.9	0.26	No cracking
56-2	5,363	20.9	0.26	No cracking

TABLE 4.17 COMPARISON OF COMPUTED CRACKING STRENGTH WITH OBSERVED RESPONSE: STATION 360,02 ONE-WAY SLABS

Slab	Static Cracking Strength, Ve 10^3 lb	Maximum Reaction, V 10^3 lb	Cracking Strength / Maximum Reaction	Observed Response
11-1	0,873	1.76	0.50	No inclined cracking
16-1	1.29	2.95	0.44	No cracking
16-2	1.42	3.43	0.41	No cracking
16-3	1.41	3.43	0.41	No inclined cracking
21-1	1.99	4.04	0.49	Possible inclined crack, one end only
21-2	1.88	4.04	0.47	No cracking
21-3	1.79	3.55	0.50	No inclined cracking
21-4	1.74	3.55	0.49	No inclined cracking
21-5	2.08	4.04	0.50	No inclined crack[illegible]
21-6	1.72	4.04	0.43	No inclined cracking
26-1	2.40	4.20	0.[illegible]	No cracking
[illegible]	2.50	4.19	[illegible].46	No cracking
26-3	2.22	4.20	0.5[illegible]	No cracking
31-1	2.64	4.32	0.61	No inclined cracking
31-2	2.80	4.32	0.65	No cracking

TABLE 4.18 COMPARISON OF COMPUTED SHEAR COMPRESSION STRENGTHS OF SLABS WITH VARIOUS COMPUTED FLEXURAL STRENGTHS: STATION 360.62 ONE-WAY SLABS

All measurements in 10^6 in-lb

Slab	Static Shear Compression Strength, M'_s	Estimated Dynamic Shear Compression Strength, 1.5 M'_s	Dynamic Yield Moment, No Axial Loads, M_y	Dynamic Ultimate Moment, No Axial Loads, M_u	Dynamic Yield Moment with Axial Loads, M_{ya}	Maximum Resisting Moment Attained
20-1	9.33	14.0	7.8	8.5	11.2	11.2
28-1	15.8	23.1	10.7	12.1	19.0	19.0
28-2	15.8	23.9	10.5	12.1	19.0	19.0
28-3	15.1	22.7	10.5	12.1	19.0	19.0
34-1	25.5	38.2	18.8	20.7	33.2	33.2
34-2	25.1	37.7	18.9	20.8	33.2	33.2
34-3	22.6	33.9	14.7	16.0	32.2	32.2
36-1	21.9	32.9	25.6	29.1	36.5	36.5
36-3	19.8	29.7	9.2	11.1	29.3	29.3
41-1	20.2	30.3	20.4	29.2	32.0 *	35.2 †
41-2	21.2	31.8	20.1	23.6	35.0 *	37.1 *
41-3	28.8	43.2	12.6	16.3	37.5 *	37.5 †
41-4	21.2	31.8	6.9	9.1	30.5 *	38.0 †
36-1	45.6	68.2	21.7	29.3	60.0 *	76.2 †
36-2	45.4	68.0	21.7	29.1	60.0 *	36.2 †

* Extrapolated on interaction diagrams.

† Obtained from calculations of elastic response under combined bending and axial loads.

TABLE 4.19 COMPARISON OF COMPUTED SHEAR-COMPRESSION STRENGTHS OF SLABS WITH VARIOUS COMPUTED FLEXURAL STRENGTHS: STATION 360.62 ONE-WAY SLABS

All measurements in 10^6 in-lb

Slab	Static Shear Compression Strength, M'_s	Estimated Dynamic Shear Compression Strength, 1.5 M'_s	Dynamic Yield Moment, No Axial Loads, M_y	Dynamic Ultimate Moment, No Axial Loads, M_u	Dynamic Yield Moment with Axial Loads, M_{ya}	Maximum Resisting Moment Attained
11-1	2.89	4.32	2.43	2.68	2.92	2.92
16-1	5.25	7.89	3.39	4.04	5.3	5.3
16-2	6.05	9.08	3.10	3.65	6.3	6.3
16-3	5.97	8.96	4.19	5.61	6.3	6.3
21-1	8.41	12.62	5.81	6.70	9.8 *	7.27 †
21-2	8.33	12.50	5.81	6.65	9.6 *	7.27 †
21-3	6.34	9.67	3.21	3.86	6.3	6.3
21-4	6.73	10.10	3.21	3.86	6.3	6.3
21-5	10.29	15.39	8.73	9.73	12.5 *	7.27 †
21-6	8.09	12.14	4.78	5.17	8.0 *	7.27 †
26-1	12.11	18.17	7.21	8.44	15.0 *	7.29 †
26-2	9.96	14.94	4.46	5.38	11.8 *	7.27 †
26-3	11.1	16.76	9.10	10.25	9.1 *	7.29 †
31-1	13.88	20.82	6.29	7.65	16.2 *	7.19 †
31-2	14.0	21.0	6.10	7.71	16.2 *	7.19 †

* Extrapolated on interaction diagrams.

† Obtained from calculations of elastic response under combined bending and axial loads.

TABLE 4.20 COMPARISON OF COMPUTED SHEAR-ANCHORAGE STRESSES AT YIELD MOMENT WITH COMPUTED SHEAR-ANCHORAGE STRESS CAPACITIES AND OBSERVED RESPONSE: STATION 300+1 ONE-WAY SLABS

Stress measurements in psi.

Slab	Shear-Anchorage Stress at Yield v_a	Shear Anchorage Stress Capacity v_u	v_a/v_u	Observed Response	Web Reinforcement
29-1	3,650	5,150	0.71	Vertical and inclined cracking, one end only	Yes
29-1	4,250	8,320	0.53	Apparent shear-anchorage failure	No
29-2	4,250	8,250	0.52	Vertical and inclined cracking, both ends	Yes
29-3	4,250	8,180	0.51	Vertical and inclined cracking, both ends	Yes
36-1	6,750	13,660	0.50	Bearing crack at one support inclined cracking, one end only	No
36-2	6,750	14,010	0.48	Bearing crack at one support	Yes
36-3	5,810	12,600	0.46	Inclined cracking, one end	No
36-4	8,010	12,610	0.64	Corner cracked at support	No
36-5	4,810	10,750	0.45	Vertical and inclined cracking, both ends	Yes
44-1*	7,400	13,110	0.56	None	No
44-2	6,500	14,310	0.45	None	Yes
44-3	6,280	[illegible]	0.47	Vertical crack at midspan	No
44-4	5,700	11,150	0.40	Vertical and inclined cracking, both ends	Yes
56-1*	6,940	14,620	0.49	None	Yes
56-2	6,940	13,480	0.51	None	No

* Slabs in 44 and 56 series did not yield. Computed shear-anchorage stresses are probably higher than those attained.

TABLE 4.21 COMPARISON OF COMPUTED SHEAR-ANCHORAGE STRESSES AT YIELD MOMENTS WITH COMPUTED SHEAR-ANCHORAGE STRESS CAPACITIES AND OBSERVED RESPONSE: STATION 300.92 ONE-WAY SLABS

Stress measurements in psi.

Slab	Shear-Anchorage Stress at Yield v_a	Shear Anchorage Stress Capacity v_u	v_a/v_u	Observed Response	Web Reinforcement
11-1	2,435	3,151	0.779	Light vertical midspan crack	Yes
16-1	2,652	3,911	0.678	None	Yes
16-2	2,356	4,241	0.556	None	No
16-3	2,356	4,150	0.570	Short vertical crack at midspan	Yes
21-1*	3,285	3,646	0.901	Light vertical cracking	No
21-7	2,385	3,819	0.675	None	Yes
21-3	2,297	3,972	0.453	Light vertical cracking	Yes
21-1	2,297	4,979	0.470	Light vertical cracking	No
21-5	4,502	4,773	0.943	Short light crack at midspan	No
21-6	3,017	4,630	0.650	Short light crack at midspan	Yes
26-1*	3,442	5,610	0.613	None	Yes
26-2	2,47	4,974	0.542	None	No
26-3	3,700	5,371	0.913	None	No
31-1*	3,700	5,832	0.629	Possible light crack at midspan	Yes
31-2	3,180	5,715	0.556	None	No

* Slabs in 21, 26, and 31 series did not yield.

TABLE 4.22 COMPARISON OF COMPUTED AVERAGE BOND STRESS WITH CYLINDER STRENGTH AND OBSERVED RESPONSE: STATION 360.01 ONE-WAY SLABS

Slab	Average Bond Stress u_a psi	Cylinder Strength f'_c psi	u_a/f'_c	Observed Response
20-1	1,477	5,410	0.273	Vertical and inclined cracking, one end only
28-1	1,477	6,679	0.221	Apparent shear-anchorage failure
28-2	1,477	6,900	0.214	Vertical and inclined cracking, both ends
28-3	1,477	6,571	0.225	Vertical and inclined cracking, both ends
36-1	1,477	6,845	0.216	Bearing crack at one support inclined cracking, one end only
36-2	1,477	7,020	0.210	Bearing crack at one support
36-3	1,477	6,852	0.216	Inclined cracking, one end
36-4	1,477	6,180	0.239	Corner cracked at support
36-5	1,478	6,310	0.234	Vertical and inclined cracking, both ends
44-1	1,478	6,209	0.238	None
44-2	1,477	6,744	0.219	None
44-3	1,478	6,238	0.237	Vertical crack at midspan
44-4	1,478	6,614	0.223	Vertical and inclined cracking, both ends
56-1	1,477	6,566	0.224	None
56-2	1,477	6,329	0.233	None

TABLE 4.23 COMPARISON OF COMPUTED AVERAGE BOND STRESS WITH CYLINDER STRENGTH AND OBSERVED RESPONSE: STATION 360.02 ONE-WAY SLABS

Slab	Average Bond Stress u_a psi	Cylinder Strength f'_c psi	u_a/f'_c	Observed Response
11-1	2,364	5,625	0.420	Vertical crack at midspan
16-1	2,364	5,442	0.434	None
16-2	2,364	5,600	0.421	None
16-3	2,364	5,535	0.427	Vertical crack at midspan, one side
21-1	2,364	6,882	0.344	Light vertical cracking
21-2	2,364	6,415	0.368	None
21-3	2,364	6,587	0.359	Light vertical cracking
21-4	2,364	6,273	0.377	Light vertical cracking
21-5	2,364	5,821	0.418	Short vertical crack at midspan
21-6	2,364	5,654	0.418	Short vertical crack at midspan
26-1	2,364	6,666	0.353	None
26-2	2,364	5,932	0.399	None
26-3	2,364	5,203	0.454	None
31-1	2,364	5,917	0.400	Possible vertical crack at midspan
31-2	2,364	6,692	0.353	None

TABLE 4.24 COMPARISON OF VARIOUS COMPUTED BEARING STRESSES WITH COMPUTED BEARING STRENGTHS AND OBSERVED RESPONSE FOR ONE-WAY SLABS AT STATION 360.0

All measurements in psi.

Slab	Bearing Stress at Yield with No Axial Loads, f_{by}	Bearing Stress at Yield with Axial Load, f_{by_a}	Maximum Bearing Stress Elastic Response $f_{b_{max}}$	Bearing Strength P_b	Observed Response in Bearing
20-1	3,250	4,925	10,870	8,250	None
28-1	3,410	6,281	11,380	10,250	None
28-2	3,410	6,281	11,380	10,325	None
28-3	3,410	6,281	11,380	10,060	None
36-1	5,270	11,250	11,800	10,470	Typical bearing failure, one end
36-2	5,270	11,250	11,800	10,730	Typical bearing failure, one end
36-3	4,410	10,218	12,000	10,450	Corner off one end
36-4	6,750	11,615	11,750	9,460	Corner off one end
36-5	3,310	9,396	12,150	9,650	None
44-1	6,940		12,080	9,500	None
44-2	5,680		12,150	10,300	None
44-3	4,400		12,220	9,540	None
44-4	3,080		12,000	10,120	Vertical crack over support, one end
56-1	5,980		12,300	10,080	None
56-2	5,999		12,300	9,650	None

TABLE 4.25 COMPARISON OF VARIOUS COMPUTED BEARING STRESSES WITH COMPUTED BEARING STRENGTHS AND OBSERVED RESPONSE FOR ONE-WAY SLABS AT STATION 360.0

All measurements in psi.

Slab	Bearing Stress at Yield with No Axial Loads, f_{by}	Bearing Stress at Yield with Axial Load, f_{by_a}	Maximum Bearing Stress Elastic Response $f_{b\ max}$	Bearing Strength P_b	Observed Response in Bearing
11-1	1,666	1,569	3,149	7,890	None
16-1	1,152	2,556	3,230	7,618	None
16-2	2,548	2,956	3,330	7,450	None
16-3	2,548	2,956	3,330	7,750	None
21-1	2,779	—	3,440	8,640	None
21-2	2,779	—	3,465	8,360	None
21-3	1,935	1,956	3,450	8,250	None
21-4	1,935	2,956	3,450	8,780	None
21-5	—	—	3,460	8,150	None
21-6	2,440	—	3,460	7,950	None
26-1	2,266	—	3,500	8,000	None
26-2	2,410	—	3,500	8,200	None
26-3	—	—	3,600	7,200	None
31-1	3,664	—	3,700	8,250	None
31-2	3,761	—	3,700	8,260	None

TABLE 4.26 COMPARISON OF COMPUTED AVERAGE SHEARING STRESS AT SUPPORTS, AT YIELD, WITH ULTIMATE CONCRETE STRENGTH AND OBSERVED RESPONSE. STATION 360.01

All measurements in psi.

Slab	Computed Average Shearing Stress Vertical Load Only v_{sy}	Computed Average Shearing Stress Combined Loading v_{sy}	Computed Ultimate Shearing Stress Equation 4.45 v_{su}	Computed Ultimate Concrete Strength Allowing for Rapid Stressing $k_3 f'_c$	Observed Response in Shear
20-1	920	1,231	730	8,280	None
28-1	729	1,274	902	10,200	None
28-2	729	1,274	932	10,550	None
28-3	729	1,274	897	10,069	None
36-1	953	1,634	924	10,476	None
36-2	953	1,634	918	10,730	None
36-3	868	1,514	922	10,450	None
36-4	1 255	1,684	834	9,460	None
36-5	380	1,400	854	9,650	None
11-1	1,055	1,893 *	852	9,500	None
11-2	849	1,598 *	838	10,500	None
11-3	659	1,956 *	810	9,540	None
11-4	423	1,988 *	842	10,120	None
36-1	707	1,505 *	893	10,080	None
36-2	707	1,505 *	889	9,650	None

* Computed using v_{max} from elastic response computations.

TABLE 4.27 COMPARISON OF COMPUTED AVERAGE SHEARING STRESS AT SUPPORTS, AT YIELD, WITH ULTIMATE CONCRETE STRENGTH AND OBSERVED RESPONSE. STATION 360.02

All measurements in psi.

Slab	Computed Average Shearing Stress Vertical Load Only v_{sy}	Computed Average Shearing Stress Combined Loading v_{sy}	Computed Ultimate Shearing Stress Equation 4.45 v_{su}	Computed Ultimate Concrete Strength Allowing for Rapid Stressing $k_3 f'_c$	Observed Response in Shear
11-1	495	565	760	7,590	None
16-1	453	617	725	7,610	None
16-2	597	716	757	7,853	None
16-3	597	716	747	7,750	None
21-1	508	748 *	929	9,646	None
21-2	508	748 *	926	8,300	None
21-3	320	544	889	9,255	None
21-4	329	343	847	8,730	None
21-5	611	748 *	786	8,159	None
21-6	432	748 *	763	7,929	None
26-1	496	628 *	903	9,360	None
26-2	313	628 *	801	8,340	None
26-3	693	628 *	702	7,290	None
31-1	371	542 *	799	8,290	None
31-2	371	542 *	903	9,369	None

* Computed using v_{max} from elastic response computations.

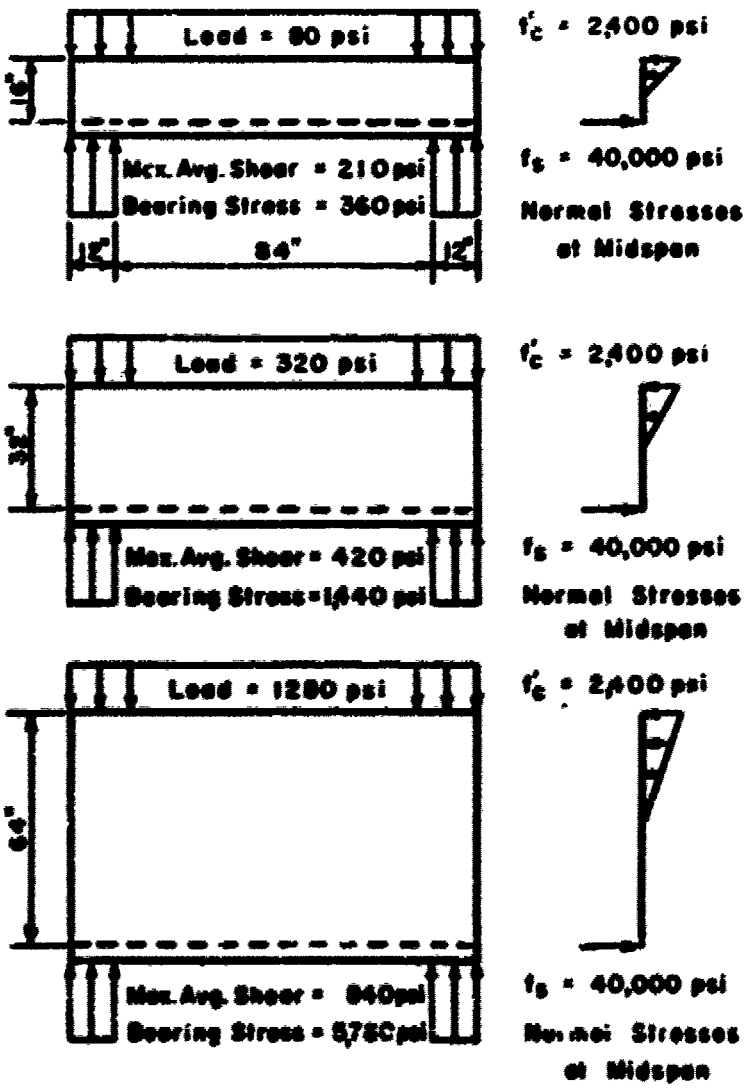

Figure 4.1 Illustration of effect of depth on loads, bearing stresses, and shearing stresses corresponding to constant nominal flexural stresses.

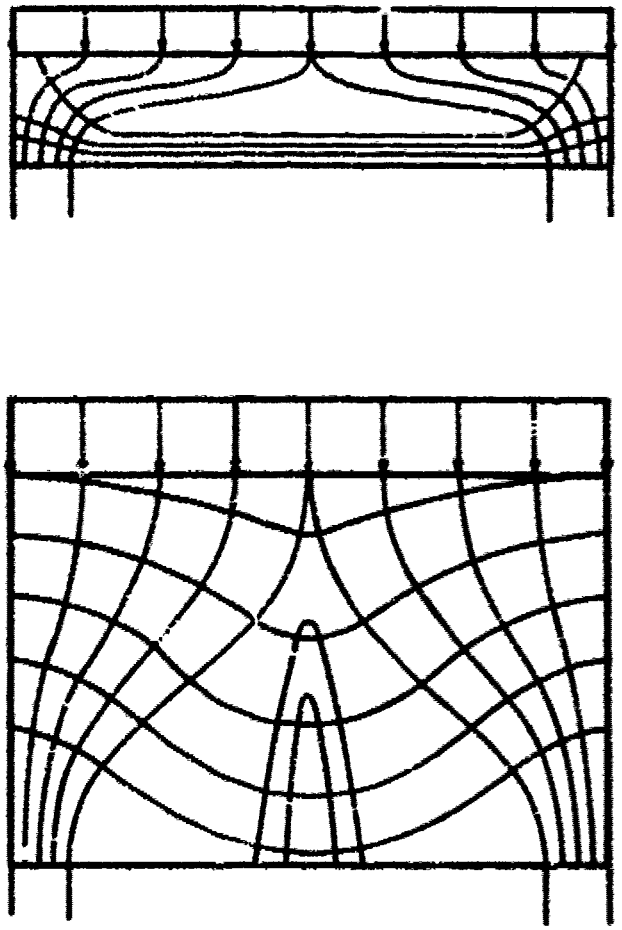

Figure 4.2 Qualitative representation of principal stress trajectories for members of two different span-depth ratios.

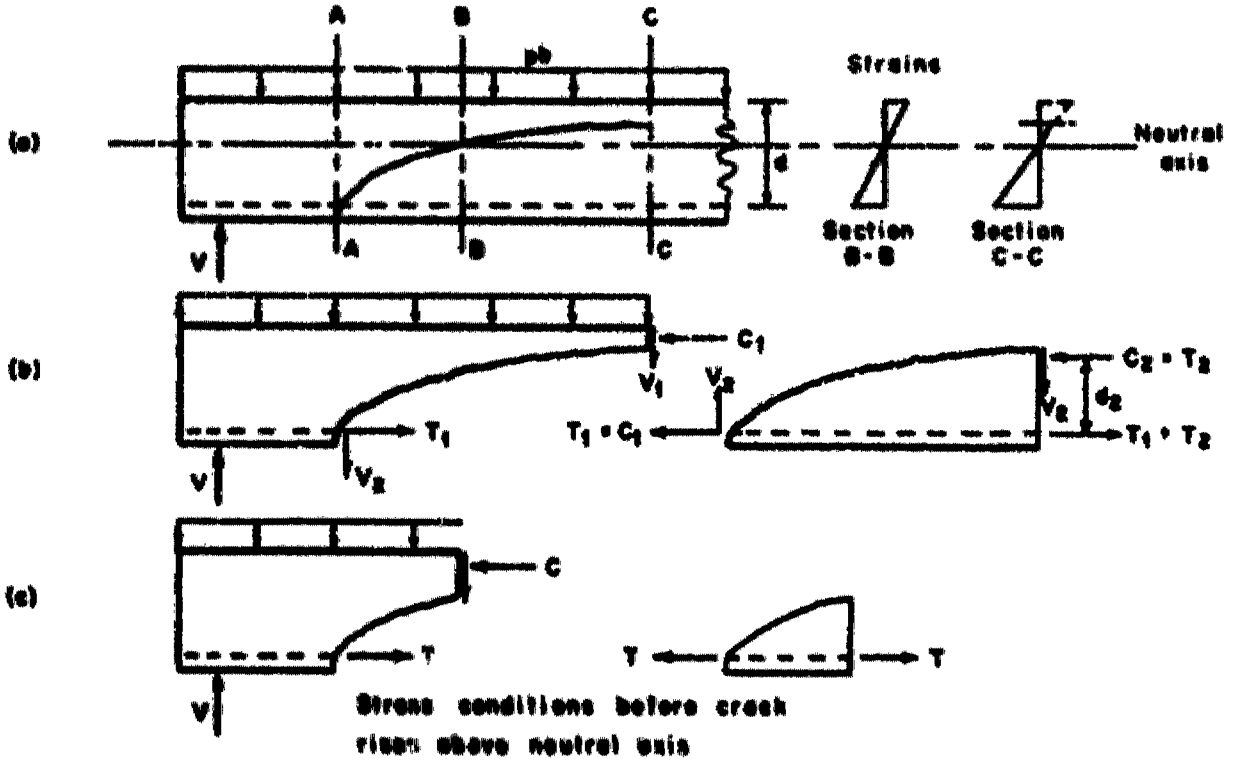

Figure 4.8 Redistribution of stresses caused by inclined cracking.

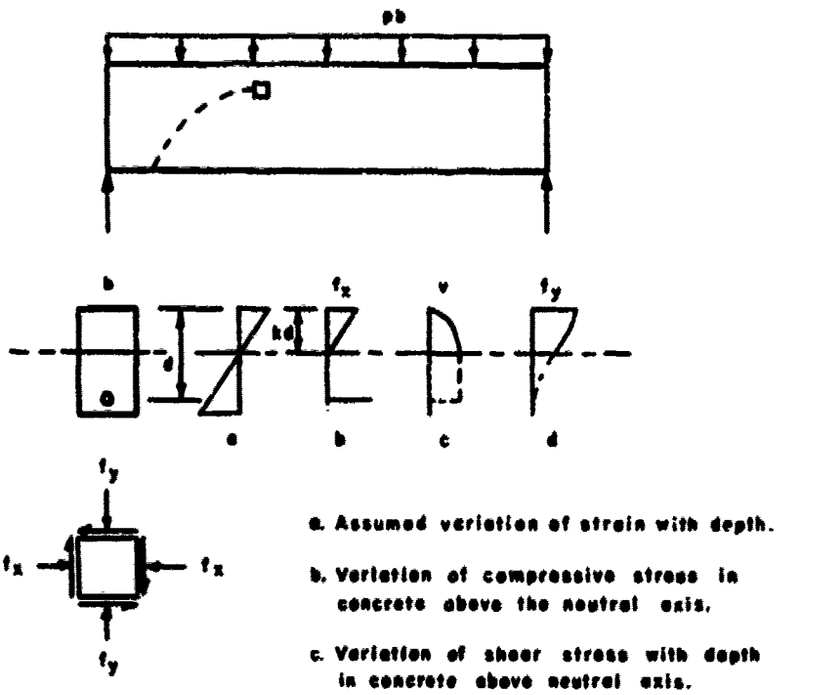

a. Assumed variation of strain with depth.

b. Variation of compressive stress in concrete above the neutral axis.

c. Variation of shear stress with depth in concrete above neutral axis.

d. Variation of vertical compressive stress with depth in concrete above neutral axis.

Figure 4.4 Combined stress conditions in the concrete above the neutral axis in a simply supported prismatic beam of reinforced concrete under uniformly distributed load. (See Appendix A.)

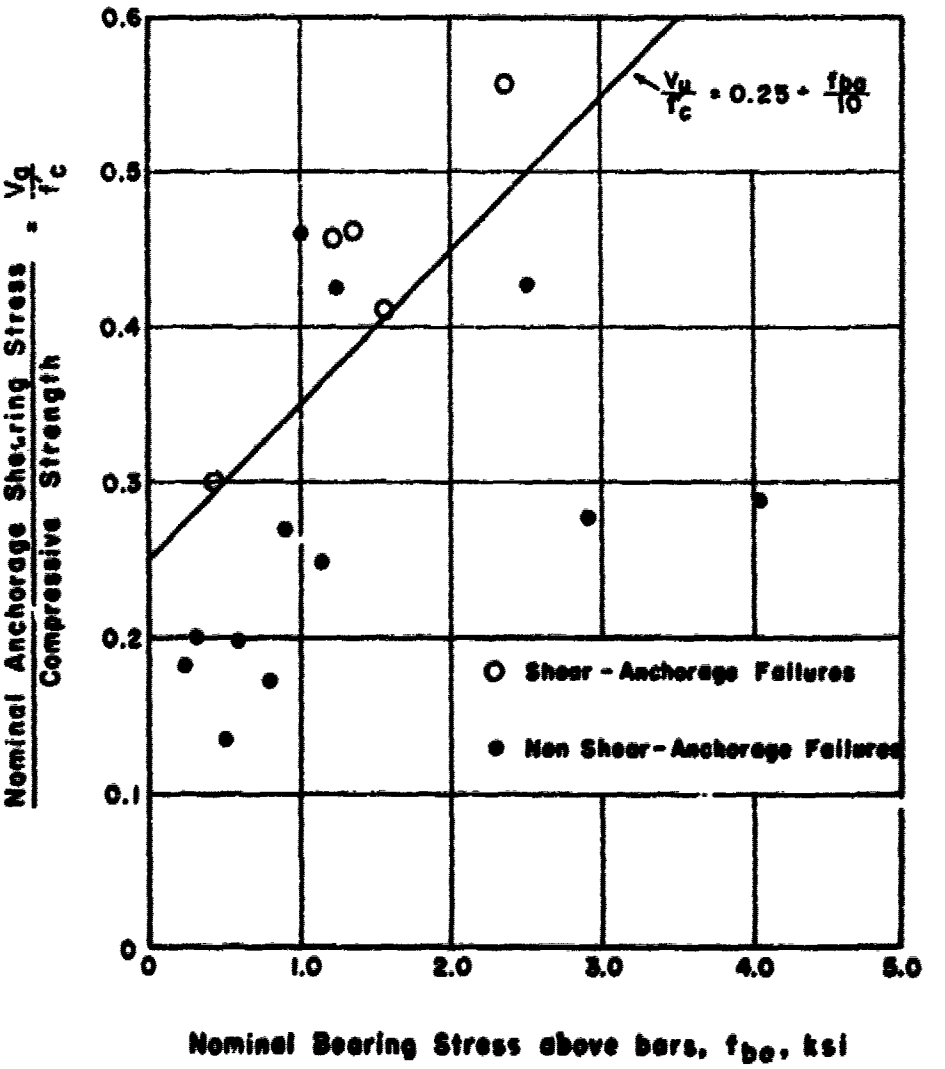

Figure 4.5 Anchorage shearing stresses at ultimate load.

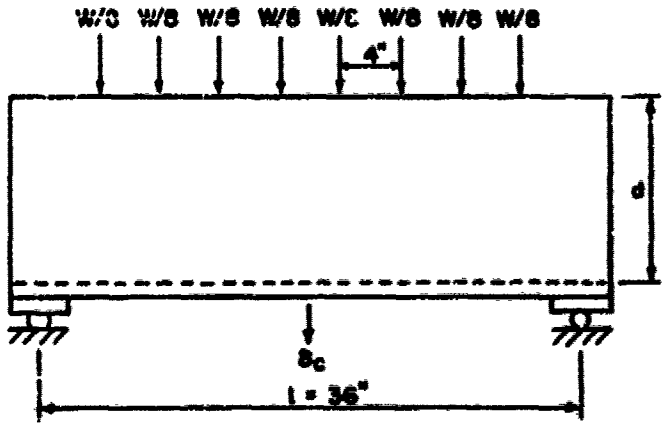

Moment at Ce: 5W in inch-kips for W in kips

Equivalent Distributed Load: $\frac{1}{8} w (36)^2 = 5W$

$$w = \frac{W}{32.4} \text{ kips/inch}$$

Center Deflection by Flexural Theory:

$$\delta_c = \frac{5}{384} \frac{wl^4}{EI} + \frac{1}{8} \frac{wl^2}{GK'A}$$

I = Moment of inertia of cracked transformed section

E = Elastic Modulus of Concrete = $\frac{30 \times 10^6}{n}$ psi

$n = 6 + \frac{10{,}000}{f'_c}$

K'A = Area effective in shear, taken as bd

G = Shearing Modulus, taken as E/2.4

l = Effective span, taken center to center of rollers

Figure 4.6 Loading on C and D series specimens of Reference 3 and method used to compute elastic deflections including shear deflection.

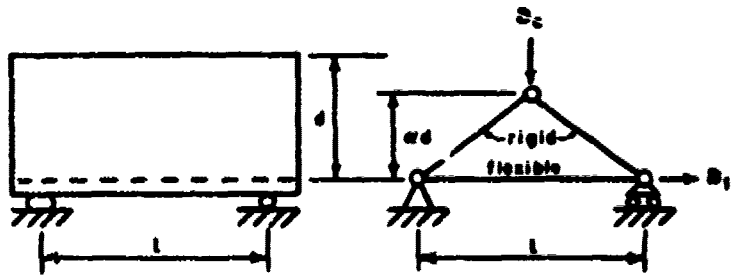

Deflections in Elastic Range

Center Deflection of Equivalent System

$$\Delta_c = \frac{1}{4\alpha d}\Delta_1$$

Assuming Δ_1 to be produced by stress in steel

$$f_s = \frac{M_s}{A_s j d}$$

$$\Delta_1 = l\varepsilon_s = \frac{M_s l}{A_s E_s j d}$$

Setting $j\alpha = \alpha'$

$$\Delta_c = \frac{M_s}{4A_s E_s d\alpha'}\frac{l^2}{d}$$

Figure 4.7 Basis for development of expression for elastic deflection of deep one-way slab.

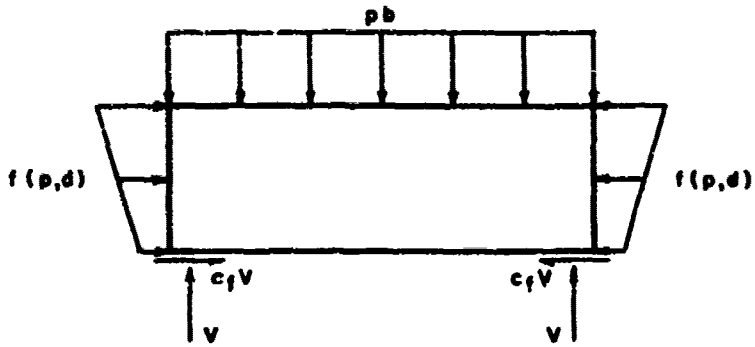

Figure 4.8 Field-test loading conditions for one-way slabs.

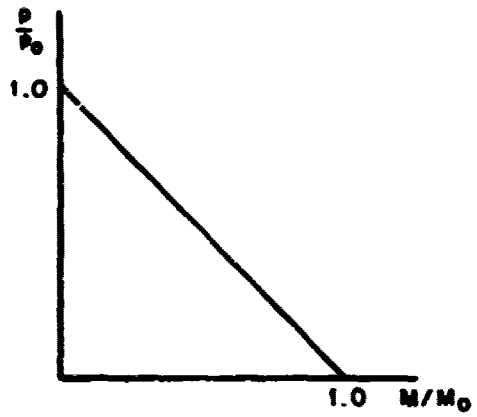

(a) Interaction diagram for member of homogeneous, elastic, isotropic material.

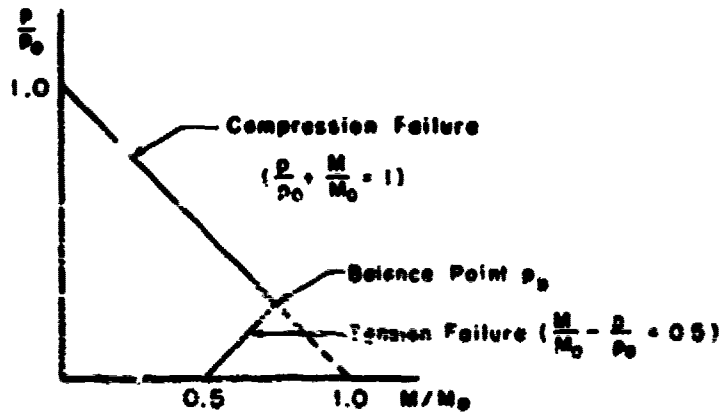

(b) Interaction diagram for member of homogeneous, elastic anisotropic material.

Figure 4.9 Typical interaction diagrams for members of homogeneous elastic material.

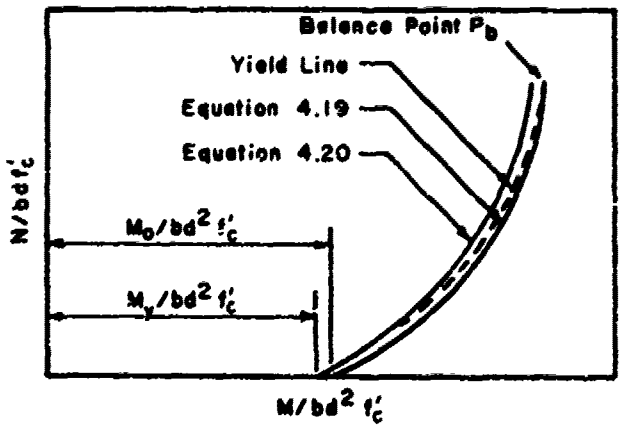

Figure 4.10 Interaction diagrams for yield and ultimate flexural capacities of reinforced-concrete members.

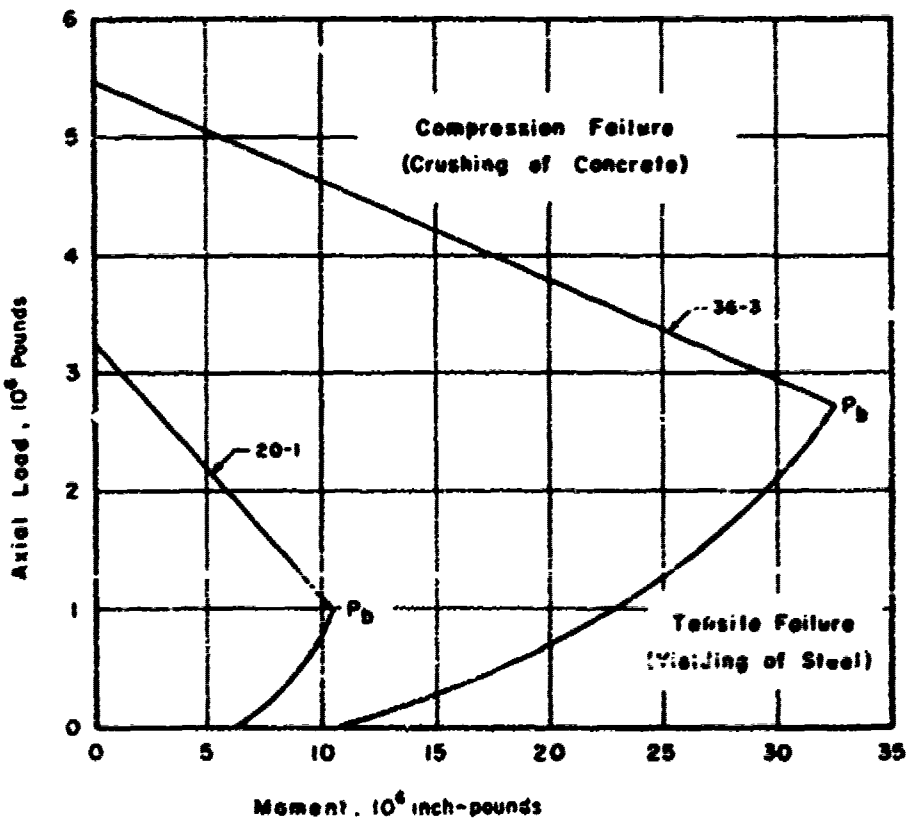

Figure 4.11 Interaction diagrams for Slabs 20-1 and 36-3, using static resistance values for concrete and tensile reinforcement.

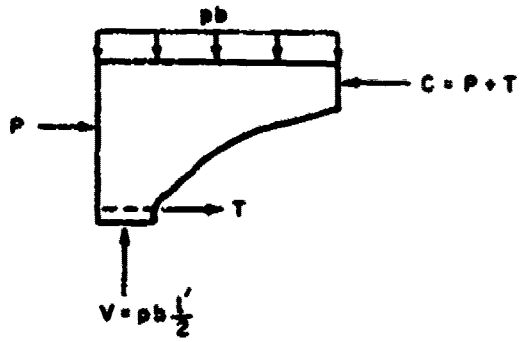

(a) Effect of lateral pressure on shear - anchorage resistance.

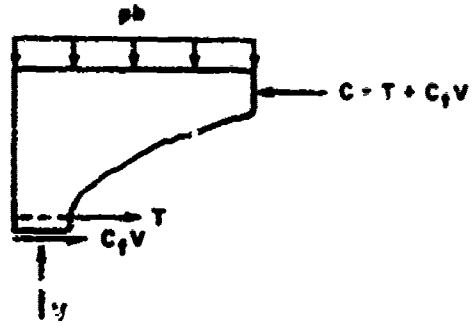

(b) Effect of friction at supports on shear - anchorage resistance.

Figure 4.12 Effects of axial loadings on shear-anchorage resistance.

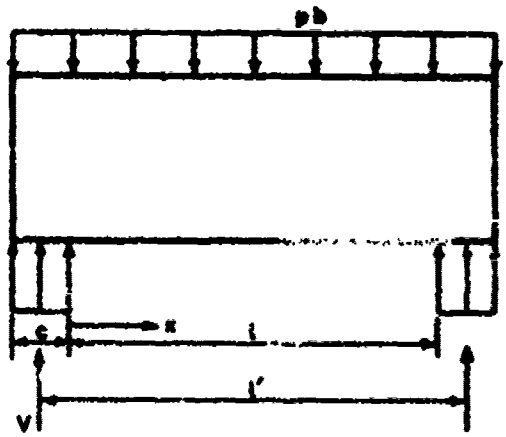

Figure 4.13 Loading conditions considering finite support dimensions.

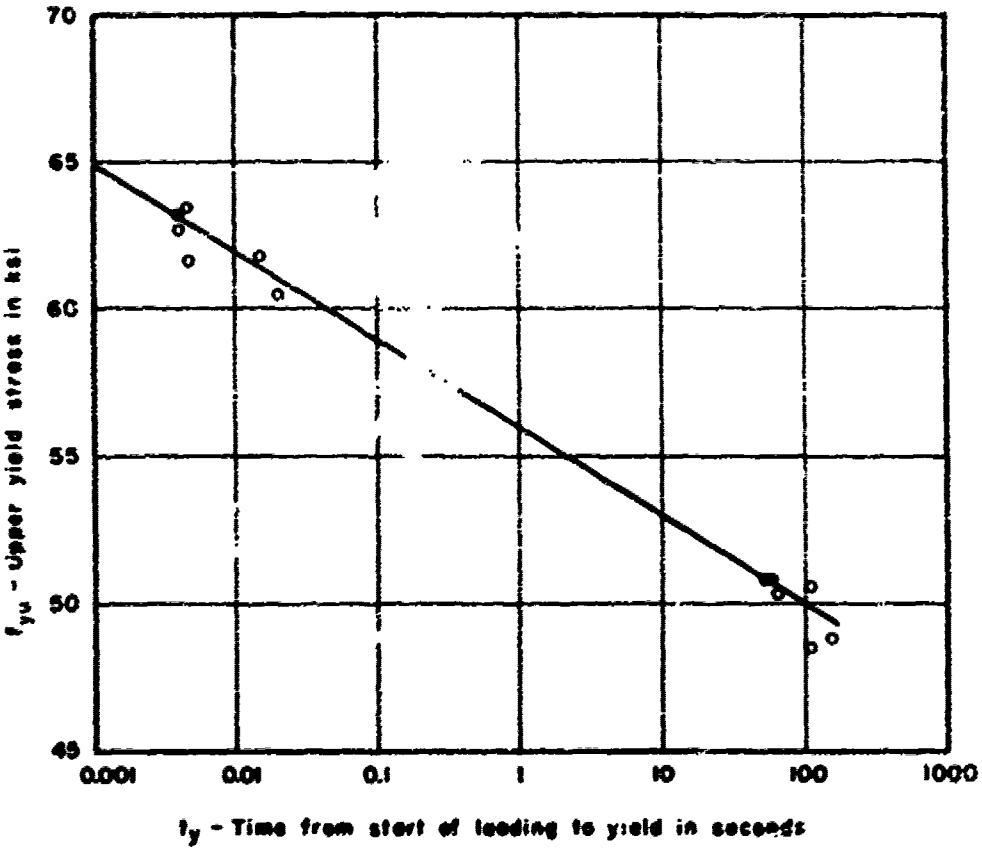

Figure 4.14 Upper yield stress versus time to yield.

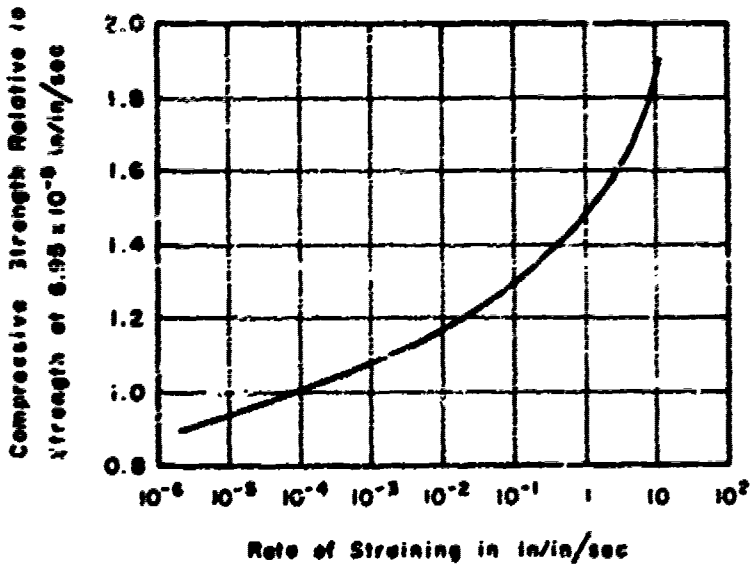

Figure 4.15 Effect of rate of straining on compressive strength of concrete.

SECRET

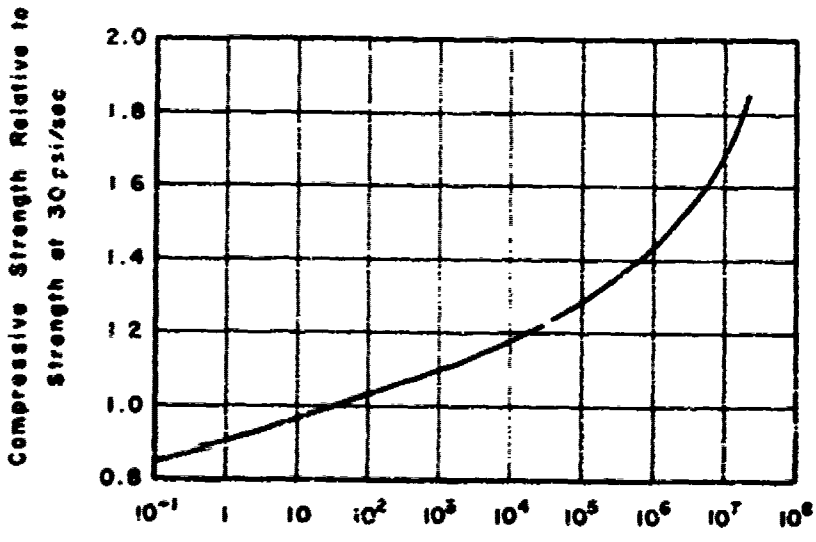

Figure 4.16 Effect of rate of stressing on compressive strength of concrete.

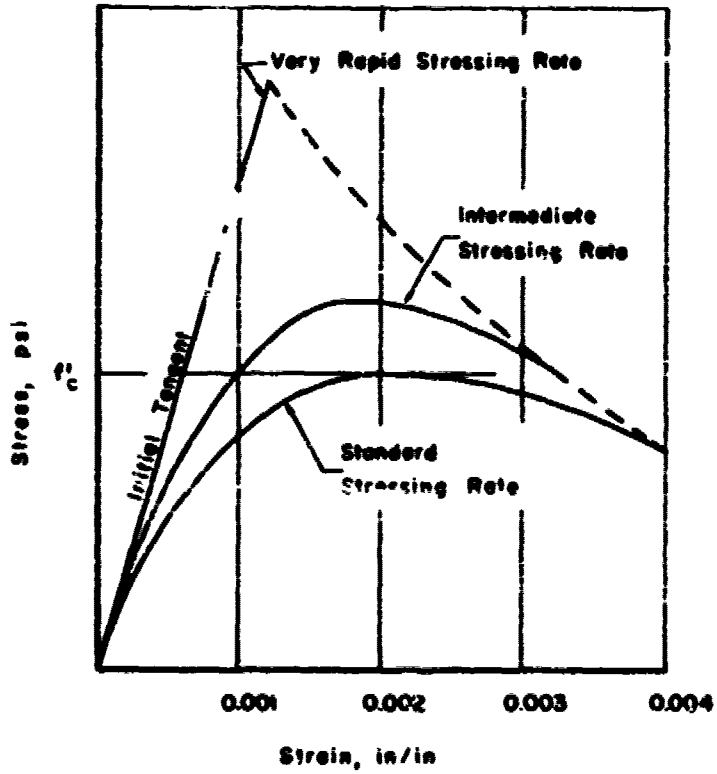

Figure 4.17 Probable effect of rapid stressing or straining rate on the shape of the stress-strain relationship in concrete.

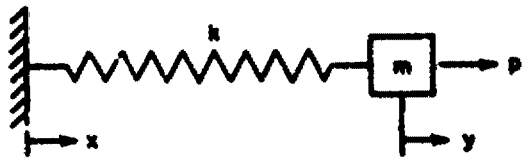

x base displacement — p forcing function
y mass displacement — m mass
k spring constant

Figure 4.18 Single-degree-of-freedom system.

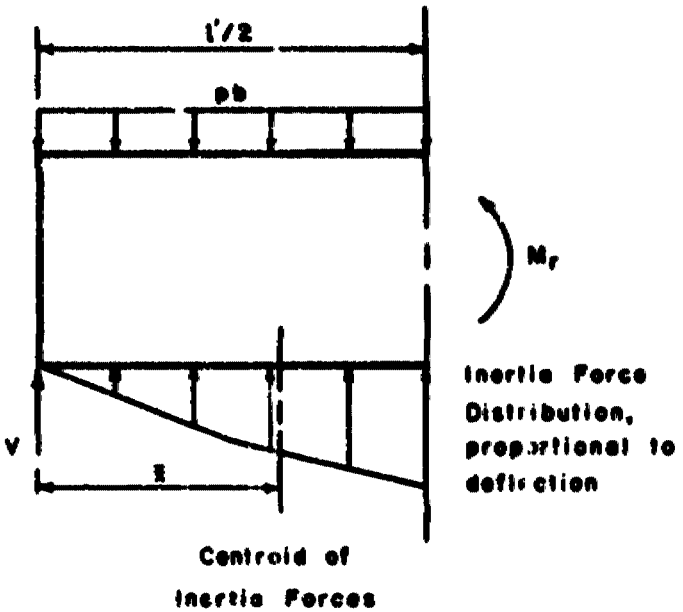

Figure 4.19 Forces on slab in dynamic response.

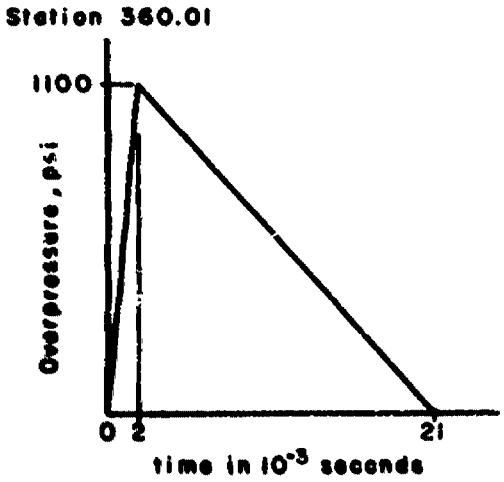

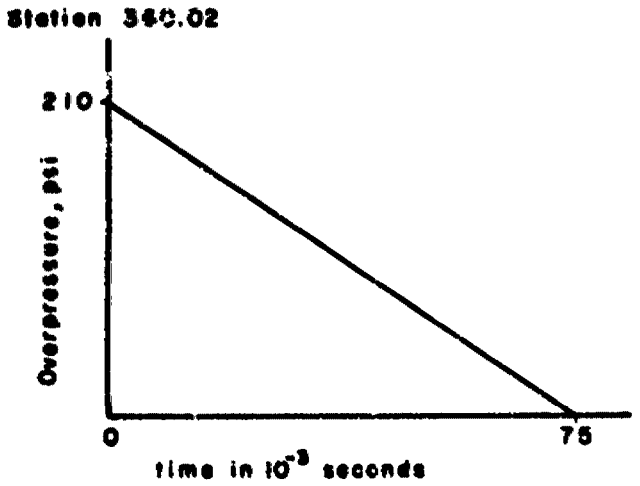

Figure 4.20 Equivalent overpressure-time curves used in response analysis.

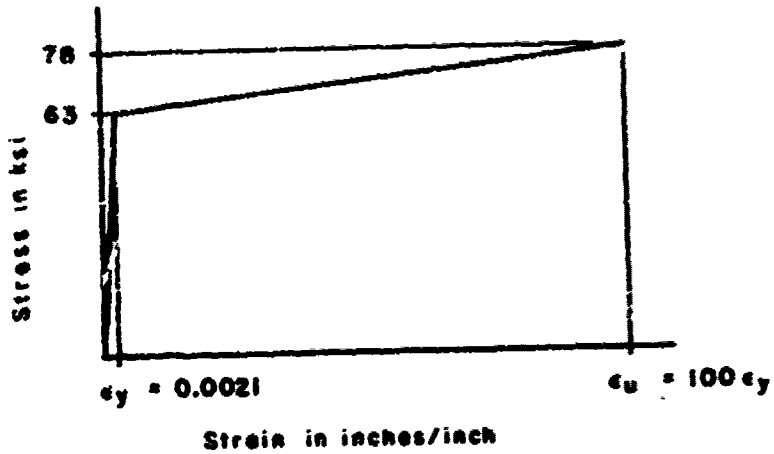

Figure 4.21 Shape used for stress-strain relation in reinforcing steel under field-test loading.

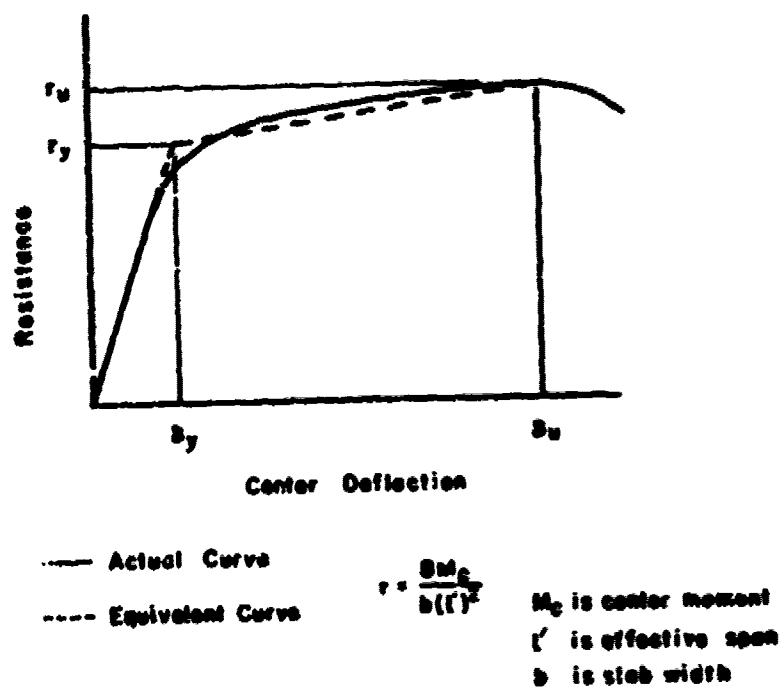

Figure 4.22 Resistance function for slab.

SECRET

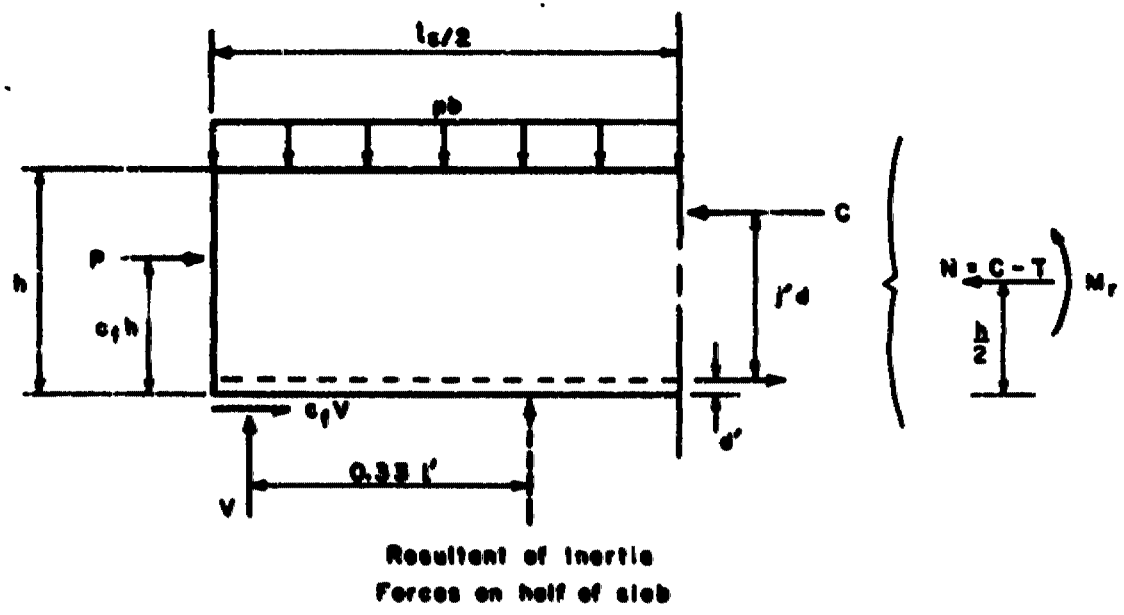

Figure 4.23 Resolution of stresses at midspan for slab in dynamic response.

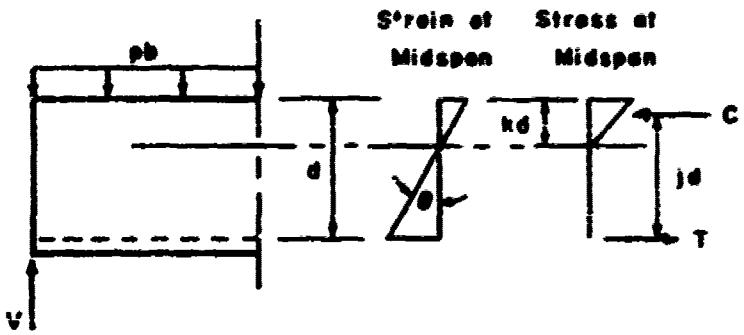

(a) Stress distribution at midspan with no axial load

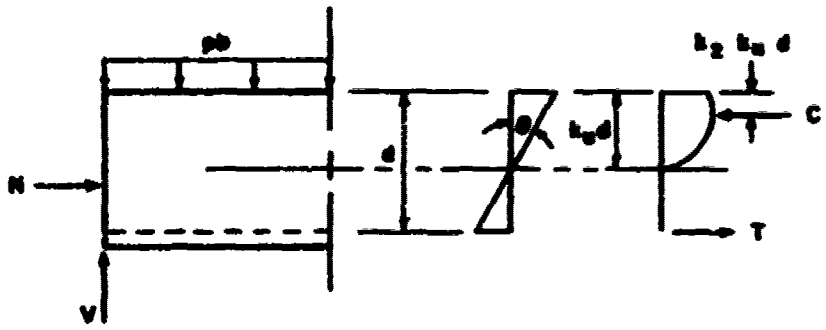

(b) Stress distribution at midspan with axial load

Figure 4.24 Effect of axial load on moment arm, and stress distribution in reinforced-concrete member for constant-angle change at section.

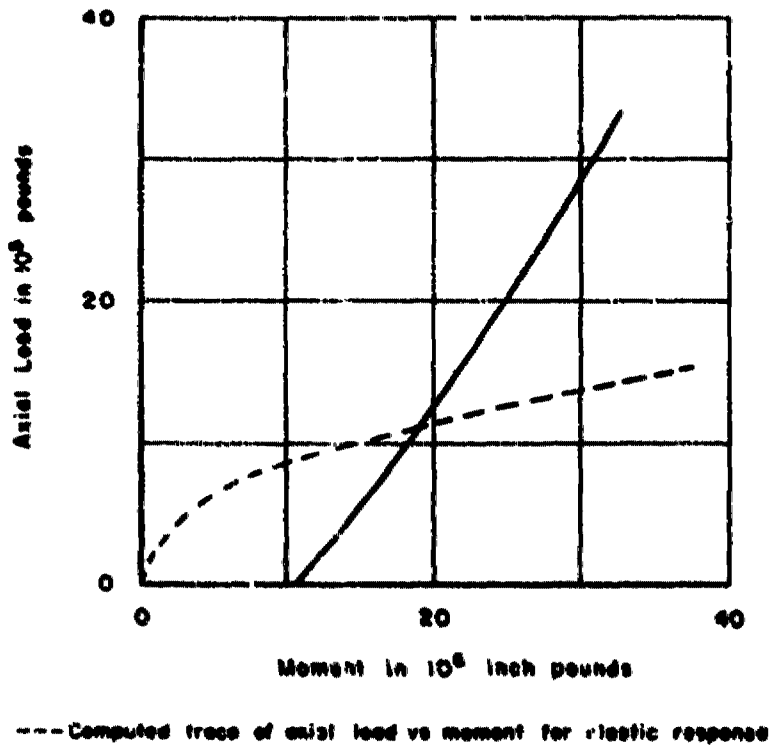

Figure 4.25 Dynamic interaction diagram for Slabs 23-1 23-2, and 23-3.

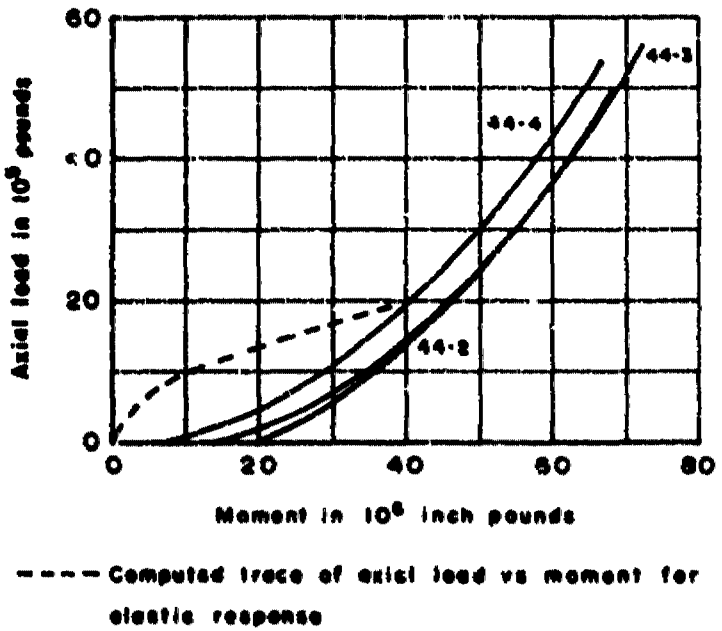

Figure 4.26 Dynamic interaction diagram for Slabs 44-2, 44-3, and 44-4.

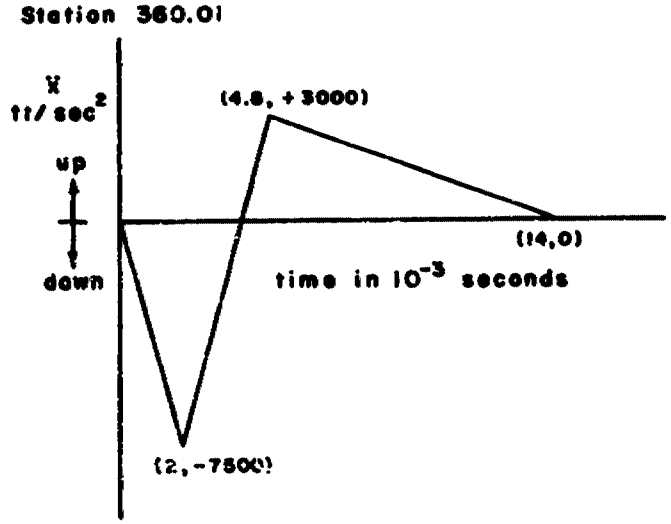

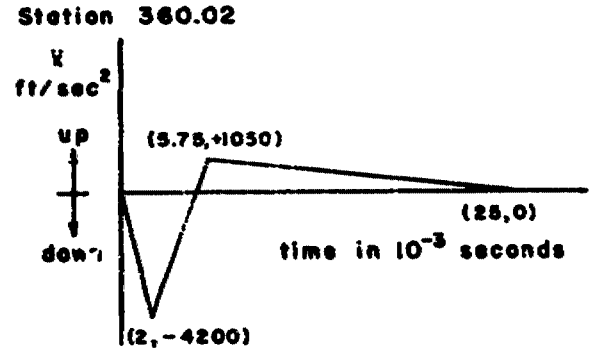

Figure 4.27 Representative linearized acceleration-time variations for slab foundations.

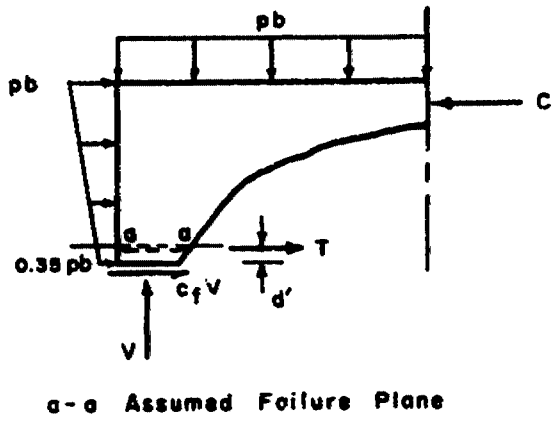

Figure 4.28 Assumed loading conditions for shear-anchorage analysis.

Chapter 5

CONCLUSIONS AND RECOMMENDATIONS

5.1 CONCLUSIONS

5.1.1 General. In terms of the original objectives of this project, the results were partially successful, at least for the one-way slabs. Despite differences between predicted and observed response, the results obtained from this project are in relative agreement with those obtained in static tests of deep beams as reported in Reference 2. The latter tests were conducted subsequent to the inception of Project 3.6 and results obtained from them were not available at the time of the preliminary design and analysis of the slabs tested under Project 3.6.

In particular, the data from laboratory tests mentioned above indicate that the present criteria for anchorage-bond and pure-shear failures are very conservative. As discussed under Section 4.1.3, it is believed that a diagonal-tension failure is not possible for a uniformly loaded, simply supported one-way slab or beam. None of the slabs tested under Project 3.6 failed in anchorage bond, pure shear, or diagonal tension.

Certain qualitative conclusions may be drawn from comparisons of the behavior of slabs that differ from each other in only one respect, and from the behavior of the slabs in general, despite the differences between predicted and observed response. In addition, tentative conclusions may be drawn from the analyses discussed in Chapter 4 of this report. These conclusions are tentative because there is no data to substantiate the various assumptions that were necessary to consider the effects of axial loads, base disturbance, and rebound, on the response of the test slabs.

5.1.2 Conclusions Drawn from Observed Behavior. Effects on Web Reinforcement. The effect of web reinforcement on the behavior of the one-way slabs tested under Project 3.6 was qualitatively the same as that obtained in static tests of deep beams. Specifically, comparing the response of Slab 28-1 with that of 28-2 and 28-3 and the response of 36-1 with 36-2, it is apparent that web reinforcement inhibits the development of major inclined cracks even in very deep members under dynamic loads.

With the exception of slight differences in concrete strengths the slabs compared had the same properties. Slab 36-1, which had no web reinforcement, developed an inclined crack at one end, whereas 36-2 did not. Slab 28-1 which also had no web reinforcement, developed major inclined cracks at both ends and failed, either in shear anchorage or during rebound. The other two slabs, 28-2 and 28-3, exhibited more distributed cracking, did not develop major inclined crack and did not fail.

It is concluded therefore that web reinforcement should be provided to insure failure in flexure rather than in some more brittle mode.

Longitudinal Compression Reinforcement. None of the test slabs were reinforced in compression, although those with web reinforcement had very small bars at the top to which the web reinforcement was tied. A large number of the slabs developed vertical cracks from top to bottom in the vicinity of midspan. It is believed that the only logical explanation for these cracks is that tensile stresses were developed at the top

surface during rebound (Section 4.3.6). It is concluded, therefore, that wherever support conditions are such that significant tensile stresses can be developed in the top of the slab, longitudinal reinforcement for resistance against rebound should be provided in accordance with Reference 27. This reinforcement will result in more ductile flexural response in the direction of the applied load.

5.1.3 Conclusions Drawn from Analyses. Flexure. It is recognized that flexural response computations are affected by certain parameters that cannot be defined with great certainty, especially if the resistance function is elastoplastic. Among these parameters are rise-time of the applied load, natural period of the structure, peak applied pressure, and yield resistance. However, it is clear from brief considerations that the maximum possible effect of variation in the first two mentioned cannot account for the differences between predicted and observed response at Station 360.01.

Because the probable variation in the peak applied pressure is on the order of ± 15 percent, it can be concluded that the yield resistances or apparent yield resistances of the slabs at Station 360.01, particularly, must have been increased greatly. Computations have indicated that axial forces and base disturbances could account for the differences noted (Section 4.3.4). Owing to a lack of data, these computations were based on assumptions the validity of which cannot be confirmed in general. Therefore, the results of these computations should be regarded as giving orders of magnitude of the effects of axial loads and base disturbances on the response of the test slabs.

Neither axial load nor base disturbance by itself appears to account for the difference between computed and observed response for all slabs. For deep members such as Slab 44-4 the effect of axial loads appears to account for the order of magnitude of the increase in yield resistance required. There are other indications that the increase in yield resistance was real rather than apparent—indications such as cracks in the bases of some of the deeper slabs over the supports. However, for the slabs with depths of 20 inches or less, the effect of axial loads was insufficient to account for the required increase in yield resistance. Therefore, it is concluded that both axial loads and base disturbances had a significant effect on the flexural resistance of the various test members, and that the former had a greater effect on the behavior of the deeper slabs whereas the latter had a greater effect on the behavior of the shallower slabs.

Other Modes of Failure. An attempt was made in Section 4.3.7 to evaluate the resistances of the slabs to failure in other modes, such as shear-compression, shear-anchorage, bond bearing and pure shear, by applying empirical expressions derived from analyses of data obtained from static tests of reinforced concrete beams. Equations 4.3, 4.4, 4.5, 4.6, and 4.7 were modified only to include, where practicable, the effect of rapid strain or stressing on the strength of the concrete. It is not clear whether the equations used are applicable to the dynamic case.

If applicable, the equations for cracking strength and shear-compression strength appear to be conservative. The former predicted inclined cracks in all members, whereas visible inclined cracks were noted in relatively few. Allowing for an increase in shear-compression strength due to the rapid straining rate, the latter predicted a shear-compression failure in only one member and that member did not fail. However, it is believed that the shear-compression strengths of all members would have been increased by the effects of the axial loads; these were not taken into consideration in the development of the equation.

With the possible exception of Slab 28-1, none of the members failed in shear-anchorage, and none were computed to have failed. However, because some of the slabs had web steel (which undoubtedly helps to resist failure in shear-anchorage) and because most of

the slabs did not develop visible inclined cracks, it is not clear whether the equation used is applicable to the dynamic case.

It is clear that there is no adequate criterion for anchorage bond strength of deep one-way slabs. The stress conditions in the concrete surrounding the tensile reinforcement above the support in a deep slab are greatly different from those in standard pullout tests upon which the present criterion is based. This fact was noted in Reference 2, which reported computed bond stresses greatly in excess of the standard bond-strength criterion in static tests of deep beams. Bond stresses on the order of 0.3 f'_c probably were developed in the slabs tested under Project 3.6 with no apparent bond failure at the anchorage.

The criterion applied for bearing strengths appears to be applicable to the dynamic case after allowance has been made for the rapid stressing rate. Good correlation was obtained between the computed bearing stresses, computed bearing strengths and observed response for the case of the assumed combined loading condition. As discussed above, the analyses of the response of the slabs to combined bending and axial loads are based on assumed magnitudes of forces not confirmed by data. Thus, the applicability of the bearing strength criterion assumed has not been established firmly.

The present criterion for pure (end) shear failure is apparently too conservative. Values of computed average shearing stresses as high as 0.43 f'_c were obtained in static tests of simply-supported deep beams without pure-shear failures as reported in Reference 2. Computations indicate that average shearing stresses as high as 0.32 f'_c were attained in the slabs tested under Project 3.6 without a shear failure.

It is believed that one of the reasons why the present criterion is too conservative is that no consideration is given to the effect of the stressing rate on the strength of the concrete. It is concluded therefore that although the value of the average shearing stress at which a pure-shear failure will occur has not been established, there is sufficient evidence available to permit a reasonable increase in the ultimate or allowable average shearing stress on the vertical section adjacent to the support.

In summary, it is concluded that, except for bearing strength, none of the criteria used to determine the strengths of the members in modes of failure other than flexure have been demonstrated to be applicable to the dynamic case. Specifically, it is emphasized that: (1) there is no adequate criterion for anchorage-bond strength; (2) the equation used for shear-compression strength is known to be conservative when the member is subjected to combined bending and axial loads, even in the static case; (3) the expression for cracking strength appears to be very conservative if it is applicable to the dynamic case at all; and (4) the criterion for pure-shear (end shear) strength appears to be very conservative.

5.2 RECOMMENDATIONS

5.2.1 Further Research on Deep One-Way Slabs. The response of deep one-way slabs to static loads is only beginning to be understood. Although some recent progress has been made, as reported in Reference 2, a great deal remains to be learned, specifically about the failure of these slabs in brittle modes such as shear-compression, shear-anchorage, pure shear, and anchorage bond.

Flexural resistance criteria developed from tests of reinforced-concrete beams of ordinary proportions (span-depth ratios of about 10) appear to be applicable to deep beams down to span-depth ratios of around 2.0. However, criteria developed similarly for cracking, shear-compression, pure-shear, and anchorage-bond strengths do not appear to be applicable to the static case, much less the dynamic. Further, the effect of axial loads on the resistance of deep members to these brittle modes of failure has not been determined for the static case. After the static case is fully understood, there is much that

remain to be investigated concerning dynamic behavior, which can best be investigated under laboratory conditions where the variables involved can be controlled. Among the important areas of investigation are: (1) periods of vibration of deep one-way slabs; (2) effects of rapid stressing or straining rates on the strength of deep reinforced-concrete slabs in flexure; (3) effects of rapid stressing or straining rates on the strength of deep reinforced-concrete slabs in shear modes; and (4) effects of axial loads including friction at the supports on the strength of deep reinforced-concrete slabs in the various modes of failure.

It is recommended, therefore, that laboratory investigations of the static and dynamic behavior of deep one-way slabs are pursued. Until more is known about the effects listed above, the design of deep one-way slabs must necessarily remain conservative.

5.2.2 Research on Deep Two-Way Slabs. Present design criteria for deep two-way slabs of reinforced concrete are based on theoretical analyses and meager static tests of medium-thick two-way slabs. Based on recent results obtained (Reference 2) from static tests of deep one-way slabs significant differences between the behavior of deep and medium-thick two-way slabs are anticipated.

To the writers' knowledge, there have been no static tests of deep two-way slabs of reinforced concrete conducted under laboratory conditions. In addition, little theoretical work has been done on deep two-way slabs even in applying the theory of elasticity to a homogeneous, isotropic material. It is recommended therefore that theoretical and experimental investigations of deep two-way slabs of reinforced concrete be pursued to establish the probable modes of failure of such members and criteria for resistance to failure in those modes.

5.2.3 Interim Design Criteria for One-Way Slabs. Until more knowledge is obtained and better criteria established, it is recommended that the criteria summarized below be used for the analysis and design of simply supported deep slabs subjected to uniformly distributed dynamic loads.

Flexure. (1) Yield resistance:

$$r_y = 0.08\, f_y\, j\, (d/l)^2\, \phi \qquad (5.1)$$

Where: r_y = yield resistance

f_y = dynamic yield stress of the tensile reinforcement

j = ratio of distance between centroids of compressive and tensile forces to the effective depth as defined by the elastic theory

d = effective depth

l = effective span (center to center of supports)

ϕ = percentage of tensile reinforcement

(2) Ultimate resistance:

$$r_u = 0.08\, f_s\, (1 - k_s k_u)\, (d/l)^2\, \phi \qquad (5.2)$$

Where: r_u = ultimate resistance

f_s = dynamic stress in tensile reinforcement associated with strain in the steel at the ultimate moment

k_z = ratio of depth of the centroid of the compressive forces to depth of the neutral axis at the ultimate moment as defined by the ultimate strength theory

k_u = ratio of the depth of the compression zone in the concrete at ultimate moment to the effective depth of the slab as defined by the ultimate strength theory

d, l', and ϕ are as defined above

(3) Yield deflection:

$$\delta_y = \frac{3.125\ r_y\ (l')^2}{\alpha\ \phi\ E_s d^2} \tag{5.3}$$

Where: δ_y = dynamic yield deflection at midspan

E_s = modulus of elasticity of the tensile reinforcement

$$\alpha = \frac{-0.01\ (l'/d)^2 + 0.22\ (l'/d) + 0.17}{\phi^{2/3}}$$

r_y, l', d and ϕ are as defined previously

(4) Ultimate deflection:

$$\delta u = \delta y + 0.2\ (l'/d)^2\ (\epsilon_{su} - \epsilon_{sy}) \tag{5.4}$$

Where: δu = dynamic ultimate deflection at midspan

ϵ_{su} = strain in the tensile reinforcement at ultimate load

ϵ_{sy} = yield strain in the tensile reinforcement

δy, l', and d are as defined previously

(5) Period of vibration:

(a) For span-depth ratios of less than 6.0 use the following:

$$T = 2\pi \sqrt{\frac{0.696\ \delta_{sc}}{g}} \tag{5.5}$$

Where: T = fundamental period of vibration

δ_{sc} = computed deflection at midspan when slab is loaded by a distributed static load equal to its own weight

g = gravity constant

(b) For span-depth ratios of 6.0 or greater use the following expression which was developed from consideration of simple support cases of Equations 5.5 and 5.29 in Reference 28:

$$T = 6.19 \times 10^{-3}\ l' \sqrt{f_y / r_y} \tag{5.6}$$

Where: T = natural period of member, msec

l' = effective span (center to center supports), inches

f_y dynamic yield stress of the tensile reinforcement, psi

r_y dynamic yield resistance of member, psi

The preceding expressions require knowledge of the stress-strain relationship in the tensile reinforcement under rapid stressing, and a considerable amount of computation For example, the computations for ultimate deflection and resistance in particular require the solution by successive approximation of the following expression:

$$\epsilon_{su} = \frac{100\ \epsilon_u\ k_1\ k_3\ f'_c}{f_s \phi} - \epsilon_u \qquad (5.7)$$

Where: ϵ_u = ultimate strain in the concrete in compression

k_1 = ratio of the area of the concrete stress block to the area of the enclosing rectangle as defined by the ultimate strength theory

k_3 = ratio of the ultimate compressive stress in the concrete to the standard cylinder strength, f'_c, taking into consideration rapid straining rate

f'_c = standard cylinder strength in psi

f_s, ϕ, and ϵ_{su} are as defined above

Equation 5.7 is based on an assumed linear variation of strain with depth at midspan and should be valid for span-depth ratios of 2.0 or more. To use the equation it is necessary to know or assume values for ϵ_u, k_1, k_3, and f'_c, and to know or assume the dynamic stress-strain relationship for the tensile reinforcement. In this report, the ultimate compressive strain in the concrete was assumed to be 0.004; k_1 was assumed to be 0.85; k_3 was obtained from Figure 4.15. For a first approximation, the straining rate may be computed by assuming the ultimate strain is attained in one-half the fundamental period.

For trial design purposes the extensive computations required to determine ultimate deflection and resistance may be avoided by using an elastoplastic resistance function. The yield resistance value can be used as the ultimate resistance. The ductility factor μ may be obtained from the following equation taken from Reference 26:

$$\mu = \frac{10}{\phi - \phi'} \qquad (5.8)$$

Where: ϕ = percentage tensile reinforcement

ϕ' = percentage compressive reinforcement

It is believed that designs based on the above equation for ductility factor, and the previously given equations for yield resistance and fundamental period will be somewhat conservative for flexural response because of the neglect of the additional energy absorption due to strain hardening in the steel and increases of the internal moment after yield.

Other Modes. (1) Shear-Compression: Use the following expression developed in Reference 9.

$$V'_s = 1.52\ bd^2\ f'_c\ k\ \left(0.57 - \frac{0.045\ f'_c}{10^3}\right)$$

Since M's $r_{sc} = \frac{b(l')^2}{s}$

$$r_{sc} = 12.16\,(d/l')^2\, f'_c\, k\,(0.57 - \frac{0.043\, f'_c}{10^3}) \quad (5.9)$$

Where: r_{sc} = resistance to shear-compression failure

k = ratio of the depth of the neutral axis to the effective depth of the slab as defined by the elastic theory

d, l', f'_c are as defined above

(2) Shear-Anchorage: (a) use the following expression developed in Reference 2 modified by the rate of stressing at the support, assuming no axial loads:

$$v_u = k_3 f'_c \left(0.25 + \frac{f_{by}}{10^4}\right) \quad (5.10)$$

Where: v_u = ultimate average shearing stress on the failure plane

f_{by} = average bearing stress at the yield resistance

k_3 and f'_c are as defined previously

(b) Equation 5.10 must be compared to the following expression to determine whether the slab will fail in shear-anchorage before the yield resistance is attained (assuming no axial force acting):

$$v_a = \frac{0.01\, f_y\, \phi\, d}{(c + 0.5\, d')} \quad (5.11)$$

Where: v_a = the average shearing stress on the failure plane when the yield resistance is reached

c = the longitudinal dimension of the supports

d' = the distance from the centroid of the tensile forces to the bottom of the slab

f_y, ϕ, and d are as defined previously

(3) Bond. Use the following expressions as indicated for shear-anchorage above:

$$u_u = 0.30\, f'_c \quad (5.12)$$

$$u_a = \frac{0.01\, f_y\, \phi\, bd}{\Sigma_o\, c} \quad (5.13)$$

Where: u_u = ultimate bond stress

u_a = average bond stress at yield resistance

Σ_o = sum of the perimeters of the tensile reinforcement

f'_c, f_y, ϕ, b and d are as defined previously

(4) Bearing. Use the following expressions, assuming no axial loads:

$$f_{bu} = k_3\, f'_c \quad (5.14)$$

$$f_{by} = \frac{V_y}{bc} \frac{l'}{c} = (0.12\, p_y + 0.38\, r_y) = 0.5\, p_y \qquad (5.15a)$$

Where: f_{bu} = ultimate bearing stress

f_{by} = bearing stress at yield

p_y = value of overpressure at yield of tensile reinforcement

l', c, and r_y are as previously defined

For most designs $p_y \approx r_y$, therefore, for most practical cases, the following expression may be used:

$$f_{by} = 0.5\, r_y \frac{l'}{c} = 0.5\, r_y \qquad (5.15b)$$

Note that Equation 5.15b is conservative except when $p_y > r_y$ (not a common condition).

(5) Pure Shear. Use the following expressions, assuming no axial loads:

$$v_{su} = 0.2\, k_3\, f'_c \qquad (5.15)$$

$$v_{sy} = \frac{V_y}{bd} = \frac{l}{d} (0.12\, p_y + 0.38\, r_y) \qquad (5.16a)$$

Where: v_{su} = ultimate shearing stress on the vertical section at the supports

v_{sy} = average shearing stress on the vertical section at the supports

l = clear span

d, p_y, and r_y are as previously defined

As indicated under (4) above the following expression may be used in lieu of (5.16a) for most practical cases.

$$v_{sy} = 0.5\, r_y \frac{l}{d} \qquad (5.16b)$$

(6) Web Reinforcement. It is recommended that the amount of web reinforcement required be determined as indicated in Section 5.1.2.1 of Reference 1 but that at least 0.5 percent of web reinforcement be used in deep beams of span-depth ratios of less than 6.0. It is believed that this minimum requirement should be met to insure a flexural failure until apparent anomalies between the behavior of deep one-way slabs under static and dynamic loads have been explained.

Axial Loads. If the values of axial loads can be predicted with reasonable accuracy as a function of time, they should be taken into account in the analysis of the member. It is apparent from the considerations in Chapter 4 that axial loads can have a marked effect on the yield resistance of the slab and on the shear-compression, shear-anchorage, bond, and pure-shear strengths of the slab. However, the values assumed in this report for the coefficient of friction at the support and the lateral component of the earth-transmitted pressure are not to be taken as accurate since there are no data to confirm them. To ignore the effects of axial loads is to be conservative; thus, it seems advisable to ignore rather than to overestimate them until more data has been obtained.

Base Disturbance. As indicated in Chapter 4, base disturbance can be harmful or beneficial depending on the variation of the disturbance with time. Again, if a reasonable prediction of the variation of the base disturbance with time is possible, it should be taken into account. For one-way slabs with shallow footings, subjected to high overpressures (within a range of pressure such that the air-shock velocity is greater than the

ground-shock velocity) it is believed that the effect of the base disturbance is to increase the apparent yield resistance of the slab. This belief is based on two considerations; the magnitude of the disturbance at shallow depths appears to be significant, and the rate of propagation of the air-induced ground shock through the soil is such that the disturbance begins before the structure attains its first maximum deflection.

No attempt was made to approach the problem of the effect of base disturbance on the response of simply supported one-way slabs in general, in this report. Therefore, no general recommendation can be made. However, it is noted that the magnitude of the effect computed for these slabs is undoubtedly much greater than that which might be expected for a structure designed to withstand pressures on the order of 200 to 1,000 psi. The depth of the footings for such a structure, even if it were not buried, would be greater than the depths of the footings for these slabs, and consequently, the magnitude of the base disturbance would be less than for the Project 3.6 slabs.

Rebound. It is recommended that consideration be given to the provision of longitudinal reinforcement to resist tensile forces developed during rebound. This can be accomplished by the use of the charts in Reference 27. It is emphasized that these charts were prepared assuming that the member has the same moment of inertia in both directions. The required resistance obtained from the charts should be multiplied by the ratio of $\sqrt{I_r/I}$. As stated in Section 4.3.6, the factor given above is an approximation which is correct only for response to an impulsive loading. Multiplication of the resistance values obtained from charts in Reference 27 by the factor given above is conservative for long-duration loads. I_r and I may be computed using transformed elastic sections.

This procedure will not prevent cracking in rebound but will prevent a flexural failure in rebound. If no steel is provided to resist tensile forces in rebound, a vertical crack might represent failure of the member, depending upon the function of the slab.

5.2.4 Interim Design Criteria for Deep Two-Way Slabs. It is recommended that deep two-way slabs be designed in accordance with the procedures outlined in Reference 28 until better criteria become available from future research.

Appendix A

DISTRIBUTION OF STRESSES IN REINFORCED-CONCRETE BEAMS, ASSUMING ELASTIC STRESS DISTRIBUTION

In the derivation for the distribution of shearing stresses in rectangular beams of an elastic, homogeneous, isotropic material, it has been shown by the application of the principles of statics that the shearing stress at any point is the integrated difference between the bending stresses on either side of a beam section. Applying the same principles to the reinforced-concrete beam, the standard shearing stress distribution may be obtained. The total shearing force on the Section pq in Figure A.1. is $vb\Delta x$, assuming a uniform distribution of shear along that surface in the direction of the width. This force is the resultant of the horizontal forces acting to the right and left on the portion of the beam above the Section pq.

$$F_m = \int_{y_1}^{kd} f_m dA \text{ and } F_n = \int_{y_1}^{kd} f_n \, dA \qquad (A.1)$$

Where: F_m = the total force on the concrete above pq at section m–m

f_m = unit compressive stress at any depth in the concrete above pq at section m–m

dA = an elemental area over which the stress acts

F_n = the total force on the concrete above pq at section n–n

f_n = unit compressive stress at any depth in the concrete above pq at section n–n

But since the stress has been assumed to vary linearly with depth:

$$f_m = \frac{Y}{kd} (f_c - \Delta f_c)$$

$$f_n = \frac{Y}{kd} (f_c)$$

and $dA = bdy$

Where: b = width of the beam

y = distance above neutral axis

kd = depth of the neutral axis

f_c = extreme fiber stress

Δf_c = an increment of stress at the extreme fiber

Thus: $vb\Delta x = b \int_{y_1}^{kd} \frac{Y}{kd} (f_c) \, dy - b \int_{y_1}^{kd} \frac{Y}{kd} (f_c - \Delta f_c) \, dy \qquad (A.2a)$

$$vb\Delta x = \frac{b\Delta f_c}{kd} \int_{y_1}^{kd} y\,dy$$

$$\text{or } v = \frac{\Delta f_c}{\Delta x} \frac{1}{kd} \int_{y_1}^{kd} y\,dy \qquad (A.2b)$$

Taking moments at the tensile steel at Section m–m in Figure A.1,

$$\frac{w\Delta x\Delta x}{2} \cdot c\,jd + V\Delta x - (c + \Delta c)\,jd = 0$$

$$\frac{w\Delta x^2}{2} \cdot (f_c - \Delta f_c) \frac{bkd\,jd}{2} + V\Delta x - \frac{f_c}{2} b\,kd\,jd \qquad (A.3a)$$

Ignoring the first term, the above may be written as

$$V\Delta x = \Delta f_c \frac{b\,kd\,jd}{2}$$

$$\text{or } \frac{\Delta f_c}{\Delta x} = \frac{2V}{b\,kd\,jd} \qquad (A.3b)$$

Substituting this in the above integral (A.2b)

$$v = \frac{2V}{b\,(kd)^2\,jd} \left[\frac{y^2}{2}\right]_{y_1}^{kd} = \frac{V}{b(kd)^2\,jd} \left[(kd)^2 - y_1^2\right] \qquad (A.4)$$

Evaluating the above for the value of v at the neutral axis,

$$v = \frac{V}{bjd}$$

This is the standard expression obtained in many references assuming that the sections m–m and n–n are so close together that $V_m = V_n$.

Then the value of the shearing force at any height above the neutral axis may be expressed as:

$$v = \frac{V}{bjd} \left[1 - \left(\frac{y}{kd}\right)^2\right] \qquad (A.5)$$

Distribution of Vertical Stresses with Depth. Again applying the principles of statics to the section, an expression for the distribution of vertical stresses induced by the applied load may be developed. The total vertical force on Section pq in Figure A.2 is $f_v b\Delta x$, again assuming a uniform distribution of stress across the section. This force is the resultant of all other vertical forces acting on the element of the beam above the section.

$$V_m = \int_{y_1}^{kd} v_m dA, \qquad V_n = \int_{y_1}^{kd} v_n dA \qquad (A.6)$$

Where: V_m = the total vertical shearing force on the concrete above pq at Section m – m

v_m = unit shearing stress at any depth in the concrete above pq at Section m – m

dA = an elemental area over which the unit shearing stress acts

V_n = the total vertical shearing force on the concrete above pq at Section n – n

v_n = unit shearing stress at any depth in the concrete above pq at Section n – n

But by Equation A.5, v_m and v_n may be expressed as follows:

$$v_m = \frac{V + \Delta V}{bjd}\left[1 - \left(\frac{y}{kd}\right)^2\right] \qquad v_n = \frac{V}{bjd}\left[1 - \left(\frac{y}{kd}\right)^2\right]$$

Taking the sum of the vertical forces:

$$f_y\, b\Delta x = w\Delta x - \frac{\Delta V}{jd}\int_{y_1}^{kd}\left[1 - \left(\frac{y}{kd}\right)^2\right] dy \qquad \text{(A.7a)}$$

$$f_y = \frac{w}{b} - \frac{\Delta V}{\Delta x}\,\frac{1}{bjd}\left[y - \frac{y^3}{3(kd)^2}\right]_{y_1}^{kd}$$

but $\frac{\Delta V}{\Delta x} = w$ and $w = pb$

Thus:

$$f_y = p - \frac{p}{jd}\left[kd - \frac{kd}{3} - y_1 + \frac{y_1^3}{3(kd)^2}\right] \qquad \text{(A.7b)}$$

$$f_y = p - \frac{p}{jd}\left[\frac{2kd}{3} - y_1 + \frac{y_1^3}{3(kd)^2}\right]$$

Evaluating the above expression for the value of fy at the neutral axis:

$$f_y = p - \frac{p}{jd}\left[\frac{2kd}{3}\right] = p\left(1 - \frac{2}{3}\,\frac{k}{j}\right) \qquad \text{(A.8)}$$

From the preceding it is apparent that the value of fy at the neutral axis is dependent upon the properties of the beam:

k	fy
0.34	0.826
0.36	0.727
0.51	0.596

The variation of vertical compressive stress with depth in reinforced-concrete beams is shown in Figure A.3 compared to the variation of vertical compressive stress with depth in a beam of homogeneous, elastic, isotropic material.

Combined Stress Conditions. From the preceding, the combined stress conditions in the concrete in compression may be written. The values of the horizontal and vertical compressive stresses and the shear stress at any depth in the compression concrete may be written as follows:

$$f_x = \frac{y}{kd}\, f_c$$

$$f_y = p - \frac{p}{jd}\left[\frac{2}{3}\, kd - y + \frac{y^3}{3(kd)^2}\right]$$

$$v = \frac{\cdot}{bjd}\left[1 - \left(\frac{y}{kd}\right)^2\right]$$

If it is assumed that a section is taken just ahead of the inclined crack, and that v_o is the height of the crack at that point, then, from Figure 4.4:

$$f_{x_o} = \frac{y_o}{kd} f_c$$

$$f_{y_o} = p - \frac{p}{jd}\left[\frac{2}{3}kd - y_o + \frac{y_o^3}{3(kd)^2}\right]$$

$$v_o = \frac{V}{bjd}\left[1 - \frac{y_o^2}{(kd)^2}\right]$$

Where y_o is height of the crack above the neutral axis and f_{x_o}, f_{y_o}, and v_o are the unit horizontal and vertical compressive stresses and the unit shearing stress respectively.

Assuming that the crack is produced by the principal tensile stress, the following combined stress equation may be written:

$$t_c = -\left(\frac{f_{x_o} - f_{y_o}}{2}\right) + \sqrt{\left(\frac{f_{x_o} - f_{y_o}}{2}\right)^2 + v_o^2} \qquad (A.9)$$

Where t_c = the ultimate strength of concrete in tension.

Since

$$M = \frac{f_c}{2} b \cdot kd \cdot jd = \frac{pbdx}{2} - \frac{pbx^2}{2}$$

$$f_c = \frac{pd(x - x^2)}{kd \cdot jd}$$

$$\text{and } f_{x_o} = \frac{y_o p\,d(x - x^2)}{(kd)^2 \cdot jd} \qquad (A.10)$$

Since $V = pbd/2 - pbx$:

$$v_o = \frac{p}{jd}\left[\left(\frac{d}{2} - x\right)\left(1 - \frac{y_o^2}{(kd)^2}\right)\right]$$

The above expressions may be used with the combined stress Equation A.9 to evaluate the height of the inclined crack if the value of t_c is known.

Even if this value is not known with certainty, it is apparent from the equations for the combined stress conditions that the inclined crack cannot proceed to the extreme fiber under these conditions, because v_o approaches zero as the crack rises and thus the principal tensile stress approaches zero. Thus, it is concluded that a diagonal-tension failure is not possible in a simply supported rectangular beam subjected to uniformly distributed load, assuming the stress-strain relationship to be elastic. Similar relationships have been developed for parabolic and trapezoidal stress-strain relationships which result in the same conclusion.

The preceding does not preclude any other mode of failure such as shear-compression. In fact, it appears to explain why simply supported rectangular reinforced-concrete members fail in shear compression rather than diagonal tension.

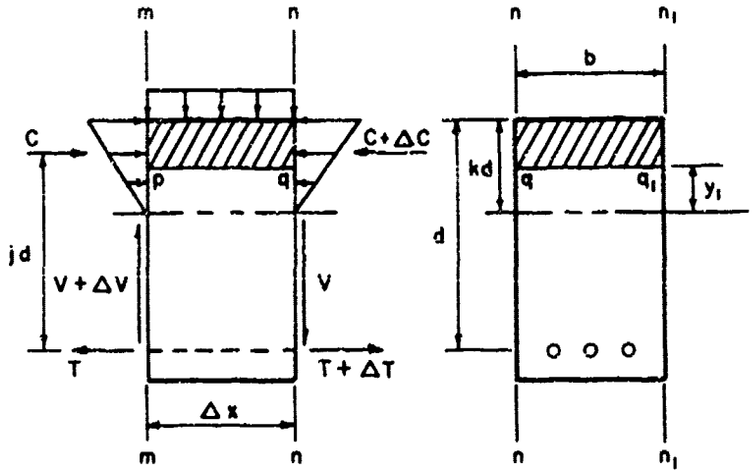

Figure A.1 Distribution of compressive stresses on an elemental length of a simply supported rectangular concrete beam subjected to uniformly distributed load.

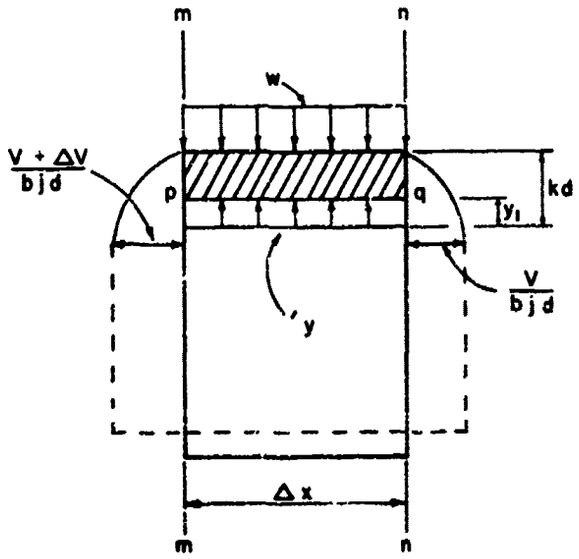

F gure A.2 Distribution of shearing stress with depth n rectangular reinforced-concrete beam subjected to uniformly distributed load.

A weight of slab per unit length, load on slab per unit length.

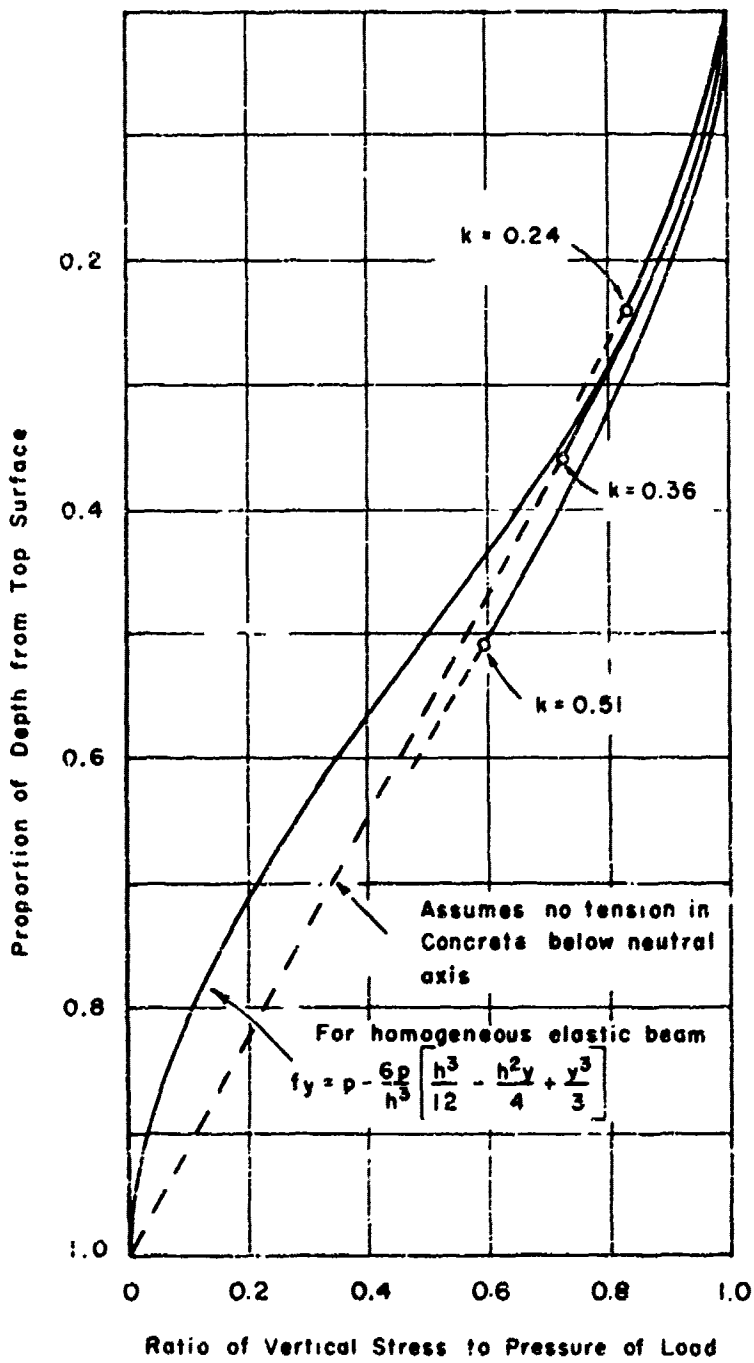

Figure A.3 Variation of vertical compressive stress with depth in a uniformly loaded beam, assuming a triangular bending stress distribution.

Appendix B

LABORATORY TESTS OF REINFORCING STEEL

Samples of the reinforcing steel used in the Project 3.6 slabs were sent to the University of Illinois for testing. These samples were of the following sizes: No. 6, 5, 4, and 3. Coupons of all the sizes were tested in tension at normal static loading rates, and coupons of the No. 6 bars were tested in tension at high loading rates comparable to those that were experienced in the field test.

The areas of the coupons were determined by weighing the bars (± 0.01 lb), measuring their lengths (± 1/32 inch in about 3 feet), and computing the areas based on a weight of 3.4 lb/in^2-ft.

B.1 STATIC TESTING

The normal loading-rate, or static, tests were performed on a 120,000-pound Baldwin Universal Hydraulic Testing Machine. The coupons as tested were the unaltered reinforcing bars; except for prick punching to support the extensometer, no machining was done on the bars. The static tests of the No. 6, 5, and 4 bars were planned so as to provide complete load-versus-deformation records from start of test through yield and up to strain hardening, and also the maximum load and corresponding strain. An autographic recorder was used to provide the load-versus-elongation record up to strain hardening. The deformation at maximum load was measured with calipers to ±1/100 inch, since the extensometer was removed after the beginning of strain hardening. It must be emphasized that this deformation at maximum load is not comparable to the usual figure of "elongation in 8 inches", since the measurement was taken before the coupon necked down.

Because the No. 3 bars were used for ties rather than reinforcement, no load-deformation record was taken. Only the yield point and maximum load were recorded.

The time from the beginning of steady stressing until the upper yield point was attained was recorded for each static test. The time readings were taken by ordinary wristwatch second hand and are not accurate to the nearest second, but they do define the rate of loading or strain rate adequately.

The results of the static tests of the Project 3.6 reinforcing steel are given in Table B.1. It is noted that the test results are relatively uniform in any bar size and in the overall grouping of No. 6, 5, and 4 bars. This steel did not exhibit pronounced upper and lower yield points.

B.2 DYNAMIC TESTING

To obtain an indication of the yield resistance of the reinforcing steel when subjected to high loading rates coupons of the No. 6 bars were tested in the University of Illinois 60-kip dynamic testing machine. This machine, described in Reference 29, is capable of applying a 60-kip load in approximately 6 msec.

The bars were tested in an unaltered form; the only change from the mill condition was produced by filing smooth a portion of each of the longitudinal ribs on opposite sides of the

bar in order to apply SR-4 strain gages. The basic instrumentation for the high-stress-rate testing was planned to yield load-versus-time and deformation-versus-time records. An aluminum dynamometer, mounted between the coupon and the machine frame, indicated the load through output from Type AD-7 SR-4 electrical resistance strain gages mounted on the dynamometer. The strain in the coupon was indicated by Type A-12-2 SR-4 electrical resistance strain gages mounted on the coupon. The outputs of load from the dynamometer SR-4 gage bridge and of strain from the coupon SR-4 gage bridges were recorded on a Hathaway S-14c magnetic oscillograph along with a 500-cps timing signal.

A complete description of the dynamic-test apparatus and instrumentation may be found in Reference 30. This report describes tests which were carried out using the same procedures as for the Project 3.6 tests.

The results of the dynamic tests of the reinforcing are given in Table B.2. The nomenclature used is defined in Figures B-1 and B-2.

As noted in Section 4.3.1, in the dynamic tests of the Project 3.6 bars, an effort was made to load the bars with a force-time function similar to that to which the bars in the field-test slabs were subjected. This objective was largely realized. Analyses of SDF systems equivalent to the one-way slabs indicated that the time from start of loading to yield in the field ranged from about 1.5 to 3.0 msec. The range in the laboratory testing was from 4.0 to 26 msec with four of the six tests near the shorter time limit. The shape of the load-time function in the laboratory was quite similar to the shape of the resistance-time function established for the field-test slabs by use of the equivalent SDF system. It is therefore believed that the curve of yield point versus time to yield as shown in Figure 4.14 gives a reliable indication of the yield resistance of the reinforcing steel under field-test conditions.

Some results from the series of tests described in Reference 30 are included here to indicate the variations in the dynamic increase in yield point for intermediate-grade reinforcing bars of different lots and manufacturers. The Project 3.6 reinforcing bars were obtained from the Judson Steel Company; the Reference 30 bars were manufactured by the Inland Steel Company. The chemical properties of the Project 3.6 bars are given in Table B.3.

In the full range of tests performed by the two projects, the variation in [illegible] load-time functions applied to the coupons became too broad for adequate representation by the time parameter t_y-time from start of loading to yield. Theoretical studies of the yielding phenomenon in steel in Reference 31 indicate that yielding, for t_y less than about 100 msec, is defined by the relation $\int f^{\alpha} dt = C$, where α is on the order of 12.5. The test data obtained is not adequate for defining the constants α and C; therefore, the results obtained cannot be expressed as values of α and C for each lot of steel. However, the high value of α indicates that the stress-time history is of major significance only at the higher stress levels. This has been confirmed experimentally by many investigations, for instance, those of Reference 32. For this reason, the time parameter to define conditions of testing was selected as the delay time t_d, the elapsed time during the test when the stress level was in excess of the static-yield level but the specimen was still elastic.

In the reduction of the laboratory-test data, the yield point was defined as the stress, strain, time, point at which the instantaneous slope of the stress-strain curve dropped to 20×10^6 psi. This criterion was selected in order to best consider tests in which the load on the coupon peaked and then oscillated before yielding occurred. Definite yielding eventually occurred if the average load level was in excess of the static yield level. However, in each cycle of vibration, before general yielding, the strain corresponding to a given load level increased by a small amount. Defining the yield point as stated above seemed most satisfactory for these conditions, and equally applicable when yielding

occurred before the load on the coupon reached a maximum. The lower yield stress (the minimum stress level after the yield point was passed) was either slightly larger or slightly smaller than the yield stress defined by this criterion. The upper yield stress (the maximum stress level occurring between the yield point and the lower yield point) was either greater than the yield stress or equal to it. For the tests of longer delay times, (20 msec or greater), it should be recognized that the scatter can be attributed to some extent to the selection of yield time. For the fast tests, with delay times less than 2 msec, it should be appreciated that the recording equipment, sensitive to 500 cps, was being pushed to the limits of its response, and that the delay time determined from the record may really represent only an order of magnitude. One other limitation of the accuracy of the results is significant in the longer delay tests. The strains were recorded on an effective gage length of 1-inch at the center of a 10-inch specimen. The specimens may have began yielding at another point before the yielding began under the strain gage. In this sense, all delay times represent maximum values. Tests described in Reference 30 conducted with two sets of strain gages 2-1/2 inches apart show that this difference in delay time with location on the specimen is insignificant when the delay time is less than 20 msec.

The presentation of dynamic-yield resistance data in the form of yield stress versus delay time is rather unsuited to use in design. For this reason the test results presented are expressed as the percent increase in lower yield stress versus effective stress rate (Figure B.3), and percent increase in lower yield stress versus effective strain rate (Figure B.4). For comparison, the results of tests described in Reference 33, which were made on mild steel at approximately constant strain rates, are included on Figure B.4. The effective stress rate is the average stress rate during the delay time period; the effective strain rate is the average strain rate during this period. These are not believed to be the ultimate methods of expressing the time criteria for dynamic effects on steel yield point, but they should apply well when the actual stress and strain rates are reasonably linear.

Test results from Reference 30 show a generally greater percentage of increase in yield stress for a given stress or strain rate than is shown by test results from Project 3.6. Reference 31 indicates that as the static-yield level increases, percentage of dynamic-yield increase tends to decrease. Thus, the generally higher static-yield points of the Project 3.6 specimens help explain the smaller dynamic effects. It is also quite possible that the deformations of the reinforcing bars may influence the dynamic-yield point. In Reference 34, it is indicated that scratches on polished specimens caused marked reductions in dynamic-yield level. The differences in deformations signify differences in the stress concentrations, which may have a major influence on the yield level.

TABLE B-1 REINFORCING STEEL STATIC TEST DATA

Specimen	Area	Yield Stress f_y	Upper Yield Stress f_{yu}	Lower Yield Stress f_{yl}	Ultimate Stress f_u	Yield Strain ϵ_y	Strain Hardening ϵ_{sh}	Strain at Ultimate ϵ_u	Elastic Modulus E	Time to Yield t_y
	in^2	ksi	ksi	ksi	ksi	in/in	in/in	in/in	10^3 ksi	sec
6A	0.422	50.2	50.9	50.9	78.9	0.00173	0.00639	0.174	28.7	53
6B	0.427	50.1	50.8	50.8	78.7	0.00151	0.00537	0.174	31.2	57
6C	0.418	49.3	49.8	49.8	78.0	0.00161	0.00509	0.177	32.9	62
6D	0.419	50.6	50.6	50.6	79.5	0.00155	0.00725	0.166	29.7	102
6E	0.424	48.1	48.1	48.1	77.8	0.00156	0.00985	0.176	29.1	105
6F	0.413	48.5	48.7	48.7	78.5	0.00156	0.01052	0.165	29.0	130
6G	0.425	48.7	48.7	48.7	77.6	0.00157	0.00751	0.181	29.2	85
6H	0.424	48.8	48.8	48.8	77.6	0.00163	0.00780	0.150	30.7	92
6I	0.423	48.5	48.9	48.9	78.5	0.00150	0.00669	0.170	29.8	93
6J	0.425	47.8	47.8	47.8	76.5	0.00152	0.01350	0.185	28.1	222
6K	0.425	48.0	48.0	48.0	76.9	0.00168	0.01610	0.178	27.5	252
6L	0.418	47.6	47.6	47.6	78.2	0.00170	0.01590	0.166	27.9	210
No. 6 Avg.	0.422	48.9	49.1	49.1	78.3	0.00160	0.00950	0.172	29.5	
5A	0.296	50.4	50.6	50.6	79.5	0.00151	0.00750	0.151	33.4	80
5B	0.302	51.1	51.8	51.8	83.2	0.00159	0.00720	0.163	34.1	100
5C	0.298	49.3	50.0	50.0	79.7	0.00155	0.00794	0.178	30.8	80
5D	0.300	50.9	51.1	51.1	81.4	0.00168	0.01585	0.178	27.8	245
No. 5 Avg.	0.300	50.4	50.9	50.9	81.0	0.00158	0.00962	0.153	31.5	
4A	0.188	50.7	51.0	51.0	81.9	0.00178	0.01010	0.162	28.6	85
4B	0.195	51.5	51.8	51.8	83.8	0.00151	0.01252	0.155	27.6	93
4C	0.195	53.0	53.3	52.0	84.0	0.00145	0.00832	0.157	36.0	85
4D	0.188	50.3	51.1	51.1	82.0	0.00167	0.01110	0.164	26.9	85
No. 4 Avg.	0.192	51.4	51.8	51.7	82.9	0.00160	0.01051	0.160	29.0	
3A	0.110		53.5		77.4					75
3B	0.116		53.8		79.0					70
3C	0.110		53.9		78.4					75
3D	0.109		53.9		78.7					58
No. 3 Avg.	0.110		53.8		78.4					

TABLE B.2 REINFORCING STEEL TEST RESULTS

Terminology defined in Figures B.1 and B.2.

Specimen Number	6A	6B	6C	6D	6E	6F
Area, in²	0.422	0.427	0.418	0.419	0.421	0.413
Static Test Results						
Yield stress, f_y, ksi	50.2	50.1	49.3	50.6	48.1	48.5
Upper yield stress, f_{yu}, ksi	50.9	50.8	49.8	50.6	48.4	48.7
Lower yield stress, f_{yl}, ksi	50.0	50.8	49.8	50.6	48.1	48.1
Yield strain, ϵ_y, 10^{-6} in in	1,730	1,510	1,610	1,550	1,660	1,560
Elastic modulus, $E \times 10^3$ ksi	28.7	31.2	32.9	29.7	29.1	29.0
Time to yield, t_y, sec	53	57	62	102	105	130
Dynamic Test Results						
Yield stress, f_y, ksi	59.3	61.0	57.0	62.3	59.8	61.8
Upper yield stress, f_{yu}, ksi	62.8	63.5	61.7	63.2	60.5	61.8
Lower yield stress, f_{yl}, ksi	61.5	62.3	61.7	62.5	59.7	61.0
Yield strain, ϵ_y, 10^{-6} in in	2,170	2,310	2,010	2,540	2,200	2,250
Initial time of loading, t_0, 10^{-3} sec	7.5	8.0	4.3	2.5	3.0	4.5
Time of static yield level, t_{sy}, 10^{-3} sec	10.7	11.2	8.5	5.8	14.1	15.7
Time of yield, t_{dy}, 10^{-3} sec	11.5	12.0	9.0	6.5	22.0	18.5
Time to yield, t_y, 10^{-3} sec	4.0	4.5	4.7	4.0	20.6	14.0
Delay time, t_d, 10^{-3} sec	0.8	1.3	0.5	0.7	7.9	2.8
Elastic modulus, E_d, ksi	[illegible]	27.1	28.4	26.2	27.7	28.1
Effective stress rate, ksi sec	11,600	8,150	15,400	16,700	1,480	4,750
Effective strain rate, in in-sec	0.424	0.261	0.542	0.638	0.0535	0.163
Dynamic f_{yu}						
Static f_{yu}	1.24	1.25	1.24	1.25	1.25	1.27
Dynamic f_{yl}						
Static f_{yl}	1.21	1.23	1.24	1.23	1.17	1.23

TABLE B.3 CHEMICAL PROPERTIES OF REINFORCING STEEL

Size	Carbon C percent	Manganese Mn percent	Phosphorus P percent	Sulfur S percent	Identification
No. 6	0.36 to 0.37	0.47 to 0.55	0.006 to 0.009	0.038 to 0.049	Deformed intermediate grade
No. 5	0.35 to 0.37	0.46 to 0.48	0.004 to 0.005	0.036 to 0.043	Deformed intermediate grade
No. 4	0.33 to 0.38	0.41 to 0.50	0.005 to 0.007	0.026 to 0.068	Deformed intermediate grade
No. 3	—	—	0.003 to 0.006	—	Deformed intermediate grade

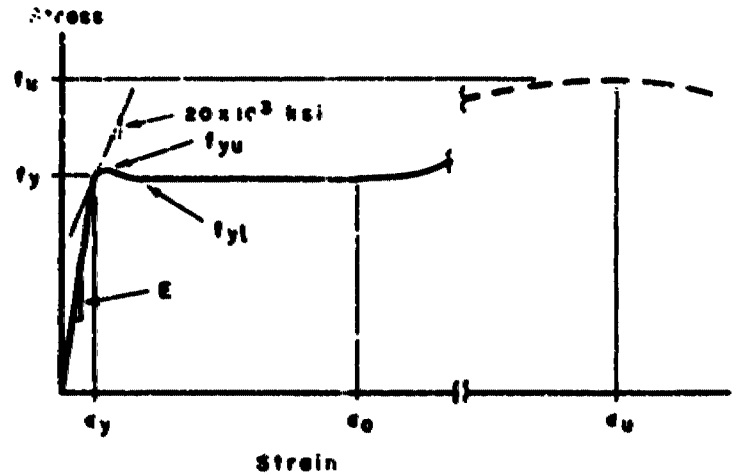

f_y stress at which tangent modulus declines to 20×10^3 ksi
f_{yu} upper yield stress
f_{yl} lower yield stress
f_u maximum nominal stress developed
ϵ_y strain corresponding to f_y
ϵ_θ strain at which strain hardening begins
ϵ_u strain corresponding to f_u
E elastic modulus - slope of straight line portion of curve

Figure B.1 Defined points on typical stress-strain curve.

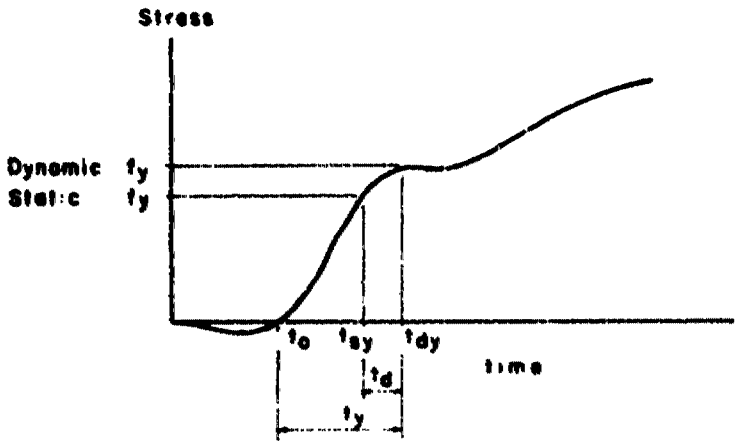

t_o time when load becomes positive
t_{sy} time when static yield stress is attained
t_{dy} time when yielding occurs
t_y time to yield ($t_{dy} - t_o$)
t_d delay time ($t_{dy} - t_{sy}$)
$\dot{f}_e$ effective stress rate is $\frac{f_y \text{ dynamic} - f_y \text{ static}}{t_d}$
$\dot{\epsilon}_e$ effective strain rate is $\frac{\dot{f}_e}{E}$

Figure 3.2 Typical dynamic test stress-time curve

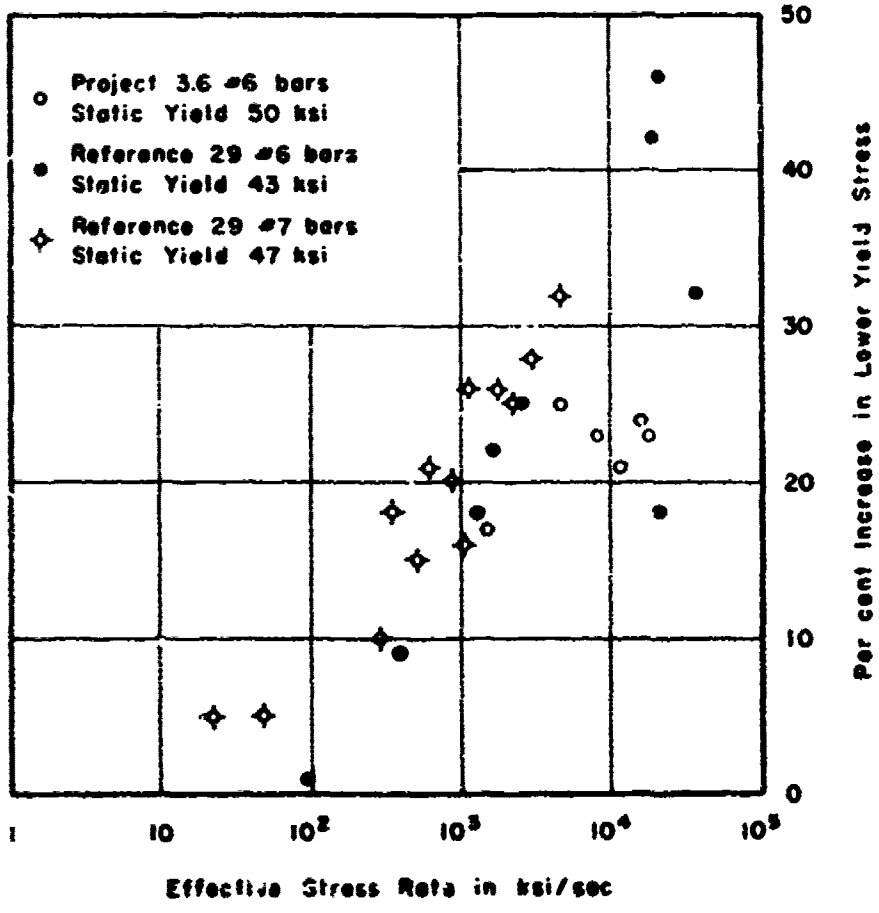

Figure B.3 Increase in lower yield stress versus stress rate for intermediate-grade reinforcing steel.

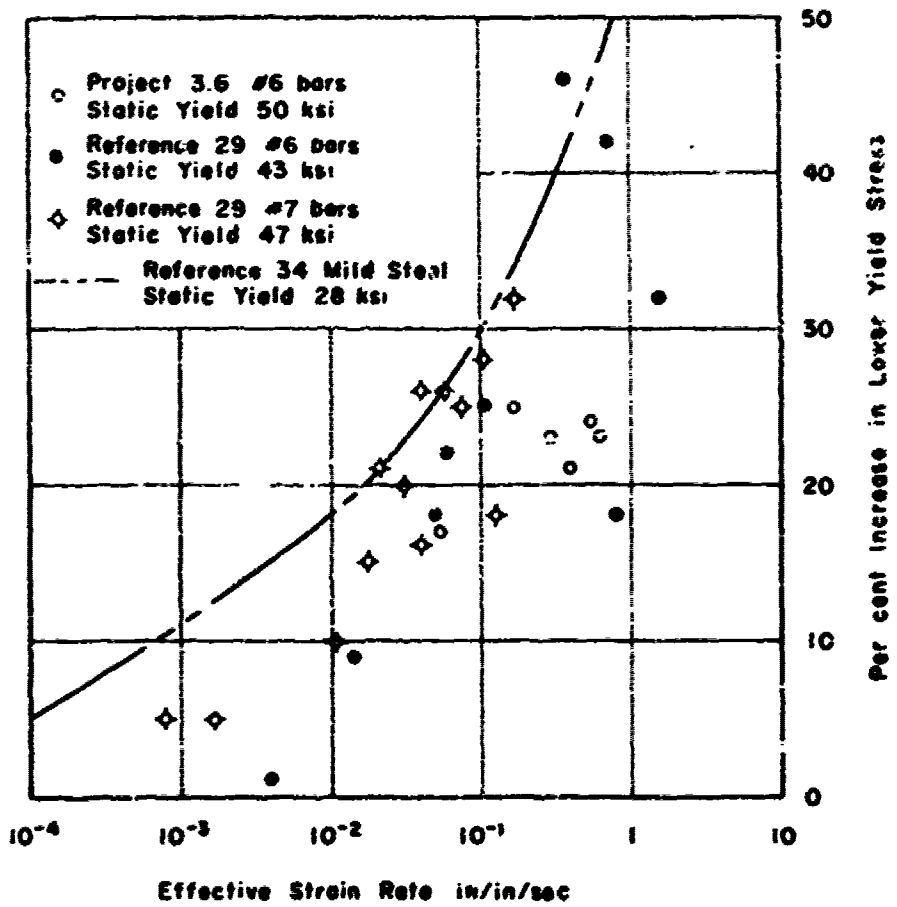

Figure B.4 Increase in lower yield stress versus strain rate for intermediate-grade reinforcing steel.

SECRET

Appendix C

DEFINITIONS OF SYMBOLS

A	area, a constant.
A_s	area of tensile reinforcement.
A'_s	area of compressive reinforcement.
a	area of tensile test specimen.
b	width of compressive zone in a concrete section; width of slab.
C	a constant; resultant vector of horizontal compressive force on concrete cross section.
c	width of the slab support in the direction of the slab span.
c_f	coefficient of friction between slab and its support.
d	the depth of a reinforced concrete cross section from the compressive surface to the centroid of the tensile reinforcing steel.
d'	the distance from the centroid of the tensile reinforcing steel to the bottom of the slab.
E	modulus of elasticity.
E_s	modulus of elasticity of the tensile reinforcing steel.
E_c	modulus of elasticity of concrete
f	a unit stress.
f_b	concrete stress in bearing.
f'_b	ultimate strength in bearing.
f_{ba}	nominal bearing stress on shear-anchorage failure plane.
f_{bc}	concrete bearing stress at time of yield of tensile reinforcing steel.
f'_c	compressive strength of standard concrete cylinder in standard test.
f_r	modulus of rupture for concrete (apparent ultimate tensile stress from test of unreinforced beam).
f_s	stress in tensile reinforcing steel.
f_y	yield stress of tensile reinforcing steel.
f_{yl}	lower yield stress.
f_{yu}	upper yield stress.

$\dot{f}_e$ effective stress rate $\frac{\text{Dynamic } f_y - \text{Static } f_y}{t_d}$.

g acceleration due to gravity.

h total depth of slab.

I moment of inertia of cross section about neutral axis.

I_r moment of inertia for rebound, I of cross section about the centroidal axis.

j the internal moment arm at a reinforced concrete cross section as a proportion of d for elastic theory.

j' the internal moment arm at a reinforced concrete cross section as a proportion of d for the general nonelastic case.

k spring constant of elastic system, dimensionless parameter used in elastic theory expressing the depth of the compressive zone of a reinforced concrete section as a proportion of d, ratio of dynamic ultimate compressive strength of concrete standard cylinder to f'_c.

ksi unit stress in 10^3 psi units.

k_u dimensionless parameter used in ultimate strength theory expressing the depth of the compression zone of a reinforced concrete section as a proportion of d.

KE kinetic energy.

k_1 coefficient expressing ratio of the area of the concrete stress block to that of the enclosing rectangle defined by $k_3 f'_c\ k_u d$.

k_2 coefficient expressing location with respect to compressive surface of resultant compressive force as a proportion of $k_u d$.

k_3 coefficient expression ratio of ultimate compressive stress to f'_c.

l clear span of slab-edge to edge of supports.

l' span of slab, center to center of supports.

l_a span of slab, center to center of anchor bolts.

l_s total length of slab.

M bending moment.

M_c bending moment at center of span.

M_r resisting moment of slab at center of slab.

M'_s slab resistance in shear compression expressed as the maximum moment capacity.

M_u slab ultimate flexural resistance expressed as the maximum resisting moment.

M_{ua} slab ultimate flexural resistance with axial loads acting expressed as the maximum resisting moment.

M_y bending moment at which the tensile reinforcing steel yields.

M_{ya} bending moment at which the tensile steel yields with axial loads acting.

m	mass of elastic system; mass of slabs per unit-plan area.
m_e	equivalent mass of slab per unit-plan area for use with equivalent single-degree-of-freedom system.
N	resultant axial force on reinforced-concrete section.
N_{cr}	axial force which would cause buckling of slab in first critical mode.
n	modular ratio of concrete E_s E_c.
P	earth-transmitted axial load on slab.
Pb	balance point of interaction diagram.
PE	potential energy.
p	overpressure loading on slab surface; reinforcing ratio A_s bd.
p_m	peak overpressure.
p_{t_0}	overpressure at t t_0.
p_y	overpressure at time of yielding of slab.
$\dot{p}$	rate of change of overpressure.
$\dot{p}_{t_0}$	rate of change of overpressure at t t_0.
psi	pressure or stress in pounds per square inch.
q	reinforcing index p f_y/f'_c.
q_y	static-yield resistance.
r	resistance of elastic system, resistance of slab expressed as force per unit-plan area.
r_a	rebound resistance as limited by anchor-bolt capacity expressed in terms of span l_a.
r'_a	rebound resistance as limited by anchor bolt capacity expressed in terms of span l'.
r_f	resistance of slab in flexure.
r_0	resistance of slab at time t t_0.
r_r	available rebound resistance of slab.
r'_r	required rebound resistance to preclude cracking of slab
r_s	rebound resistance as limited by soil friction expressed in terms of span l.
r'_s	rebound resistance as limited by soil friction expressed in terms of span l'.
r_{sc}	resistance of slab in shear compression.
r_{sp}	resistance of slab in pure shear.
r_{sw}	resistance of slab in diagonal tension.
r_u	ultimate resistance of slab.
r_y	yield resistance of slab.

r	rate of change of resistance.
$\dot{r}_o$	rate of change of resistance at $t = t_o$.
T	longest natural period of elastic system; resultant tensile force on reinforced-concrete section.
T_y	tensile force in reinforcing steel at yield.
t	time.
t_d	duration of overpressure pulse, delay time in steel testing $t_{dy} - t_{sy}$.
t_{dy}	time at which coupon yields in steel testing.
t_o	initial time; initial time of positive stressing in steel testing.
t_{sy}	time at which static-yield stress is achieved in steel testing.
t_y	time to yield in steel testing $t_{dy} - t_o$.
u	relative displacement between mass center and support in single-degree-of-freedom system.
u_a	average bond stress.
u_c	ultimate bond stress.
$\dot{u}$	rate of change of u, relative velocity.
$\ddot{u}$	rate of change of $\dot{u}$, relative acceleration.
V	shear force; shear in slab at support.
V_a	shear which anchor bolts can transmit to slab.
V_c	shear at support calculated to produce diagonal cracking.
V_y	shear at support at time of slab yielding.
V_1	shear in slab carried by concrete.
V_2	shear in slab carried by dowel action of reinforcing steel.
v	shearing stress.
v_a	average shear stress on failure plane for shear anchorage.
v_c	unit shear at supports at which diagonal cracking is calculated to occur $v_c = \frac{8}{7}\frac{V_c}{bd}$
v_{su}	ultimate average shearing stress on vertical section at the supports.
v_{sy}	average shearing stress on vertical section at the supports at the time of slab yielding.
v_u	maximum unit shear resistance on failure plane for shear anchorage.
W_u	total load on beam at ultimate.
W_y	total load on beam at yield.

w	weight of slab per unit length; load on slab per unit length.
x	a displacement.
x_o	displacement at $t = t_o$.
x_m	maximum displacement of single-degree-of-freedom system.
x_y	yield displacement of single-degree-of-freedom system.
$\dot{x}$	velocity.
$\ddot{x}$	acceleration.
y	displacement.
$\dot{y}$	velocity.
$\ddot{y}$	acceleration.
α	a phase angle in response analysis; dimensionless parameter for deflection computations.
β	a dimensionless parameter for deflection computations.
o_c	deflection of slab at center.
o_m	maximum center deflection of slab.
o_s	static deflection of slab under its own weight.
o_{sc}	static center deflection of slab under its own weight.
o_{sq}	static quarter point deflection of slab under its own weight.
o_{sp}	static center deflection of slab under load p_m.
o_u	ultimate center deflection of slab.
o_y	yield center deflection of slab.
ϵ	unit strain.
ϵ_o	strain in steel coupons at beginning of strain hardening.
ϵ_s	strain in tensile reinforcing steel.
ϵ_{su}	strain in tensile reinforcing steel at ultimate load.
ϵ_{sy}	strain in tensile reinforcing steel at yield.
ϵ_u	ultimate compressive strain of concrete.
ϵ_y	yield strain of reinforcing steel.
$\dot{\epsilon}$	effective strain rate = $\dot{f}_e/E$.
λ	a dimensionless parameter expressing distribution of strain in tensile steel.
μ	slab mass per unit length; ductility factor: ultimate deflection/yield deflection.
ρ	percentage of tensile reinforcing = $100 \frac{A_s}{bd}$.
ρ'	percentage of compressive reinforcing = $100 \frac{A'_s}{bd}$.

Σ	summation symbol for finite summation.
Σ_o	sum of reinforcing-bar perimeters.
ω	natural frequency of elastic system.
ω_a	natural frequency of elastic system with axial loads acting.

REFERENCES

1. J. L. Merritt and N. M. Newmark; "Design of Underground Structures to Resist Blast"; Draft Vol. 2, Final Report prepared under Contract DA-49-129-eng-312 with OCE, December 1957; Unclassified.

2. W. J. Austin and others; "An Investigation of the Behavior of Deep Members of Reinforced Concrete and Steel"; Report on Contract AF 29(601)-468, Civil Engineering Department, University of Illinois; February 1959; Unclassified.

3. W. J. Austin and others; "Behavior and Design of Deep Structural Members; Vol. 2: Influence of Web and Compressive Reinforcement on the Behavior of Deep Beams; Vol. 3: Flexural Behavior of Reinforced Concrete Deep Beams under Uniform Static Loading"; Report on Contract AF 29(601)-468, Civil Engineering Department, University of Illinois, 1959; Unclassified.

4. G. G. Balmer; "Shearing Strength of Concrete Under High Triaxial Stress-Computation of Mohr's Envelope as a Curve"; U. S. Bureau of Reclamation, Research and Geology Division, Structural Research Laboratory Report No. SP-23; October 1949; Unclassified.

5. "Yield Line Theory for the Ultimate Flexural Strength of Reinforced Concrete Slabs"; Bulletin No. 4, The Reinforced Concrete Research Council of the Engineering Foundation, Reprint from the Journal of the American Concrete Institute, March 1953; Unclassified.

6. J. J. Meszaros and others; "Air-Blast Phenomena and Instrumentation of Structures"; Project 1.7, Operation Hardtack, ITR-1612, August 1958; Headquarters Field Command, Armed Forces Special Weapons Project, Sandia Base, New Mexico; Secret Formerly Restricted Data.

7. L. M. Swift and D. C. Sachs; "Ground Motion Produced by Nuclear Detonations"; Project 1.8, Operation Hardtack, ITR-1613, August 14, 1958; Headquarters Field Command, Armed Forces Special Weapons Project, Sandia Base, New Mexico; Secret Formerly Restricted Data.

8. W. J. Austin and W. Egger; "Review of the Literature Pertaining to the Behavior and Design of Deep Structural Members"; Report on Contract AF 29(601)-168, Civil Engineering Department, University of Illinois, June 1958; Unclassified.

9. S. Bernaert and C. P. Siess; "Strength in Shear of Reinforced Concrete Beams under Uniform Load"; Civil Engineering Studies, Structural Research Series No. 120, University of Illinois, June 1956; Unclassified.

10. C. Bach and O. Graf; "Versuche mit Eisenbetonbalken zur Emittlung der Widerstandsfahigkeit Verschiedener Bewehrung gegen Schubkrafte, Dritter Teil"; Deutscher Ausschuss fur Eisenbeton, Heft 20, Berlin, 1912; Unclassified.

11. C. Bach and O. Graf; "Versuche mit Eisenbetonbalken zur Emittlung der Widerstandsfahigkeit Verschiedener Bewehrung gegen Schubkrafte, Vierter Teil"; Deutscher

Ausschuss für Eisenbeton, Heft 48, Berlin, 1921; Unclassified.

12. D. Watstein and R. G. Mathey, "Strains in Beams having Diagonal Cracks"; Journal of the American Concrete Institute, Vol. 30, No. 6, Pages 717-728; December 1958; Unclassified.

13. H. Nylander and H. Holst; "Nagra Undersökningar Rorande Skivor Och Hoga Balkor Av Armerad Betong"; Transactions Royal Technical University, Stockholm, No. 2, 1946; Unclassified.

14. "Design of Deep Girders"; Concrete Information, ST 66, Portland Cement Association, USA; Unclassified.

15. E. H. Bultmann, Jr., G. F. McDonough, and G. K. Sinnamon; "Loading on Buried Simulated Structures in High-Overpressure Regions"; Operation Hardtack, Project 1.9, WT-1611 (Draft manuscript), 1960, University of Illinois, Urbana, Illinois, Secret Formerly Restricted Data.

16. E. Hognestad; "A Study of Combined Bending and Axial Load in Reinforced Concrete Members"; University of Illinois Engineering Experiment Station, Bulletin 399, 1951, Unclassified.

17. M. J. Baron and C. P. Siess, "Effect of Axial Load on the Shear Strength of Reinforced Concrete Beams"; Civil Engineering Studies, Structural Research Series No. 121, University of Illinois, June 1956; Unclassified.

18. R. Diaz de Cossio and C. P. Siess; " Development of Design Criteria for Reinforced Concrete Box Culverts; Part 1: Strength and Behavior of Reinforced Concrete Beams and Frames"; Civil Engineering Studies, Structural Research Series No. 163, University of Illinois, 1958; Unclassified.

19. F. E. Richart and others, "A Study of the Failure of Concrete under Combined Compressive Stresses"; University of Illinois Engineering Experiment Station, Bulletin 185, 1928; Unclassified.

20. D. McHenry and J. J. Shideler, "Review of Data on Effect of Speed in Mechanical Testing of Concrete"; Research and Development Laboratories, Bulletin D9, Portland Cement Association, USA, 1956; Unclassified.

21. D. Watstein; "Effect of Straining Rate on the compressive Strength and Elastic Properties of Concrete"; Proceedings of the American Concrete Institute, Vol. 49, Page 729; 1953; Unclassified.

22. L. S. Jacobsen and R. S. Ayre; "Engineering Vibrations"; McGraw-Hill Book Company, Inc. New York, 1958; Unclassified.

23. J. W. Klein and S. Sutcliffe; "Development of Procedures for Rapid Computation of Dynamic Structural Response"; Civil Engineering Studies, Structural Research Series No. 171; University of Illinois, 1959; Unclassified.

24. H. L. Brode; "Numerical Solution of Spherical Blast Waves"; Journal of Applied Physics, Vol. 26, No. 6, Pages 766-775; June 1955; Unclassified.

25. H. L. Brode, "Close-in H-Bomb Effects (U)"; RAND Research Memorandum RM-1583-1, The RAND Corporation, Santa Monica, California, February 1956; Secret.

26. S. Timoshenko and D. H. Young; "Vibration Problems in Engineering", D. Van Nostrand Company, New York, 1955; Unclassified.

27. N. M. Newmark and W. J. Hall; "Studies of Design Methods for Underground Protective Structures"; Interim Technical Report No. 1 on Contract AF 29(601)-1171, 6 January 1959; Unclassified.

28. Newmark, Hansen, and Associates; "Comments on Protective Construction (U)", Contract SD-52, The Office of the Assistant Secretary of Defense, Properties and Installations, Technical Division, Directorate of Construction, Vols. I and II, 13 April 1959 Secret.

29. W. Egger; "60 Kip Capacity Slow or Rapid Loading Apparatus"; AFSWC-TR-57-22; June 1957, Air Force Special Weapons Center, Kirtland AFB, New Mexico; Unclassified.

30. W. A. Keenan; "The Yield Strength of Intermediate Grade Reinforcing Bars Under Rapid Loading"; Master Thesis, University of Illinois, 1959; Unclassified.

31. J. D. Campbell and J. Duby: "Delayed Yield and Other Dynamic Loading Phenomena in a Medium Carbon Steel"; Proceedings of the Conference on the Properties of Metals at High Rates of Strain; The Institute of Mechanical Engineers, London, 1957; Unclassified.

32. J. M. Massard and R. A. Collins; "The Engineering Behavior of Structural Metals Under Slow and Rapid Loading"; Civil Engineering Studies, Structural Research Series No. 161, 1958; Unclassified.

33. M. J. Manjoine; "Influence of Rate of Strain and Temperature on Yield Stresses in Mild Steel"; Journal of Applied Mechanics, December 1944, Unclassified.

34. R. O. Belsheim; "Delayed-Yield Time Effects in Mild Steel Under Oscillating Axial Loads"; Transactions, American Society of Mechanical Engineers, Vol. 79, 1957, 1619; Unclassified.

DISTRIBUTION

Military Distribution Categories

[illegible], D.C.

[illegible], D.C. ATTN: [illegible]

[illegible], D.C. ATTN: [illegible]

[illegible], D.C. ATTN: [illegible]

[illegible], Washington, D.C.

[illegible] Office of Director of Defense Research and Engineering, Washington, D.C.

[illegible] Chief of Army Civil Affairs, Ft. [illegible]

[illegible] Development [illegible]

[illegible] Tex. ATTN: Capt. Chester [illegible]

President, U.S. Army Artillery Board, Ft. Sill, Okla.

President, U.S. Army Air Defense Board, Ft. Bliss, Tex.

Commandant, U.S. Army Command & General Staff College, Ft. Leavenworth, Kansas. ATTN: ARCHIVES

Commandant, U.S. Army Air Defense School, Ft. Bliss, Tex. ATTN: Command & Staff Dept.

Commandant, U.S. Army Armor School, Ft. Knox, Ky.

Commandant, U.S. Army Artillery and Missile School, Ft. Sill, Okla. ATTN: Combat Developments Department

Commandant, U.S. Army Aviation School, Ft. Rucker, Ala.

Commandant, U.S. Army Infantry School, Ft. Benning, Ga. ATTN: C.D.D.

Commanding General, Chemical Corps Training Cmd., Ft. McClellan, Ala.

Commandant, USA Transportation School, Ft. Eustis, Va. ATTN: Security and Info. Off.

Commanding General, The Engineer Center, Ft. Belvoir, Va. ATTN: Asst. Cmdt., Engr. School

Director, Armed Forces Institute of Pathology, Walter Reed Army Med. Center, [illegible] 16th St., NW, Washington 25, D.C.

[illegible]

Commandant, Walter Reed Army Inst. of Res., Walter Reed Army Medical Center, Washington 25, D.C.

Commanding General, U.S. Army Chemical Corps, Research and Development Cmd., Washington 25, D.C

Commanding Officer, Chemical Corps Materiel Command, Chemical Center, Md. ATTN: Tech. Library

Commanding General, Engineer Research and Dev. Lab., Ft. Belvoir, Va. ATTN: Chief, Tech. Support Branch

Director, Waterways Experiment Station, P.O. Box 631, Vicksburg, Miss. ATTN: Library

Commanding General, Aberdeen Proving Ground, Md. ATTN: Director, Ballistics Research Laboratory

Commanding General, Frankford Arsenal, Philadelphia 37, Pa.

Director, Operations Research Office, Johns Hopkins University, 6410 Connecticut Ave., Chevy Chase 15, Md.

NAVY ACTIVITIES

Chief of Naval Operations, OP-03, Washington 25, D.C. ATTN: [illegible]

Chief of Naval Operations, OP-07, Washington 25, D.C. ATTN: OP-07

[illegible] Naval Material [illegible]

Chief, Bureau of [illegible], Code [illegible]

Chief, Bureau of [illegible], Code [illegible]

Chief, Bureau of [illegible] D.C. ATTN: [illegible]

Director, U.S. Naval Research Laboratory, Washington 25, D.C. ATTN: Mrs. Katherine H. Cass

Commander, U.S. Naval Ordnance Laboratory, White Oak, Silver Spring 19, Md.

Commanding Officer, U.S. Naval Radiological Defense Laboratory, San Francisco, Calif. ATTN: Tech. Info. Div.

Commanding Officer and Director, U.S. Naval Engineering Experiment Station, Annapolis, Md. ATTN: Code 240

Commanding Officer, U.S. Naval Schools Command, U.S. Naval Station, Treasure Island, San Francisco, Calif.

Superintendent, U.S. Naval Postgraduate School, Monterey, Calif.

Officer-in-Charge, U.S. Naval School, CEC Officers, Naval Construction Bn. Center, Port Hueneme, Calif.

Commanding Officer, Nuclear Weapons Training Center, Atlantic, U.S. Naval Base, Norfolk 11, Va. ATTN: Nuclear Warfare Dept.

Commanding Officer, Nuclear Weapons Training Center, Pacific, Naval Station, San Diego, Calif.

Commanding Officer, U.S. Naval Damage Control Training Center, Naval Base, Philadelphia, Pa. ATTN: ABC Defense Course

Commanding Officer, U.S. Naval Medical Research Institute, National Naval Medical Center, Bethesda, Md.

Commanding Officer and Director, David W. Taylor Model Basin, Washington 7, D.C. ATTN: Library

Officer-in-Charge, U.S. Naval Supply Research and Development Facility, Naval Supply Center, Bayonne, N.J.

Commander, Norfolk Naval Shipyard, Portsmouth, Va. ATTN: Underwater Explosion Research Division

Commandant, U.S. Marine Corps, Washington 25, D.C. ATTN: Code AO3H

Commanding General, Fleet Marine Force Atlantic, Norfolk, Va.

Director, Marine Corps Landing Force Development Center, M&D, Quantico, Va.

Commanding Officer, U.S. Naval CIC School, U.S. Naval Air Station, Glynco, Brunswick, Ga.

Chief, Bureau of Naval Weapons, Navy Department, Washington 25, D.C. ATTN: RM

AIR FORCE ACTIVITIES

[illegible], D.C.

Hq. USAF, ATTN: Operations Analysis Office, Office, Vice Chief of Staff, Washington 25, D.C.

Director of Civil Engineering, Hq. USAF, Washington 25, D.C. ATTN: [illegible]

Hq. USAF, Washington 25, D.C. ATTN: [illegible]

Director of Research and Development, DCS/D, Hq. USAF, Washington 25, D.C. ATTN: Guidance and Weapons Div.

SECRET

SUPPLEMENTARY

INFORMATION

Defense Nuclear Agency
6801 Telegraph Road
Alexandria, Virginia 22310-3398

ISST

ERRATA
AD-360623L

29 January 1996

MEMORANDUM FOR DEFENSE TECHNICAL INFORMATION CENTER
ATTENTION: OCD/Mr. Bill Bush

SUBJECT: Declassification of AD-360623L

The Defense Nuclear Agency Security Office (OPSSI) has declassified the following report:

WT-1630 (AD-360623L).

Distribution statement "A" applies.

Judith Jarrett

FOR JOSEPHINE B. WOOD
Chief, Technical Support Branch